NASA CR 73349

AVAILABLE TO THE PUBLIC

[redacted]

EXOTECH
INCORPORATED

N72-12378 (NASA-CR-73349) DESIGN, DEVELOPMENT AND FABRICATION OF A SOLAR EXPERIMENT ALIGNMENT SENSOR (SEAS) Final Report J.R. Bancroft, et al (Exotech, Inc., Gaithersburg, Md.) Apr. 1971 104 p CSCL 14B G3/14

Unclas
09482

\wf

FINAL REPORT

on the

Design, Development and Fabrication of a Solar Experiment Alignment Sensor (SEAS)

Prepared Under Contract
NAS2-4835 for the

National Aeronautics and Space Administration
Ames Research Center
Moffett Field, California 94305

by

J. R. Bancroft/M. Z. Fain/ D. F. Johnson

EXOTECH INCORPORATED
1200 Quince Orchard Blvd
Gaithersburg, Maryland 20760

April 1971 TR IC039

TABLE OF CONTENTS

TABLE OF CONTENTS

LIST OF ILLUSTRATIONS

LIST OF ILLUSTRATIONS

TABLES

ADDENDUM

This final report is the result of a laboratory feasibility investigation of the SEAS concept, described in the following sections.

After the investigation was completed, the recommendation in Section 6 to build a flight version was adopted. Subsequently a flight qualified version for sounding rockets was completed by Exotech in January 1971.

The first flight of the SEAS is scheduled in the summer of 1971. Results from this flight will be available shortly after launch by contacting the NASA-Ames Research Center Technical Monitor, R. K. Melugin.

ABSTRACT

This report summarizes the design, development and testing of a laboratory SEAS (Solar Experiment Alignment Sensor) system capable of overcoming traditional alignment and calibration problems to permit pointing anywhere on the solar disc to an accuracy of five arc seconds.

The concept, development and laboratory testing phases of the program are discussed in detail, and particular attention has been given to specific problems associated with selection of materials, and components.

The conclusions summarize performance capability and discuss areas for further study including the effects of solar limb darkening and effects of annual variations in the apparent solar diameter.

SECTION 1 - Introduction

The Solar Experiment Alignment Sensor (SEAS) system is an attitude measurement system which actively senses the absolute alignment of a solar oriented telescope axis relative to the solar axis and provides control information to permit pointing the experiment anywhere on the solar disc to an absolute accuracy on the order of two arc seconds in the center and five arc seconds on the limb.

In late 1966 Exotech successfully completed a flight hardware development program for NASA, Ames Research Center for a Precision Autocollimating Solar Sensor[1] (PASS) which measured the real-time solar pointing error of the early Solar Pointing Aerobee Rocket Control System[2] (SPARCS) flights. By an integral autocollimator, the PASS measured its own alignment with respect to a reference surface. Although this technique proved successful, the application of PASS as a solar-experiment control sensor was limited, in terms of absolute accuracy, by the potential instabilities of the experiment to PASS mechanical interface plus instabilities within the experiment itself to shock, vibration and thermal stresses. Furthermore, offset pointing accuracy was limited to about 1% by the accuracy with which solar cells could be calibrated.

To overcome these limitations, Exotech began development of a Solar Experiment Alignment Sensor (SEAS) for NASA, Ames Research Center. Much of the technology proven in the PASS was utilized in the SEAS. Conceptually, instead of an autocollimator, the SEAS was designed with a collimator sensor oriented to view an infrared (IR) light source through the experiment optics. This technique permits a direct, continuous, precise determination of the optical axis of the experiment.

For development purposes, only a single axis of the two axis sensor was completely fabricated. The full two axis capability of the SEAS could be obtained with additional components. The electronics were breadboarded without special packaging considerations, but the basic circuitry and components were selected for ready adaptation to flight hardware.

Figure 1-1 shows the breadboard SEAS system which includes its three basic components:

1. A sensor assembly which senses experiment to solar-vector alignment.

2. A focal plane IR source.

3. An electronics package which provides control and amplification functions for the sensor and IR source.

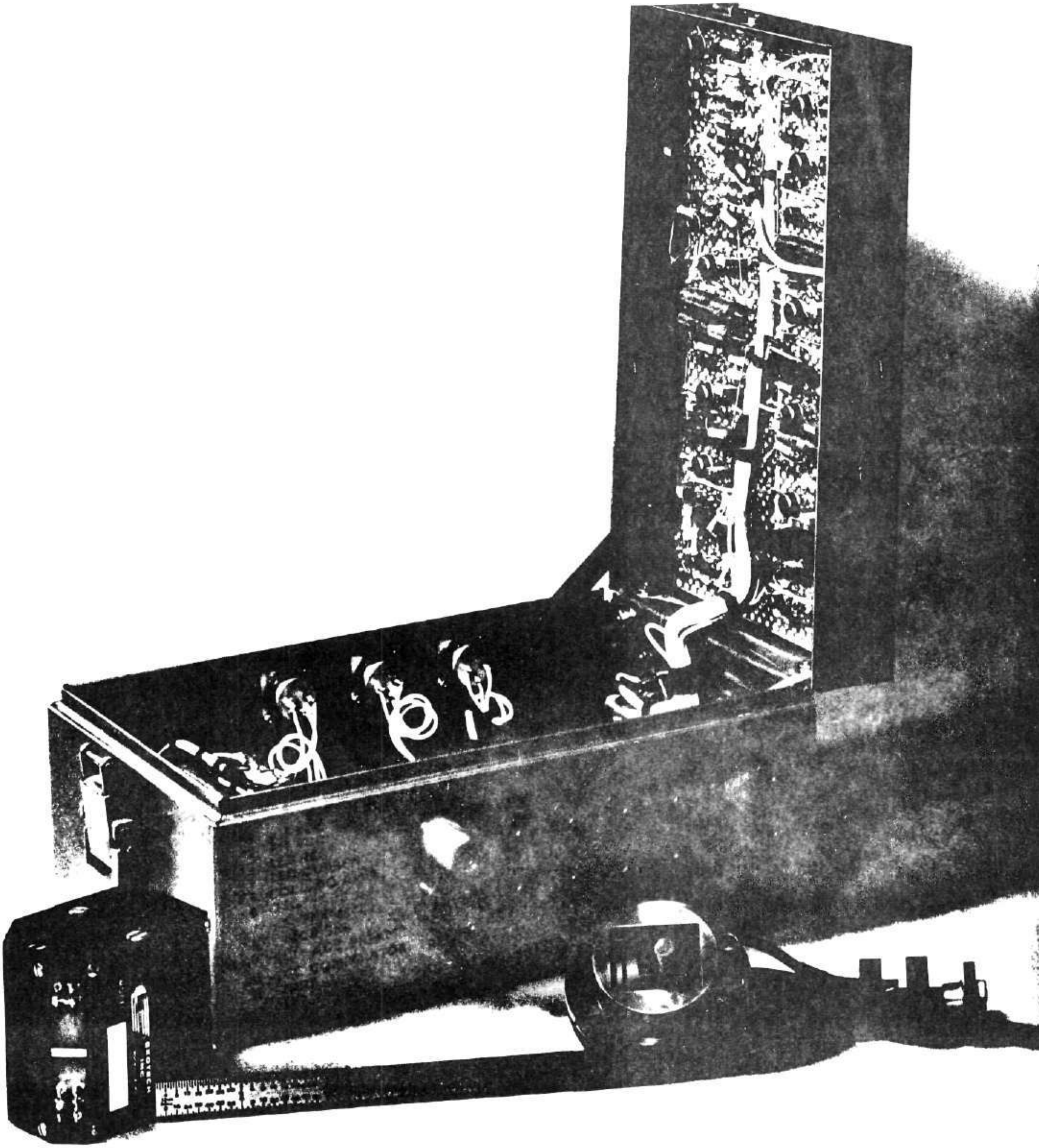

FIGURE 1-1 SEAS System Breadboard

SECTION 2 - SUMMARY

Two major problems in accurately pointing rocket-borne solar experiments at the sun are: the initial alignment of the vehicle control sensor with the experiment, and the maintenance of this alignment through subsequent changes in environment. These problems are overcome with the SEAS concept, which is based on a stable, dual-function sensor which observes the sun in one direction while monitoring an experiment oriented IR source in the opposite direction to continuously measure the experiment-axis to solar-vector alignment. Functional goals and performance goals of the SEAS are based on a desire to achieve an absolute pointing accuracy on the order of 5 arc seconds anywhere on the solar disc.

The SEAS concept shifts the burden of alignment stability from the experiment to the relative stability between solar and collimator sensors. As such, the SEAS design approach is based on fabrication of both sensors within a monolithic structure to provide superior thermal and mechanical stability. A comparative analysis of various structural materials was carried out to find those having the best dimensional stability. Also, a series of tests were conducted on four different cements to determine their stability with respect to curing, temperature cycling and aging.

Since the absolute responsivity and relative responsivity of the detector cells affect sensor performance, the thermal stability characteristics of silicon solar cells have been closely examined. Also, the desirability of obtaining a linear solar sensor transfer characteristic necessitated tests on the influence of defocussing to control the transfer characteristic shape.

Two focal-plane IR-source aperture configurations were considered, each using fiber optics to convey IR from a remotely located source to the experiment focal plane. The first was an aperture in the form of four narrow slits arranged in a square around the experiment aperture but this was replaced by a simpler round aperture at a small sacrifice in gain. Selection of an IR source for the experiment focal plane was based on complex considerations and after a detailed comparison of tungsten sources and light emitting diodes, a diode was selected for use in the SEAS system.

The SEAS electronic system was developed to take maximum advantage of integrated operational amplifier circuits which have now become generally accepted for spacecraft use. Where necessary, their performance limitations were supplemented by additional components, and every effort was made to employ "flight approved" components to permit rapid adaptation of the electronic breadboard to flight hardware.

The SEAS as a system may be described in terms of three functional subsystems:

1. A solar sensor including optics, amplifiers and AGC circuitry
2. A collimator sensor including optics, amplifiers, and IR modulation and signal demodulation circuitry
3. A 28 volt DC to DC voltage regulator

A comprehensive test program was carried out to establish performance characteristics of the SEAS system which could be evaluated in terms of the original performance goals. This was begun with a series of electronic system tests to establish the influence of the electronics on subsequent optical system tests. Sensor tests demonstrated that excellent linearity was obtainable, and most performance goals were either achieved or it was shown that they were attainable.

During these tests, an unexpected phenomenon manifested itself in the form of a variation in incremental responsivity of silicon photovoltaic cells with ambient light. This was first noticed as a shift in the collimator sensor output as the solar simulator was turned off or on. The implication here was that a shift in the collimator sensor output would occur between ground and space conditions.

Further study has indicated that the incremental responsivity of the silicon cell with ambient light is apparently not frequency or spectral dependent. This phenomena varies according to manufacturing process, with Planar passivated types showing the least effect. To further reduce the effect, a narrow band spectral filter is used to attenuate the solar radiation but not the IR from the focal plane source.

SECTION 3 - Sensor Considerations

SUBSECTION - Pointing Requirements

THE GENERAL SOLAR POINTING PROBLEM

In addition to dynamic stability, two major problems in accurately pointing rocket-borne solar experiments at the sun are: the initial alignment of the vehicle control sensor with the experiment, and the maintenance of this alignment through subsequent changes in environment.

Many problems arise in the design of sounding-rocket and spacecraft attitude control systems, capable of pointing solar experiments at the sun with an absolute angular accuracy of better than 5 arc seconds. Initially there is concern with dynamic pointing stability which is basically a function of the control sensor noise and control system limit cycle performance. Fortunately, due to the sun's high energy output, solar sensors operate with very low equivalent noise levels, and recently developed control systems have achieved pointing stabilities in the order of 1 arc second with an improvement to 0.1 arc second anticipated. In fact, the primary problem in reducing jitter is the control of vehicle disturbance torques.

Absolute accuracy depends primarily on achieving an initial alignment between the solar experiment and the control sensor, and maintaining this alignment through temperature changes, launch vibration, vehicle bending, and the space environment. A detailed discussion of various alignment difficulties can be based on a typical solar experiment arrangement shown in Figure 3-1. Initial alignment between the control sensor and experiment should be carried out using a precision solar simulator having sufficient aperture to illuminate both control sensor and experiment simultaneously. In addition, a fairly elaborate test set-up is required and great care must be exercised in taking measurements. As a result, alignment checks are very inconvenient and time consuming and after alignment has been achieved, there is no guarantee of permanence because of the many mechanical interfaces between the two which are subject to thermal, gravitational, and mechanical stresses. Misalignment of sensor and experiment caused by vehicle flexure can be overcome to some extent by mounting both items on a rigid baseplate but changing temperatures may warp the plate if it is not made of the same material as the vehicle. Furthermore, if the solar experiment is optically complex, its design becomes increasingly difficult when arc second stability is desired, and if proper mounting techniques are not employed, acceleration and vibration during vehicle launch can cause serious alignment shifts due to wear on mating surfaces. In theory, all of these problems are solvable on an individual basis, but when considered together, the solutions become impractical because of the great care required to implement each one. Obviously, a concept such as SEAS which solves these problems is desirable.

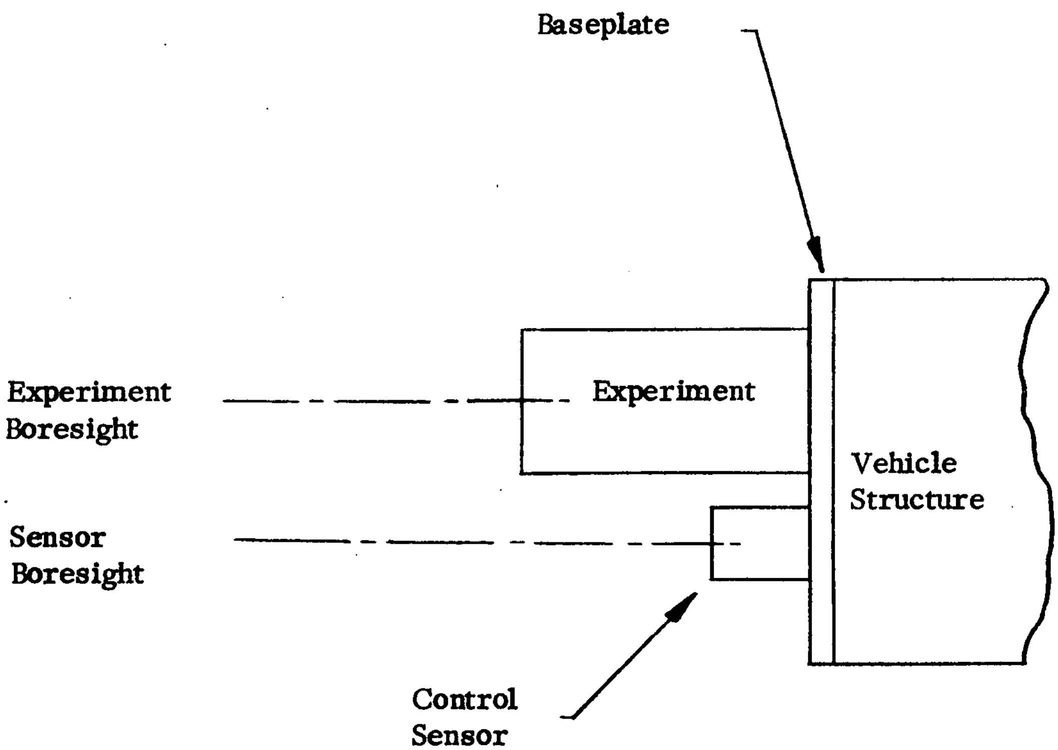

FIGURE 3-1 Typical Sensor-Payload Mounting Configuration

SECTION 3 - Sensor Considerations

SUBSECTION - Sensor

DESCRIPTION OF THE SEAS CONCEPT

The SEAS concept is based on a stable, dual-function, sensor which observes the sun in one direction while monitoring an experiment-oriented IR source in the reciprocal direction to measure the experiment-axis to solar-vector alignment.

The SEAS concept is based on the ability to accurately define the optical axis of an imaging type experiment by means of an IR source located in the focal plane of the instrument. If the experiment is considered basically as a telescope, then IR from a circular source in the center of the focal plane will be collimated parallel to the instrument axis, and to an external observer the source will appear as a distant sun with a decollimation angle dependent on the source diameter and system focal length. An external sensor operating on the same principles as a solar aspect sensor can be located as shown in Figure 3-2 to observe the source and give an electrical output signal proportional to the angular displacement between the sensor boresight and the experiment axis. This collimator sensor may be rigidly attached to a solar aspect sensor looking along a reciprocal path at the sun. The solar sensor output will be proportional to the angular deviation between the solar vector and the sensor boresight, so that by combining both sensor signals it is possible to determine the experiment-axis to solar-vector alignment. Such a combined sensor will be referred to as a Solar Experiment Alignment Sensor (SEAS). The absolute stability of this system is primarily dependent on the relative stability of the two sensor boresights which can be very good because both devices can be fabricated within a single compact structure.

It is particularly important to note that the SEAS system is insensitive to angular rotation of the SEAS alone because each sensor would observe equal but opposite alignment errors and their combined outputs would cancel. As a result, mounting of the SEAS is simplified because it need not be rigidly mounted in the arc second sense and any movement occurring during vehicle launch vibration will not be detrimental to final pointing accuracy. Also, since the collimator sensor observes the experiment directly, any changes in its alignment due to vibration or temperature induced component shifts will be detected and compensated so that experiment design is also simplified.

A complete SEAS system is illustrated in Figure 3-2 which depicts an imaging solar experiment with its aperture slightly obscured by a two axis SEAS control sensor mounted immediately in front of it. The solar sensor and collimator sensor outputs are electronically summed to give an output proportional to the misalignment between the solar vector and experiment axis in each control axis (pitch and yaw).

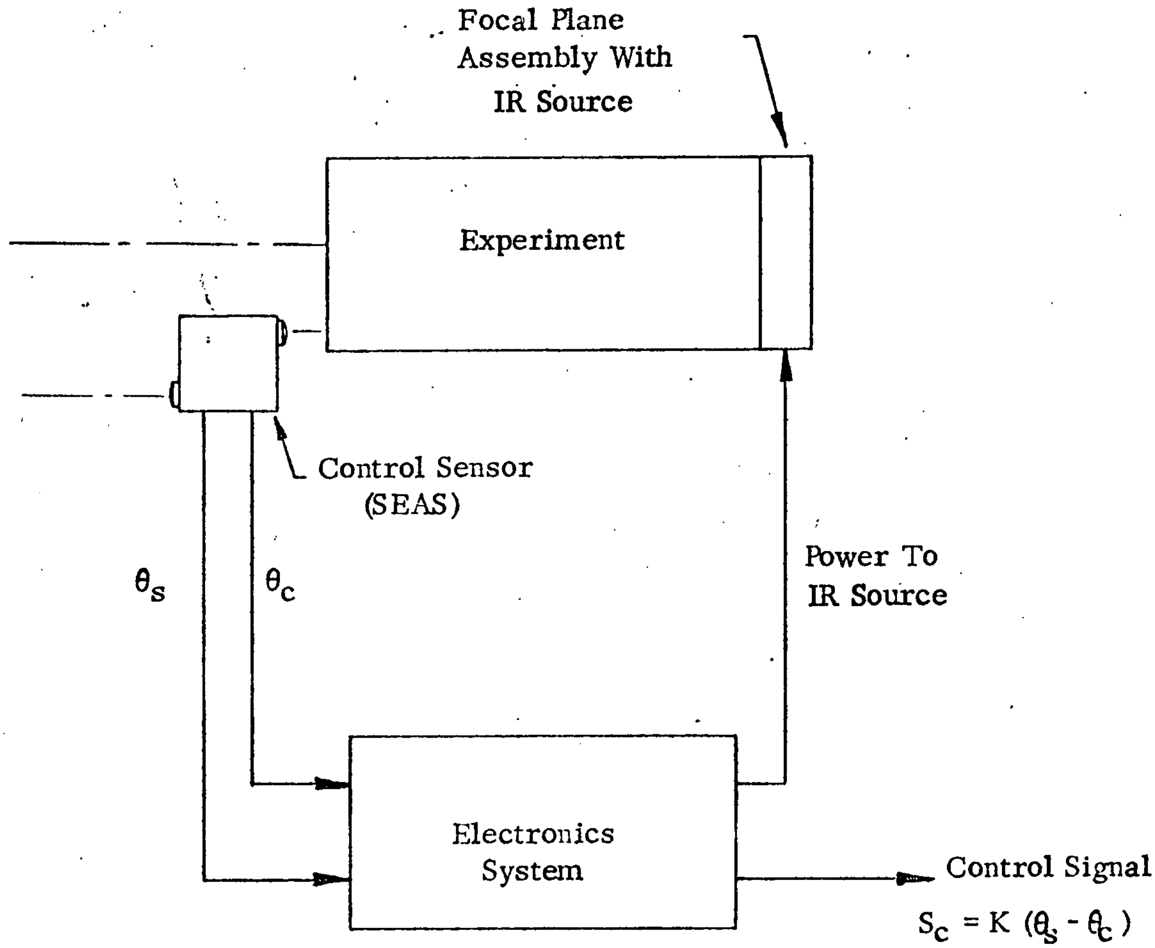

FIGURE 3-2 - Illustration Of SEAS System

SECTION 3 - Sensor Considerations

SUBSECTION - Sensor

DERIVATION OF SYSTEM GOALS

The functional and performance goals of the SEAS are based on a desire to achieve an absolute pointing accuracy on the order of 5 arc seconds anywhere on the solar disc.

Any realistic set of sensor design goals must ultimately be based on future solar experiment requirements, but at this time a complete set of objectives is not available. We have therefore set up an arbitrary goal of being able to point anywhere on the solar disc with an accuracy of 5 arc seconds. This has been interpreted into detailed design goals for specific SEAS parameters such as null stability, dynamic range, and linearity. In addition, criteria for gain control, calibration, and the collimator IR source have been developed.

Null Stability - The boresight, or null stability of each sensor refers to the permanence of its null indication when aligned to a target direction vector. This stability is affected by differential variations in detector conversion efficiency (in the case of an energy balance sensor) or mechanical-structural changes brought on by vibration or a fluctuating thermal environment. In the case of a SEAS, the null stability of each sensor must be better than 1 arc second, and the relative stability of the two sensors must also be of a high order. A goal of 0.5 arc seconds was chosen for the latter so that a combined boresight change should not exceed 1.5 arc seconds.

Dynamic Range - In order to permit pointing to the solar limb or slightly beyond, the dynamic range of the solar sensor should be greater than ± 20 arc minutes. However, the collimator sensor's dynamic range need be only sufficient for accommodation of alignment changes within the solar experiment and movement of the SEAS itself. A range of about ± 1 arc minute should be sufficient for this purpose but since the first SEAS was to be of an experimental nature, a range in excess of ± 2 arc minutes was set as a goal.

Linearity - Sensor linearity is of considerable importance in offset pointing because both solar sensor and collimator sensor must have the same gain in order to correct exactly for movement of the SEAS or the solar experiment. If, for example, the solar sensor and collimator sensor gains differ by 2%, then a 30 arc second change in the SEAS mounting alignment will result in a pointing error of 30 x .02 = 0.6 arc seconds. Based on this result the linearity of the two sensors should be within ± 1% as a goal. It should be emphasized that by calibrating the sensor transfer characteristic to 0.1%, even more accurate offset pointing could be achieved.

Gain Accuracy - Offset pointing accuracy is ultimately limited by the absolute accuracy of the solar sensor gain calibration which may be on the order of 1%, provided accurate calibration standards are available, great care in calibration is exercised, and corrections are made for the annual variations in solar constant due to the eccentricity of the earth's orbit. Even with this accuracy, offset pointing in the vicinity of the limb (16 arc minutes) can result in a pointing error of 16 x 60 x .01 = 9.6 arc seconds. Clearly, some method of calibration in space or some method of automatic gain control with an accuracy approaching 0.1% is desirable. On the other hand, calibration of the collimator sensor can be carried out on the ground with relative ease to an accuracy of better than 1% which is sufficient for its limited dynamic range.

Radiation Source - Since the IR source emits energy within the experiment itself, one of the primary considerations must be the minimization of possible interference with experiment measurements. To this end a monochromatic source seems desirable since scattered IR could be more easily filtered, and controlled. Also, a remotely located source with light transmitted to the experiment through an optical system appears desirable to minimize heating and electrical interference.

Parameter	Performance Goal
Solar Sensor Boresight Stability	< 1 arc second
Collimator Sensor Boresight Stability	< 1 arc second
Relative Stability of Sensor Boresights	< 0.5 arc seconds
Combined Stability	< 1.5 arc seconds
Dynamic Range of Collimator Sensor	> ± 2 arc minutes
Solar Sensor Linearity	± 1%
Collimator Sensor Linearity	± 1%
Solar Sensor Gain Calibration	± .1%

TABLE 3-1 - Summary Of SEAS Performance Goals

SECTION 4 - System Design

SUBSECTION - System Description

DESCRIPTION OF THE SEAS SYSTEM

The SEAS system is comprised of three distinct components: a sensor assembly (SEAS), an experiment focal-plane assembly, and an electronics package.

A block diagram of the SEAS system is shown in Figure 4-1 which depicts a solar experiment with its associated SEAS system components. These include a focal-plane assembly located at the rear of the experiment, a SEAS mounted in front of the experiment, and an electronics system.

Focal Plane Assembly - After undergoing considerable evolution, the experiment focal plane assembly adopted for the SEAS system is based on a light emitting diode (LED) whose monochromatic output, modulated at 1.5 Kilohertz, is transmitted to a circular aperture in the experiment focal plane through a glass-fiber bundle. In addition, the fiber bundle transmits a small portion of the emitted IR to a silicon cell whose output controls a regulator circuit to maintain a constant LED output.

SEAS - The Solar Experiment Alignment Sensor employs imaging-type, energy-balance sensors in which the source (sun or collimator source) is focussed on an energy-dividing optical assembly to which differentially-connected photovoltaic silicon cells are attached. When the sensor is aligned to the source vector, the source image is centered on the assembly and each cell receives equal energy so their combined outputs cancel. As the sensor is rotated, unequal portions of the image energy fall on each cell so that the net output is proportional to the angular rotation of the sensor. In addition, the SEAS contains an AGC sensor cell which receives constant solar energy over a relatively large angular range. It functions as part of a gain control circuit which maintains the solar-sensor gain at some present level to completely eliminate the need for accurate ground calibration.

Electronics - Figure 4-1 illustrates the principle functions performed by the electronics system which include, regulation of the LED output, amplification of the solar-sensor signal with a gain-controlled amplifier, amplification and demodulation of the ac collimator-sensor signal, and summation of the sensor signals to generate a control signal.

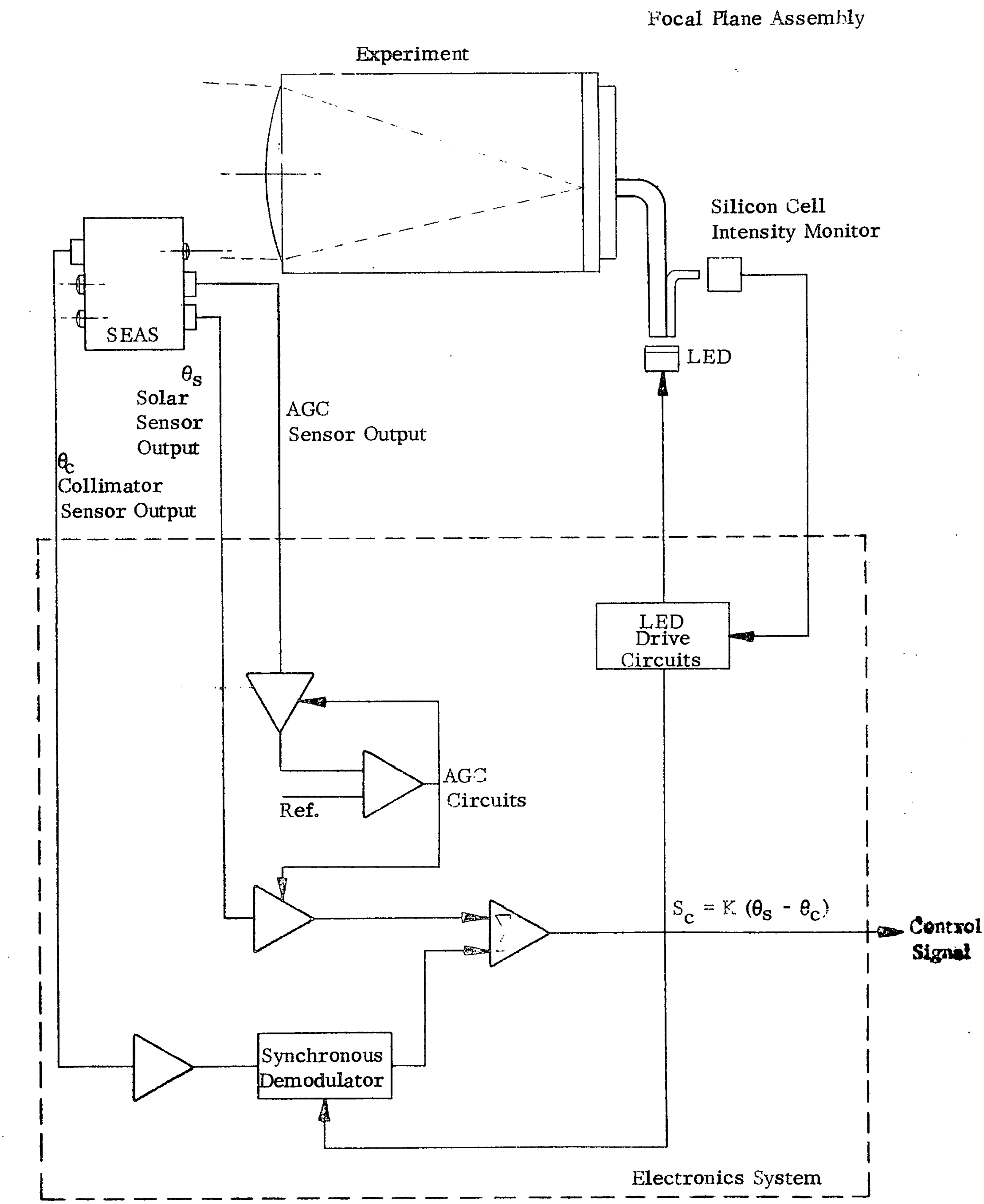

FIGURE 4-1 - SEAS System Block Diagram

SECTION 4 - System Design

SUBSECTION - Sensor

SENSOR DESIGN APPROACH

Since the burden of maintaining accurate alignment falls on the relative stability between solar and collimator sensors, the SEAS design approach taken by Exotech is based on fabrication of both sensors within a monolithic structure to provide thermal and mechanical stability.

Prior to deciding on an overall SEAS design approach, it was necessary to choose between imaging and non-imaging sensors. These two fundamental types were the subject of a previous Exotech study which shows the imaging sensor to have several outstanding advantages for angular aspect sensing, particularly in the case of the collimator sensor which operates at low source intensity levels and can take advantage of the fact that for limited linear dimensions, the imaging sensor has a much higher gain than a non-imaging sensor. This is because a focussed system achieves higher energy densities in the focal plane. Also, the imaging sensor is less sensitive to obscuration of its entrance aperture by dust particles. It must be mentioned, however, that the linearity of an imaging sensor is dependent on the shape of the source (sun or collimator source) but small non-linearities arising from a circular source may be corrected by slightly defocussing the image, resulting in a hybrid sensor, somewhere between an imaging and non-imaging type.

The essential features of an imaging type sensor are shown in Figure 4-2a. These include the lens and detector assembly, which must remain stable with respect to one another and with respect to associated sensor elements. To achieve this stability, two basic approaches were considered for fabrication of a complete SEAS requiring two single axis sun sensors and two single axis collimator sensors.

1) A PASS[1] type system consisting of quartz detector assemblies cemented to solid quartz lens blocks which are in turn cemented to each other.
2) A system consisting of quartz detector assemblies and lenses cemented to a solid structural block having holes cored through it for light paths (Figure 4-2b).

Although the first approach is suitable for single axis sensor pairs as used in PASS, it becomes very difficult to implement where four sensors are involved because it is difficult to obtain optical isolation between sensor assemblies while employing the thin glue layers required for a thermally stable assembly. In contrast, the solid structural block has the advantage that the only critical glue joints are those holding the lenses and reticles, and it is easier to assemble. For these reasons, the solid block approach was adopted.

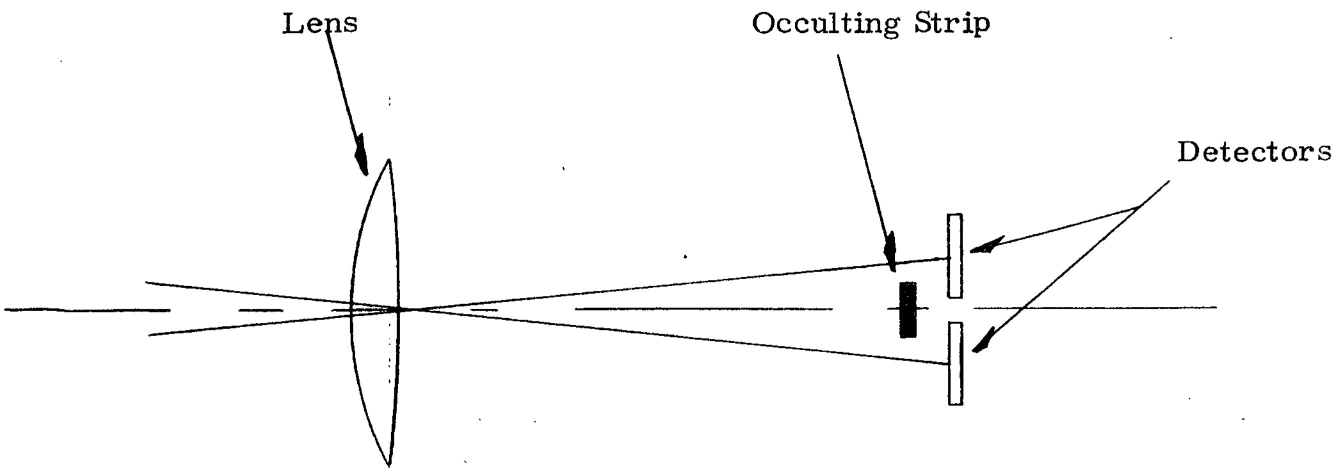

Figure 4-2a - Essential Features of an Imaging-Type Angular Aspect Sensor

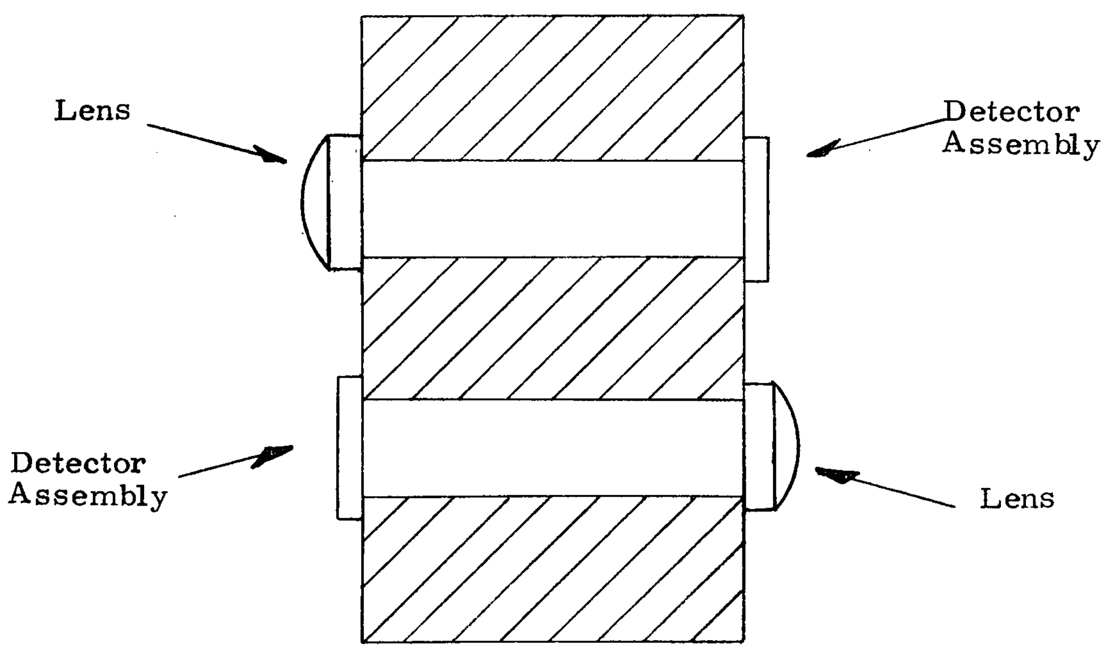

Figure 4-2b - Solid-Block Sensor Approach

SECTION 4 - System Design

SUBSECTION - Sensor

DESIGN OF SENSOR BLOCK AND RETICLE

The sensor block is designed to contain two single-axis sensor pairs in a small package which can be easily assembled and stably mounted.

Sensor Block - One of the primary sensor block design considerations was to minimize the overall size and weight so that it would have a small shadowing effect on the experiment optical system and be easy to mount. At the same time, it had to be simple to fabricate. The desired result was achieved by coring holes through the block for mounting bolts as well as for the sensors so that the general configuration shown in Figure 4-3a was obtained. This approach reduced fabrication of the block to simple sawing and boring operations which were applicable to ULE quartz, the material selected for the block. Optical isolation was obtained by coating the inside of each hole with an opaque epoxy paint.

Each sensor contained within the block consists of two principle components; a one inch focal length lens cemented over one end of a hole, and a reticle assembly located on the opposite side of the block approximately at the lens focal plane. The reticle assembly, shown in Figure 4-3b, is based on a quartz reticle substrate which has a thin opaque reticle deposited on one face, onto which the source is imaged. In the case of a solar sensor, the strip is about .0078 inches wide or about .81 solar image diameters and has no edge irregularities greater than 2×10^{-8} square inches which is very important in minimizing cross coupling effects as the source image is moved parallel to the reticle. Any light not occulted by the reticle passes into two dividing prisms whose inclined reflective surfaces deflect it onto one of two silicon detectors mounted on kovar pads which are cemented to the prisms.

The opaque reticle serves two functions:

1) It limits the energy on each cell at null so that the effects of differential cell drift are minimized.
2) It contributes to linearity of the sensor transfer characteristic.

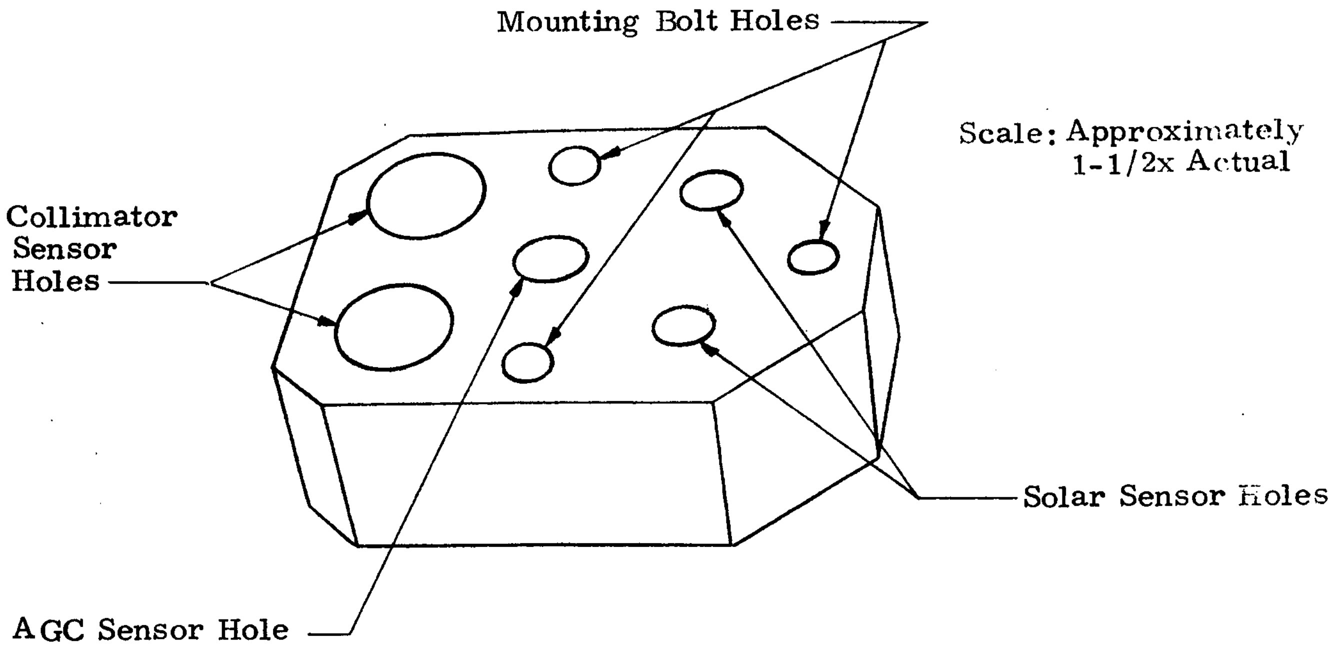

Figure 4-3a - Sensor Block Configuration

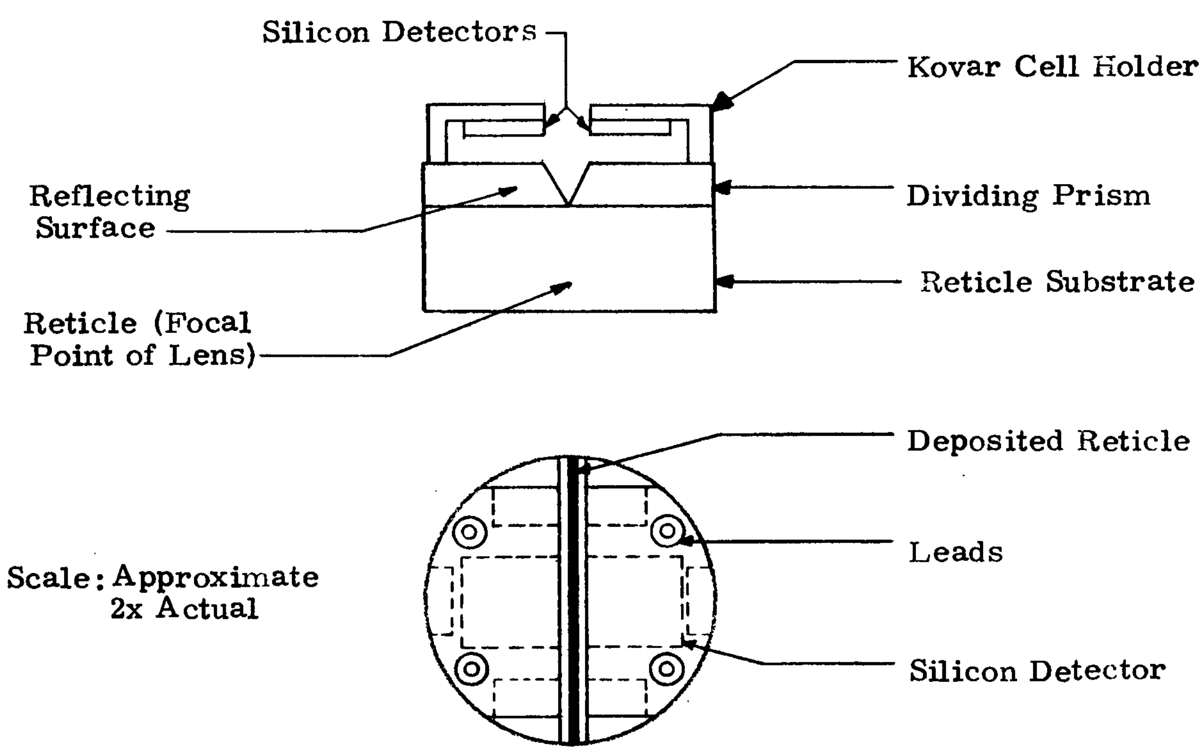

Figure 4-3b - Sensor Reticle Assembly

SECTION 4 - System Design

SUBSECTION - Sensor

SELECTION OF MATERIALS

A comparative analysis of various structural materials revealed that ULE quartz had the best combination of properties for a structural sensor block.

Prior to selecting a sensor block material, it is necessary to define those structural and thermal properties which contribute to dimensional stability. From a purely mechanical standpoint, Young's Modulus, E, is of great interest because those materials having a large modulus are more resistant to bending under a given set of loads. However, when considering vibration environments with given accelerations, a low density material generates smaller loads so that the ratio, density/E, is of interest. Also, it is necessary to check the material yield point to ensure that anticipated stresses will not exceed the elastic limit, resulting in failure or permanent strains. From a thermal standpoint, somewhat more subtle considerations must be made. Obviously a low thermal coefficient of expansion (α) is important, but when materials with similar expansion coefficients are compared it is necessary to consider the effects of a constant heat flux applied to one side which is the most likely in practice. Under these conditions, a thermal gradient inversely proportional to the thermal conductivity, K, would be established, resulting in an angular deflection proportional to the thermal gradient and the coefficient of expansion. Therefore, materials with low α/K ratios are desirable. Other material features which must be considered are machinability, opacity, ease of mounting, and magnetic properties.

To facilitate selection of a sensor block material, Table 4-1 was drawn up, showing potential materials and their physical properties. Although attractive from a machining standpoint, aluminum was ruled out because attaching lenses and sensor assemblies of quartz would be complicated by the large differences in thermal expansion. Invar was also eliminated because of its high density, and undesirable magnetic properties. By using Corning's ULE quartz for the sensor block, thermal problems virtually disappear. With a coefficient of expansion of $2 \times 10^{-8}/°C$ the structure would not change its dimensions appreciably over the maximum environmental temperature range, and resistance to bending caused by thermal gradients is such that a 100°C/inch gradient would be required to produce bending on the order of one arc second. In fact, its only apparent drawback is its transparency which permits optical coupling but this is easily eliminated by coring holes in the block and coating the inside with an opaque epoxy.

	α Coef. Exp. cm cm^{-1} °C^{-1} x10^{-6}	k Conductivity cal cm^{-2} cm °C^{-1} sec^{-1}	ρ Density gm cm^{3}	E Elastic Modulus PSI x 10^{6}	Ys Min. Tensile Yield PSI	Cp Spec. Heat cal gm^{-1}	α/k x 10^{-3} cm sec Cal^{-1}
Aluminum 7075-T6	23.2	0.31	2.80	10.4	72,000	0.21	0.078
Aluminum 6061-T6	23.2	0.40	2.80	10.4	35,000	0.21	0.057
Aluminum 1060-0	23.2	0.56	2.80	10.0	2,500	0.21	0.041
Invar (36% Ni)	1.6	0.025	8.05	20.5	40,000	0.123	.064
Kovar (42.5% Ni)	7.3	0.029	8.12	21.0	40,000	0.12	0.25
Quartz #7940	0.56	0.0032	2.202	10.6	7,200 rupture	0.17	0.18
Quartz ULE #7971	0.02	0.00313	2.213	9.8	6,500 rupture	0.183	0.0064
Pyrex #7740	3.25	0.0027	2.23	9.5	6,100 rupture	0.18	1.2

Table 4-1 Comparison of Physical Properties of Materials for Sensor Construction

SECTION 4 - System Design

SUBSECTION - Sensor

SELECTION OF CEMENTS

Since overall SEAS accuracy is dependent on the stability of glued joints, a series of tests were carried out on four different cements to determine their bonding properties in terms of curing, temperature cycling, and aging.

The basic structural technique employed with the SEAS is that of bonding functional elements such as lenses and detector assemblies to a mechanically stable quartz block. It is essential that these elements not move relative to the block since a 1 arc second error can result from a lateral reticle translation of five microinches. Therefore, a search for a suitable cement was instituted and four were finally selected for extensive testing. Of these, two were epoxy cements and two were optical cements, each formulated and recommended by their manufacturers specifically for the purpose of bonding glass to produce joints of high optical quality. Although the most critical cement joints in the SEAS are not in an optical path, it was felt that the elimination of pigments and fillers from the cements would be advantageous because the same cements could be used where transparency was required, and fillerless cements generally have lower viscosities which permit the formation of thin cement lines. They also absorb less solar energy.

Table 4-2 lists the selected cements which were tested according to a set of carefully developed test procedures which are fully described in Appendix C. A brief description is given below:

1) Two pairs of one inch quartz cubes were cemented together with each cement to form eight "test blocks".
2) One 1" x 2" face on each of the test blocks was polished and silvered.
3) Angular rotation of one cube with respect to another was determined periodically by autocollimation measurements on the silvered surfaces.

Test results are summarized in the curves on Figure 4-4 which shows changes in cube alignment with time. It is interesting to note that all cements exhibited considerable creep for a period of about two weeks before settling down. On the basis of these tests, Hysol 0151 and Summers Lab C-59 appeared to be the most stable, and from these two the Summers Lab C-59 was selected for SEAS, because it is a Mil Spec cement.

Cement	Description
Armstrong #A-271	Two component epoxy for optical use
Hysol #0151	Two component epoxy for optical use
Summers Lab #C-59	Two component polyester resin optical cement
American Optical #805	Single component thermoplastic optical cement

Table 4-2 - List of Cements Tested

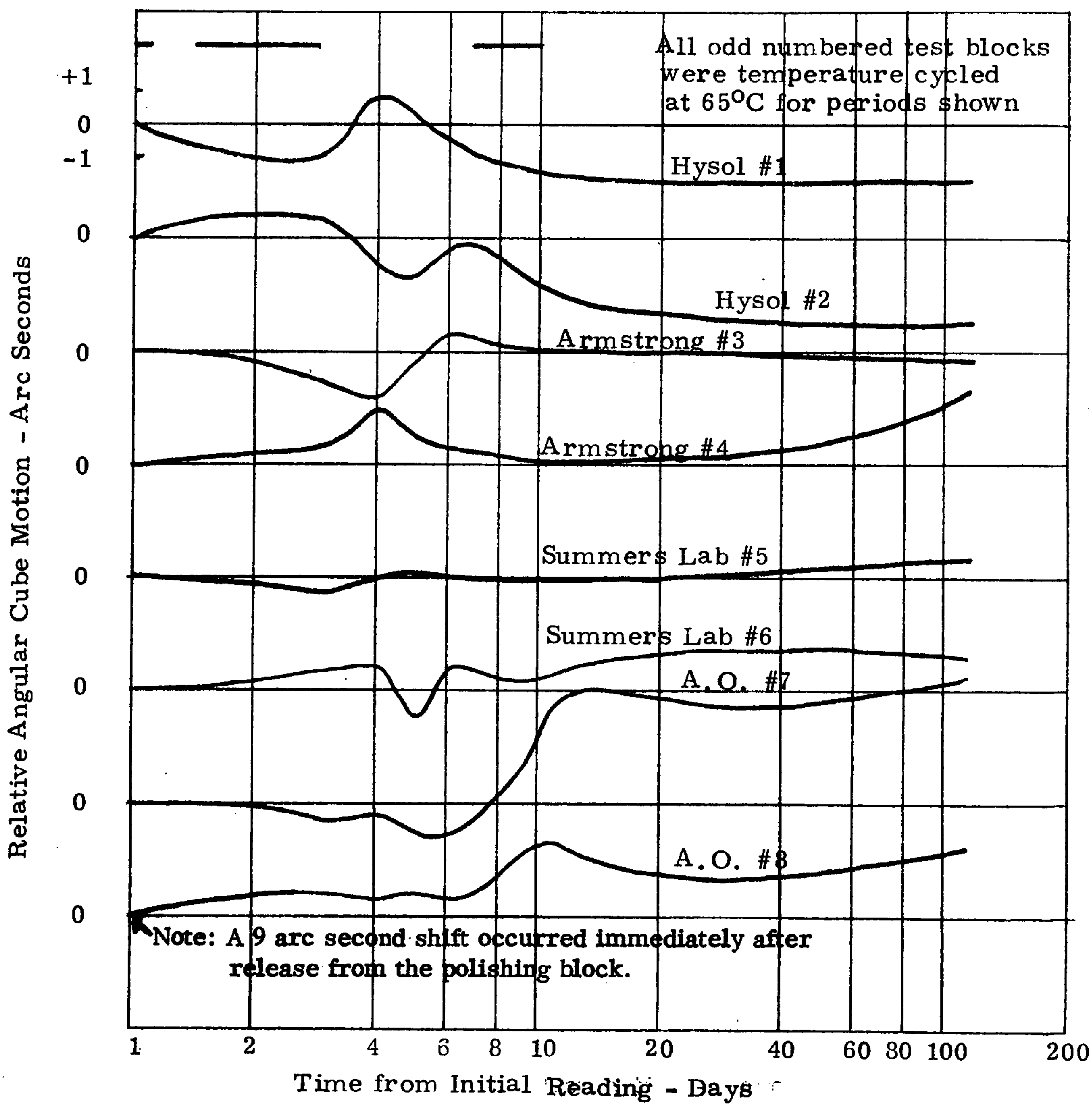

Figure 4-4 - Graph of Cement Stability

SECTION 4 - System Design

SUBSECTION - Sensor

PROPERTIES OF SILICON SOLAR CELLS

Silicon solar cells have been well established as the best detectors for solar aspect sensing but because increased performance capabilities are being sought, a critical review of silicon cell properties was undertaken.

Silicon solar cells are the best detectors for energy-balance solar sensors because of their linear response characteristics combined with simplicity, ruggedness, stability, and low noise. Their major problem is a variation in responsivity with changing temperature, but this can be overcome by proper spectral filtering as demonstrated by the Exotech solar-cell experiment carried out in conjunction with the PASS [3] program.

For practical purposes the equivalent circuit of a silicon solar cell may be considered as a current generator shunted by a silicon junction diode and a high resistance (10^5 ohms at 25°C). There is also a small series resistance in the order of a few ohms which may be neglected at current levels below 10 Ma. The equivalent generator current is a linear function of incident radiation flux and may be accurately determined by measuring the cell's short circuit current, a condition under which no current flows through the diode or shunt resistance. This short circuit current is also a function of incident light wavelength as shown by the spectral response curve in Figure 4-5, as well as a function of temperature. Increased minority carrier lifetime is responsible for a positive temperature coefficient at longer wavelengths while coating effects produce a negative temperature coefficient at shorter wavelengths.

In selecting a pair of silicon cells, two parameters must be considered. First is the absolute stability of cell responsivity which affects sensor gain, and the second is relative stability which affects boresight stability. As a result of the PASS[1] solar cell experiment, it was established that by proper selection of a spectral filter the temperature coefficient of responsivity can be reduced to .01%/°C over a 20°C temperature range. The SEAS spectral filter characteristics are shown in Figure 4-5.

In the case of the collimator sensor, the light from the LED IR source is nearly monochromatic at a wavelength of .92 microns, a spectral region where the cells exhibit a significant positive temperature coefficient. To overcome this problem a LED regulation system was employed which used a silicon cell to monitor LED output. Since this cell was matched to the collimator sensors it was possible to maintain a relatively constant collimator sensor gain.

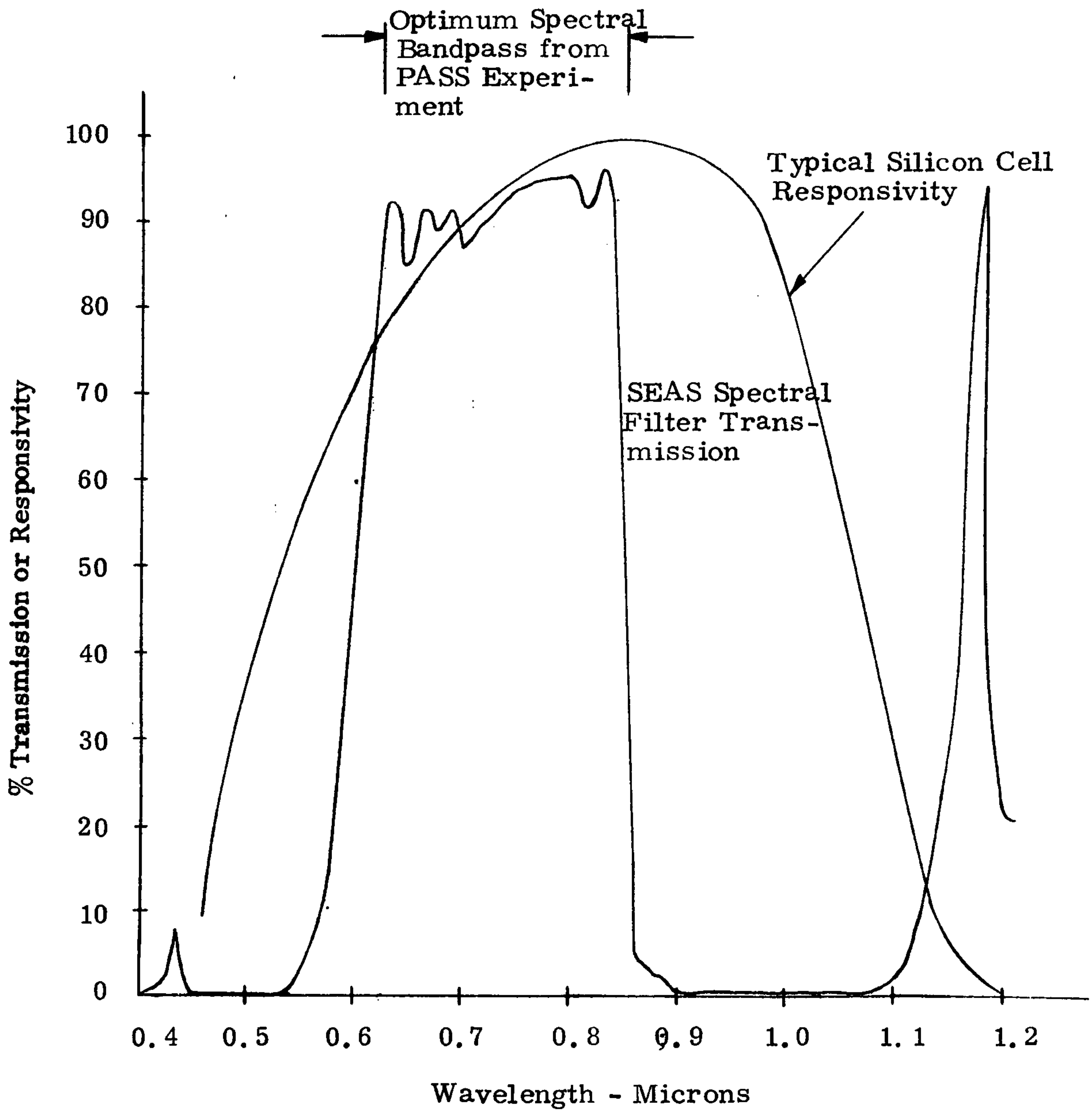

Figure 4-5 - Silicon Solar Cell Responsivity with SEAS Spectral Filter Data

SECTION 4 - System Design

SUBSECTION - Sensor

LINEARIZATION OF SENSOR TRANSFER CHARACTERISTICS

Because linearity is important in offset pointing, methods of controlling the shape of sensor transfer characteristics were investigated.

The shape of a sensor transfer characteristic is primarily dependent on the energy distribution of the source image in the sensor focal plane. If an ideal lens is employed to obtain a perfectly focussed solar image in a sensor's detector plane, the energy distribution is circular so that a non-linear sensor transfer characteristic will be obtained. Prediction of the exact shape is complicated somewhat by the effects of solar limb darkening which is a wavelength dependent phenomenon.

Limited control of transfer characteristics can be obtained under these conditions by adjusting the width of the occulted region (i.e., the reticle width) but a method of changing image energy distribution in the focal plane to control linearity is desirable.

Lens abberations, both spherical and chromatic can affect image energy distribution but their effects cannot readily be studied without a great deal of computation. Also, any departure from spherical lenses will cause fabrication and testing difficulties. In contrast, simple defocussing will produce a blurred image having a more uniform energy distribution, and its effects can be studied on an experimental basis with little difficulty. Following this line of attack, a special test fixture was set up to permit close control of lens to reticle spacing and a series of transfer characteristics were obtained using a tungsten solar simulator. Each curve was fitted with a best straight line, and peak deviations were noted. These results are summarized in Figure 4-6 which shows peak deviation from best fit straight lines (over ranges of ± 15 arc minutes and ± 20 arc minutes) versus location of reticle. With the lens and reticle combination used, it was possible to obtain good linearity over a range of ± 15 arc minutes for several lens to reticle spacings. However, with the reticle located .045 inches in front of the lens focal plane, a clear point of optimum linearity over a ± 20 arc minute range was obtained.

These results were incorporated into the final sensor design and after the lens focal lengths were measured, the final quartz sensor block thickness was specified to give the desired amount of defocussing.

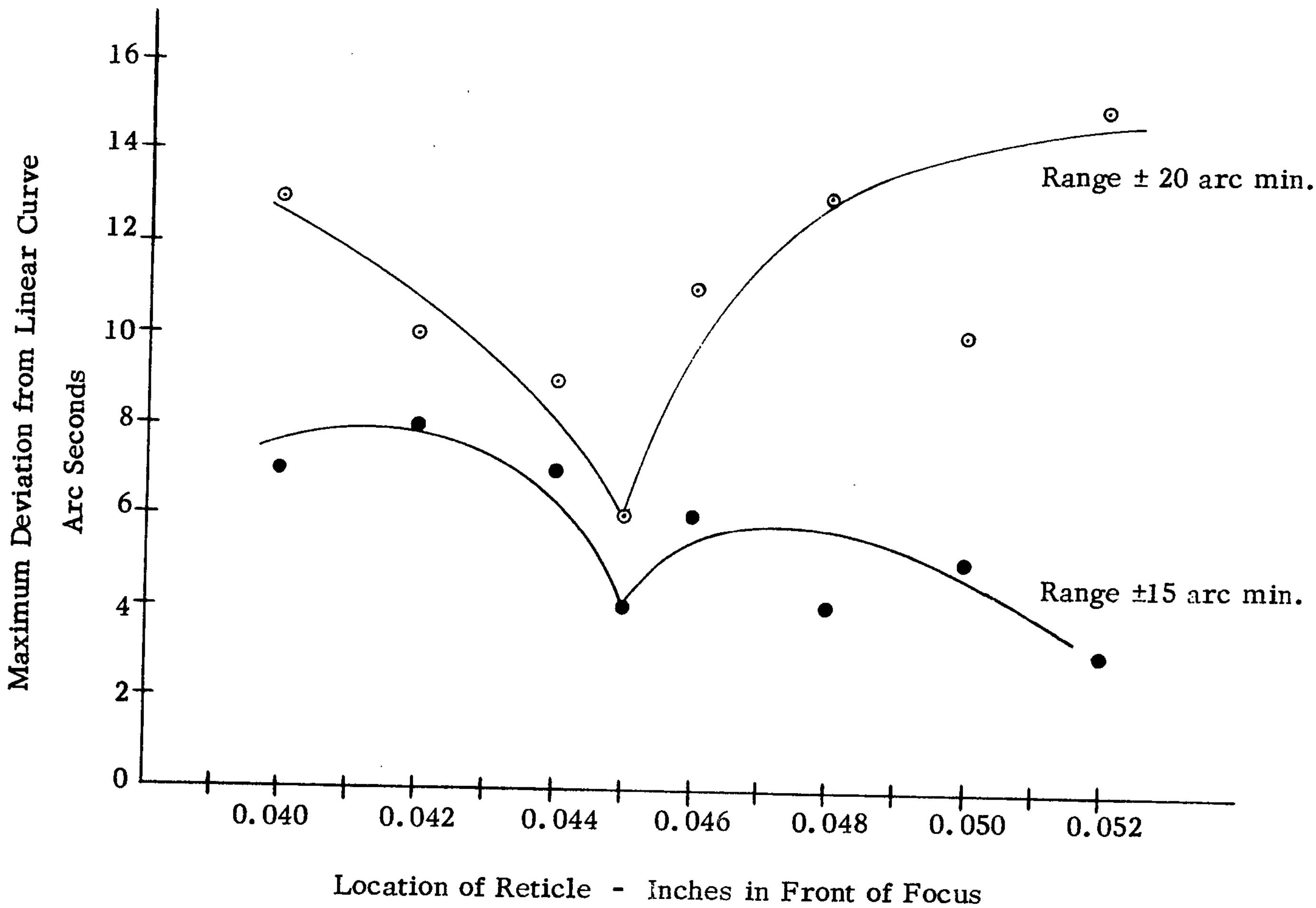

Figure 4-6 - Optimization of Solar Sensor Linearity

SECTION 4 - System Design

SUBSECTION - Sensor

DESCRIPTION OF COMPLETE SENSOR

The complete SEAS employs a variety of components cemented to a monolithic quartz block to form two collimator sensors, two solar sensors and an AGC sensor.

A detailed drawing of the complete SEAS is presented in Figure 4-7. All major SEAS components are illustrated in cross section A-A in which one of the two collimator sensors is shown pointing downward. This sensor's quartz lens, mounted on the lower side of the quartz block has an aperture precisely defined by an annular ring cemented to the lens. The detector assembly is mounted on the upper side of the quartz block. This assembly consists of: a quartz reticle substrate on which a thin-film reticle strip (0.0078 inches wide) is deposited; two dividing prisms which reflect energy onto a pair of silicon cells mounted on kovar pads; and a support ring which surrounds the whole assembly and supports a terminal board.

The solar sensors are similar to the collimator sensors, except for having smaller apertures to limit the incident energy to reasonable levels, and the addition of a 10 arc minute deviation wedge to effect final alignment of the sensor axes. A thin-film spectral filter having a bandpass from approximately 0.6 to 0.8 microns is deposited on the wedge to obtain low solar cell temperature coefficients.

Section B-B, taken through the center of the block shows the AGC sensor. This sensor consists of a single solar cell opposite a quartz lens, upon which a spectral filter similar to that used on the solar sensor, has been deposited.

Section B-B also illustrates the technique used for mounting the quartz sensor support block which is sandwiched between two aluminum end plates. The plates are clamped together by three bolts passing through the block and secured in the lower plate. Washers are used as pads between the quartz block and end plate while Bellville washers under the bolt heads are used to control compression forces.

Coarse alignment of the entire SEAS to its mating surface is maintained through the use of three mounting pads whose bearing surfaces have been polished flat.

The end view (lower left) illustrates the relative sensor positioning on the quartz block.

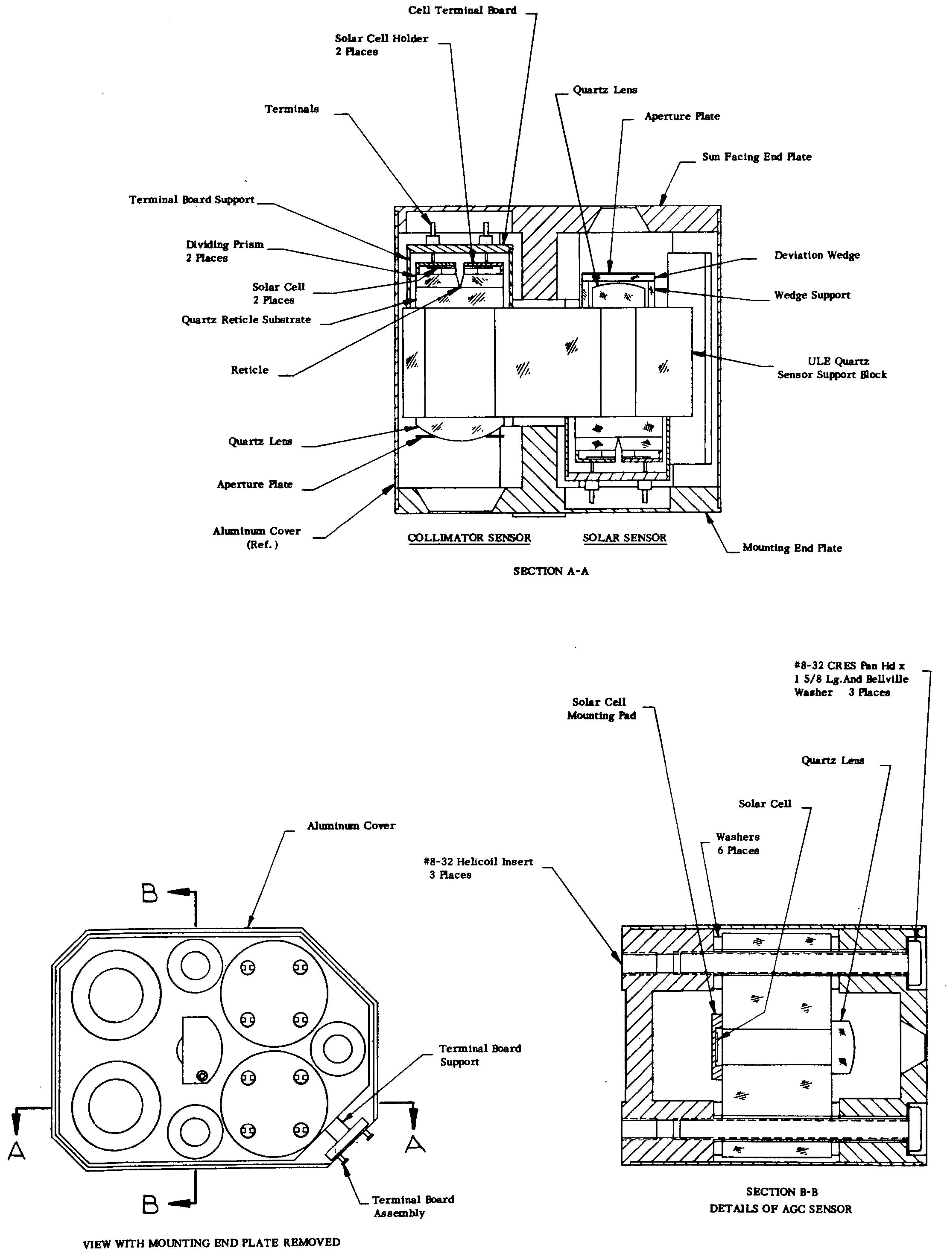

Figure 4-7 SEAS Details

SECTION 4 - System Design

SUBSECTION - Experiment

SELECTION OF EXPERIMENT FOCAL PLANE LIGHT SOURCE

Selection of a solid-state light emitting diode (LED) for the experiment focal plane light source was based on complex considerations.

A preliminary study of light source considerations revealed that, in long focal-length experiments, energy levels at the collimator sensor would be very low. This implied that the source would have to be modulated so that ac amplification of the collimator-sensor signals could be used to render the system insensitive to stray light. Starting from this basis, a set of selection criteria were established taking into account a variety of considerations.

Although source efficiency is important as a performance criterion, a more meaningful evaluation must consider the signal-to-noise ratio obtainable from the collimator sensor amplifier. This is primarily dependent on the chopping frequency since solid-state amplifier, narrow-band noise figures exhibit 1/f characteristics at low frequencies where a tungsten lamp would have to operate. Other selection criteria include reliability, operating life, thermal stability, regulation requirements, and more importantly, compatibility with potential solar experiments. The latter is difficult to define precisely but it was felt that light from a narrow spectral band source could be most easily filtered out of an experiment if interference occurred.

Several potential sources were considered, including the sun, tungsten lamps, and LED's. The first of these ranks high in reliability but it was rejected because of problems associated with chopping. These include complexity of electro-optical and mechanical choppers plus geometrical modulations of the source, arising from mechanical chopping. The tungsten and LED sources were then compared in detail as summarized in Table 4-3.

The LED was finally selected as the source for the reasons listed below:

1) Although the conversion efficiency of tungsten at 2800°K is higher than the LED, the latter can be operated at higher chopper frequencies with more uniform emission characteristics and simpler optics to give potentially lower (by a factor of up to 10) noise equivalent angles per watt of source input power.
2) The LED has longer life than a tungsten lamp whose life can only be increased by a reduction in operating temperature which is accompanied by a reduction in output efficiency.
3) The monochromatic output of the LED is more amendable to control and is less likely to cause experiment interference.

	* LED	TUNGSTEN LAMP
Wavelength Region	Monochromatic .92 μ	Requires Bandpass Filter .6 - .8 μ
Efficiency Usable power/watt	0.5% at 25°C	2% (may be less if a diffuser is used)
Thermal Stability	Output varies about 1%/°C This can be overcome with closed loop control	Output virtually independent of ambient temperature
Maximum Chopping Frequency	>10 K Hz	1-10 Hz
Obtainable Amplifier Narrow-Band Noise Figure	1 db	10-20 db
Life	Output Efficiency is reduced about 3%/1000 hrs	Approximately 1000 hrs
Reliability	Good. (Potentially better than Tungsten Lamp)	Good
Relative S/N per Watt Normalized to Tungsten	2.5 (up to 10 if diffuser is used with Tungsten)	1
Regulation Requirements	Closed Loop	Closed Loop or voltage regulated supply

*Diode Selected - Texas Instruments TIXL03
P-N Planar Gallium Arsenide Diode Light Source
Output is approximately 15 mW at .92 microns with an excitation of 2 amps at 1.5 volts.
A complete specification sheet is included in Appendix B

TABLE 4-3 Comparison Of Light Source Characteristics

SECTION 4 - System Design

SUBSECTION - Experiment

APPLICATION OF FIBER OPTICS TO THE EXPERIMENT FOCAL PLANE ASSEMBLY

Fiber optics were adopted for use with the experiment focal-plane assembly to permit remote location of the LED infrared energy source.

Since preliminary studies of the SEAS system indicated a requirement for a source input power of several watts, a decision was made to locate the source away from the experiment focal plane to prevent undesirable heating of the focal plane assembly, and isolate the relatively high-power, source-excitation signals. Obviously some optical system was required to convey from the source to the focal plane, and it was decided to study the application of fiber optics to this requirement, because of their functional flexibility which would permit the use of almost any shape and number of focal-plane apertures without resorting to complicated optical systems or multiple sources. Optically transmitting fibers consist basically of very thin dielectric cylinders surrounded by another material having a lower refractive index as illustrated in Figure 4-8. Any light ray within the fiber which impinges on the wall at some angle less than the critical angle undergoes total reflection and thus propagates down the fiber. However, if a ray is incident at steeper angles it will not be reflected but will be lost. This implies a limit to the acceptance angle of a fiber which is a function of the refractive indices of the core and surrounding material. The exact relationship is given in Equation 4-1 which relates the various indices of refraction to the maximum fiber acceptance angle, θ_m. A second parameter, commonly used in fiber specifications, is called the numerical aperture (N. A.) which is defined in Equation 4-2.

The fibers adopted for the SEAS program were Corning Glass Works Number 5900 clad fibers having the following specifications:

Fiber diameter	-	.0025 inches
Numerical Aperture	-	.67
Transmission	-	60% at .9μ for a one foot fiber with polished ends

For SEAS applications the fibers were formed into a round bundle containing approximately 13,000 fibers (.25 inch diameter bundle). After cutting to size, the ends were potted in epoxy to permit polishing, and once the exact bundle shape was achieved, heat shrinkable tubing was applied as a protective jacket.

n = refractive index of air
n_o = refractive index of fiber
n_1 = refractive index of surrounding material
θ_m = maximum acceptance angle for ray propagation
N. A. = numerical aperture

$$\theta_{max} = \sin^{-1} \frac{n_o^{\,2} - n_1^{\,2}}{n} \qquad (4\text{-}1)$$

$$\text{N. A.} = n \sin \theta \qquad (4\text{-}2)$$

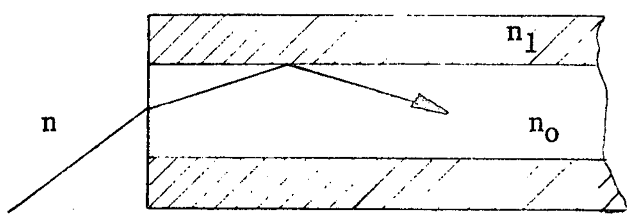

Figure 4-8 Transmitting Fiber

SECTION 4 System Design

SUBSECTION Experiment

DESIGN OF EXPERIMENT FOCAL PLANE ASSEMBLY

Two focal-plane radiation-aperture configurations were considered for the SEAS system, each employing fiber optics to convey infrared energy from a remotely located source to the experiment.

One feature of the fiber optics approach is that IR source energy can be spatially distributed in an arbitrary manner by a suitable arrangement of the fibers (i.e., a round bundle can be fanned out into a narrow strip). Originally it was intended to have a focal-plane aperture in the form of four narrow slits arranged approximately in the form of a square around the experiment aperture to give two axis information. This configuration has the advantage that with an imaging-type collimator sensor, the imaged aperture has a high energy gradient in a direction perpendicular to the slit axis so that great sensitivity is obtained as the image traverses the edges of a sensor reticle whose axis is parallel to the slit. Obviously the dynamic range of such a scheme is limited by the slit width but this is not a problem with a collimator sensor which needs only sufficient range to accommodate sensor or experiment movements in the order of ± 1 arc minute. In practice, however, imperfect focussing and lens abberations in the SEAS tend to smear the image so that performance is somewhat degraded. Obviously, a carefully focussed high-quality lens would eliminate the problem, but fabrication and procurement problems would be incurred.

An alternative to the slit scheme is a simple circular aperture which appears to the collimator sensor as a distant sun. This has the advantage that only a single fiber bundle is required and the same reticle can be employed in all sensors. Such an approach was finally adopted with only a small decrease in gain.

A diagram of the complete focal-plane radiation-source assembly is shown in Figure 4-9. IR energy from the LED is collimated by a small lens, and the resulting beam impinges on one end of a fiber bundle which transmits energy to the focal plane. A small portion of the bundle branches out to supply the LED intensity monitor cell which regulates LED output.

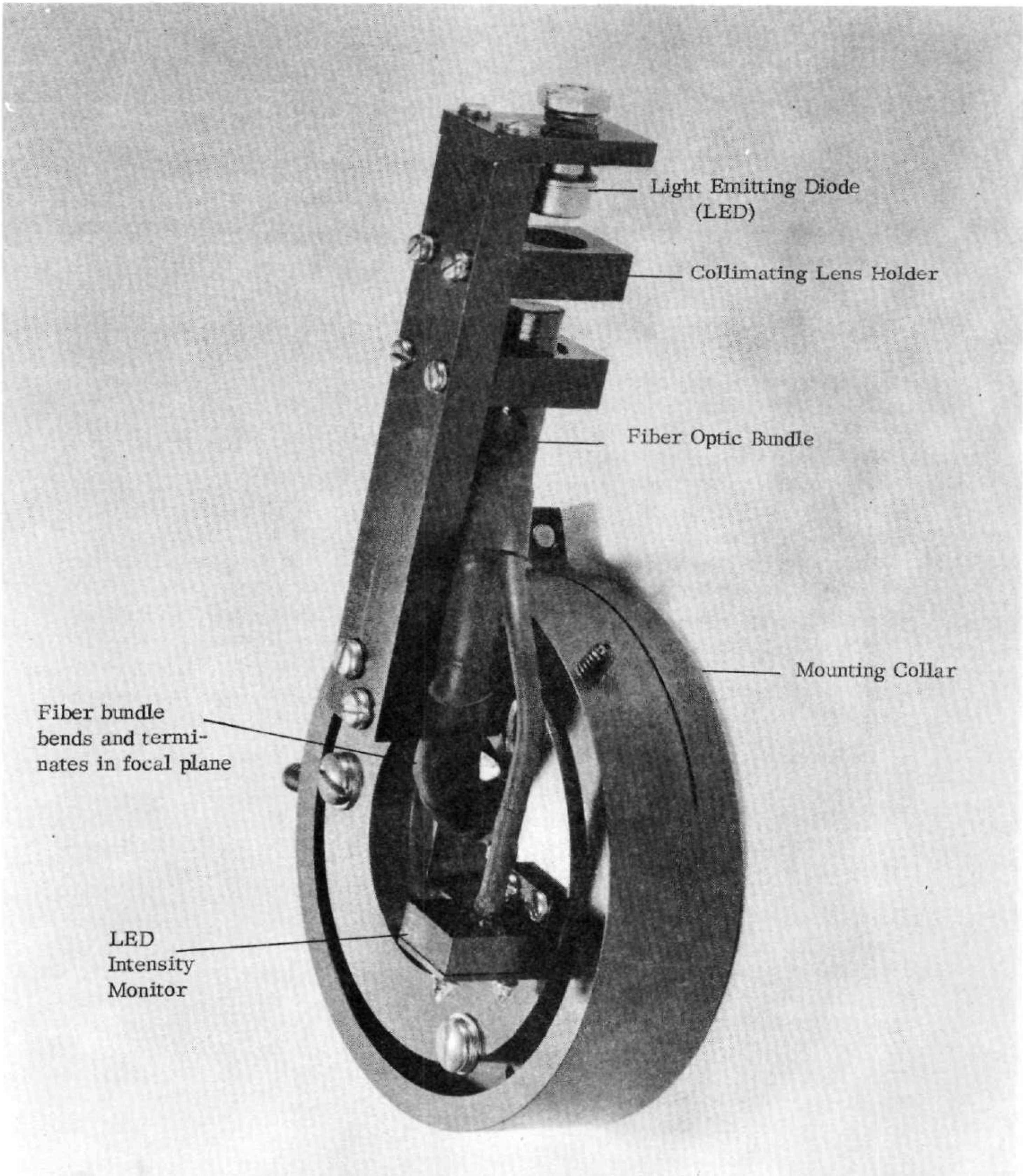

Figure 4-9 Experiment Focal-Plane Assembly

SECTION 4 - System Design

SUBSECTION - Electronics

DEVELOPMENT OF ELECTRONICS SYSTEM

The SEAS electronics system may be described in terms of three specific subsystems: a regulated power supply, a solar sensor amplifier, and a source regulator with associated collimator sensor amplifier.

A complete block diagram of the SEAS electronics is shown in Figure 4-10. All system power is derived from a dc-to-dc converter operating from a 28 to 32 volt dc supply, and highly stable voltage regulators with enough capacity to supply a complete two axis system providing ± 15 vdc and + 15 vdc to all circuits.

As was pointed out in Section 3, DERIVATION OF SYSTEM GOALS, some method of achieving an automatic solar-sensor gain calibration of better than 1% is essential if accurate offset pointing is to be achieved. Exotech has achieved this capability through the design of a sun-sensor AGC scheme outlined in the block diagram. In this approach identical variable-gain amplifiers, A1 and A2, are employed with the solar sensor and an AGC sensor respectively. Each amplifier has a switchable feedback resistor so that the average gain of both can be continuously adjusted between two limits by varying the duty cycle of the switching waveform. The AGC channel is a closed loop control system in which the AGC sensor output is amplifier by A1 and compared with a reference level, V_{Ref}. The resulting error signal is then compared with a high frequency sawtooth waveform, to obtain a variable duty cycle square wave which is fed back to control the gain of A1 and A2.

The modulation frequency employed with the AGC system is 3.0 Khz so that no restrictions are imposed on sensor frequency response, and the only accuracy limitations are the tracking of the variable gain amplifiers and differential responsivity changes between the solar-sensor cells and the AGC cell with temperature.

The lower portion of the block diagram shows the LED drive system in which the LED is supplied through a transformer with a 1 to 2 volt square wave at 1.5 Khz. A portion of the LED energy is transmitted through a fiber bundle to a silicon cell intensity monitor whose amplified output is demodulated and compared with a reference to control the LED output so collimator-sensor gain will remain constant, providing the collimator sensor cells track the LED intensity monitor. The collimator sensor output is amplified and fed to a synchronous demodulator whose dc output is filtered and summed with the solar sensor signal to yield a control signal.

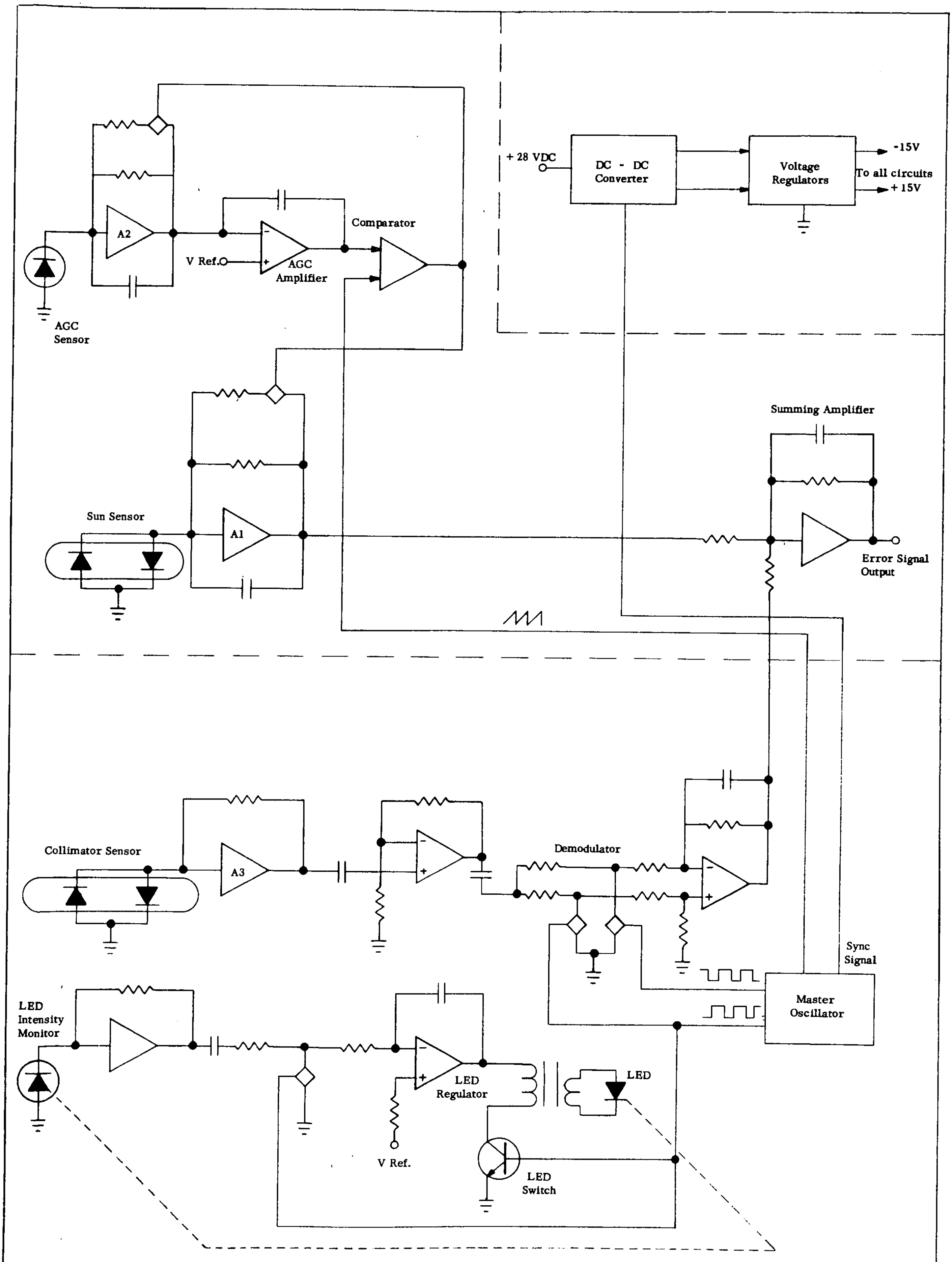

FIGURE 4-10 SEAS ELECTRONICS BLOCK DIAGRAM

SECTION 4 - System Design

SUBSECTION - Electronics

DC TO DC CONVERTER

A blocking oscillator power converter is used to provide ± 21 volts to the voltage regulators from a 28 to 32 volt dc source.

The dc to dc converter is of conventional design utilizing 2N1486 switching transistors in a push-pull blocking oscillator circuit. Dual isolated 21 volt outputs are provided from separate secondary windings driving full-wave diode bridges and single section RC filters. A third winding is used to supply a sync signal for the unijunction oscillator in the demodulator and LED drive circuitry.

This converter is identical to the one used successfully in the PASS (Precision Autocollimating Sun Sensor) system.

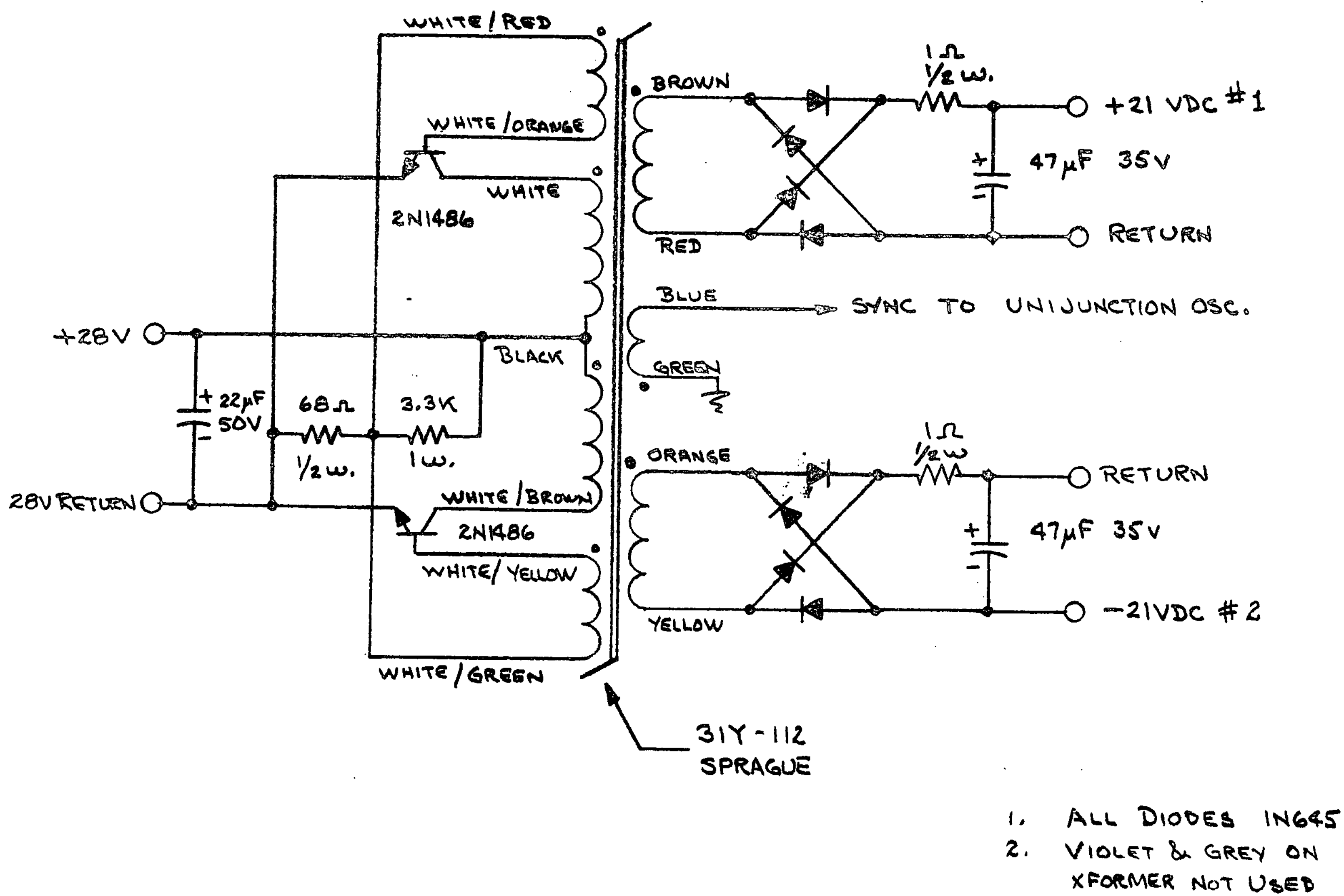

Figure 4-11 - DC to DC Converter

SECTION 4 - System Design

SUBSECTION - Electronics

VOLTAGE REGULATORS

Integrated operational amplifiers have been incorporated into conventional feedback regulator circuitry to provide highly stable ± 15 VDC system power.

The μA709 integrated operational amplifier is ideally suited to supply the stable, high dc gain required for a feedback regulator circuit. Each amplifier drives a pair of cascaded current amplifiers, also included in the feedback loop, to achieve the necessary 400 ma capability. An additional transistor in each regulator, Q3 and Q 6, provides current limiting to avoid undue stress or damage to series regulating transistors in the event of short circuits or overloads during testing. This type of limiter results in a "straight line" limiting characteristic which avoids starting or latch up conditions sometimes encountered in "foldback" circuits. In addition, starting is assured by supplying power to the μA709's from a point ahead of the series regulating transistors, Q1 and Q4.

A voltage reference is supplied by a temperature-compensated zener diode (the IN4566A designated CR1 and CR2 in the + 15 V and - 15V regulators respectively) which has a maximum temperature coefficient at 0.5 ma of 0.005%/°C from -55 to 100°C. This reference zener was selected, aside from its excellent temperature characteristics, for its low operating current. Since the input bias current to the μA709 varies from approximately 350 nA at -20°C to less than 150 nA at 80°C, the zener current of 5×10^5 nA is virtually constant over that temperature range.

The availability of floating, independent 21 volt outputs from the dc to dc converter permits the use of identical, rather than complementary, regulator circuits. This is accomplished by regulating the ground or return line of the -15 VDC supply. Of course, the reference zener diode is referenced to ground in both cases. The high gain of the μA709 (25,000 min.) even after the approximate 3:1 reduction resulting from the voltage sensing divider, provides an output impedance roughly equal to the 1.8 Ω current sense resistor divided by 8,000 or $< 0.2 \times 10^{-4}$ ohms. However, the output impedance of the converter degrades this figure, and actual tests show approximately 0.4 mV change as the load is varied from 200 to 300 ma. A summary of test results appears below:

Characteristic	Test Conditions	Output Variation
Line Regulation	30 ± 2V	± < 1.0 mV
Load Regulation	Δ 100 ma	Δ < 0.5 mV
Temperature Drift	± 45°C	± 0.1%

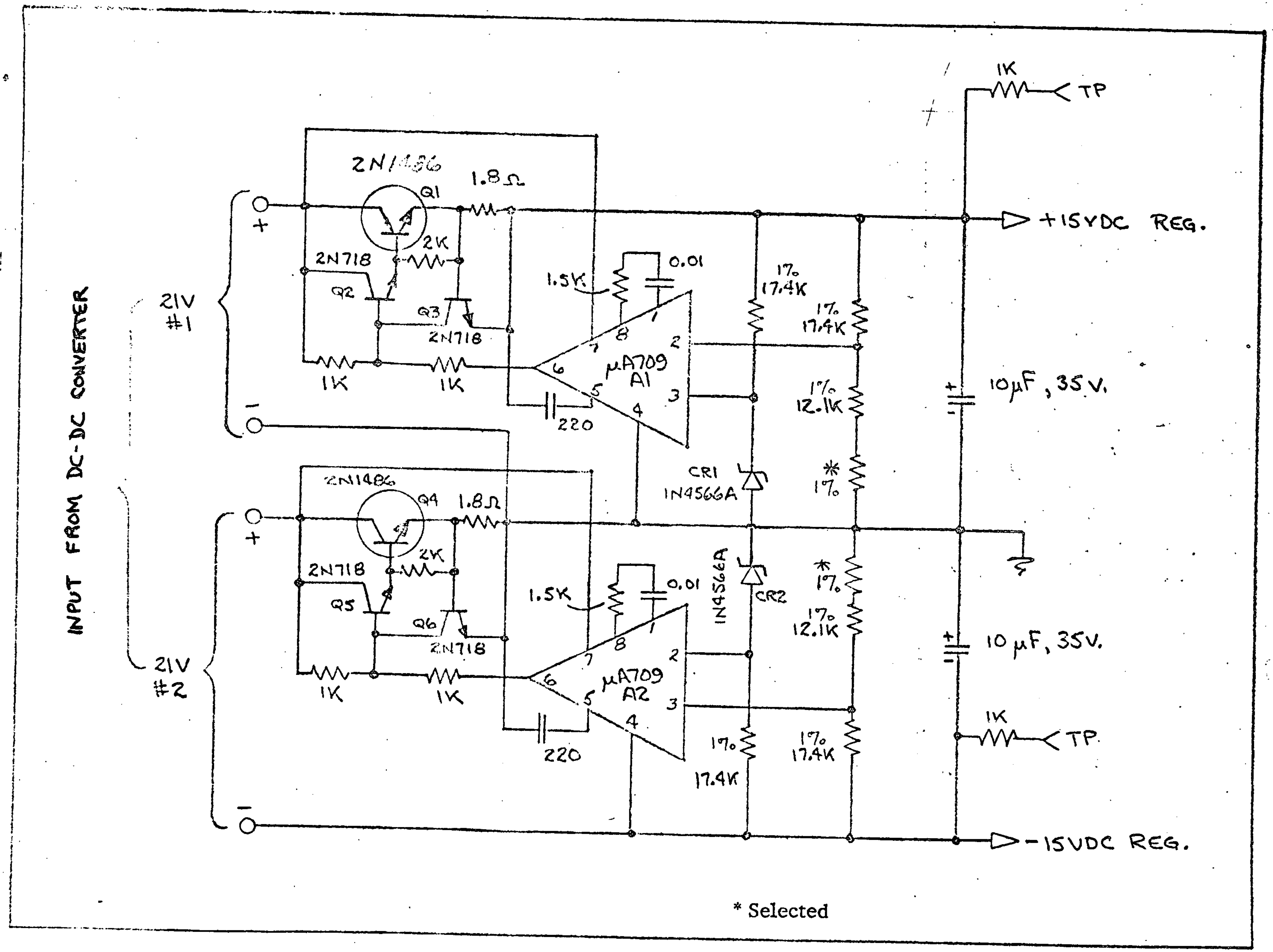

Figure 4-12 - Voltage Regulators

SECTION 4 - System Design

SUBSECTION - Electronics

SUN SENSOR AUTOMATIC GAIN CONTROL (AGC)

The sun sensor AGC provides constant sensor gain despite as much as ± 20% variation in illuminance.

An accurate AGC system removes the requirement for accurate ground calibration of sensor gain. A very precise gain control system can be devised using a scheme similar to that found in pulse width modulators (PWM). A modification frequency is selected at least ten times higher than the desired sensor bandpass (in this case $BW_{sensor} = 15\ H_Z$, and $F_m = 1500\ H_Z$). However, in an AGC application, the modulated width is used to switch in and out a feedback resistor (R 1) in parallel with a fixed feedback resistor (R 2) around an operational amplifier. Thus the gain becomes proportional to R 2 in parallel with R 1 times the pulse "on" duty cycle. Since R 1 is either completely in or out of the circuit, as switched by the field effect transistor (Q 1), gain control is essentially a time function. This is a distinct advantage over systems which use an FET as a variable resistance element in which matching of the slave FET is critical, linearity is poor, and dynamic range is limited. In addition, the PWM-type AGC can readily be trimmed to achieve very precise control by varying the value of R 1 or R 2. Bandpass of the AGC channel can be extremely low since the sun intensity is, of course, not expected to vary rapidly.

The variable pulse width is generated by using a reference amplifier (A 2) and a voltage comparator (A 3), which has a sawtooth reference voltage on its inverting input. The signal from a sun AGC sensor is amplified by control amplifier A 1 whose output is compared with a reference voltage set up by divider R3 and R 4. If V_{out} is smaller (more positive) than V_{ref}, A 2's output will move in a negative direction, causing the sawtooth to be more positive than A2's output for a greater percentage of the pulse period. Since the sawtooth is applied to the inverting input, the output of A3 will be negative, Q 1 will be "off" reducing the amount of feedback and increasing the gain. Initial nominal operating point (e.g. 50% duty cycle) can be achieved by adjusting the reference divider (R 3 and R 4). The PWM waveforms shown clarify the circuit operation. During pulses A, D, and E, gain is too low. Similarly, during B and C, too high.

System tests show less than 0.1% gain change in the slave channel over the entire ± 20% intensity range.

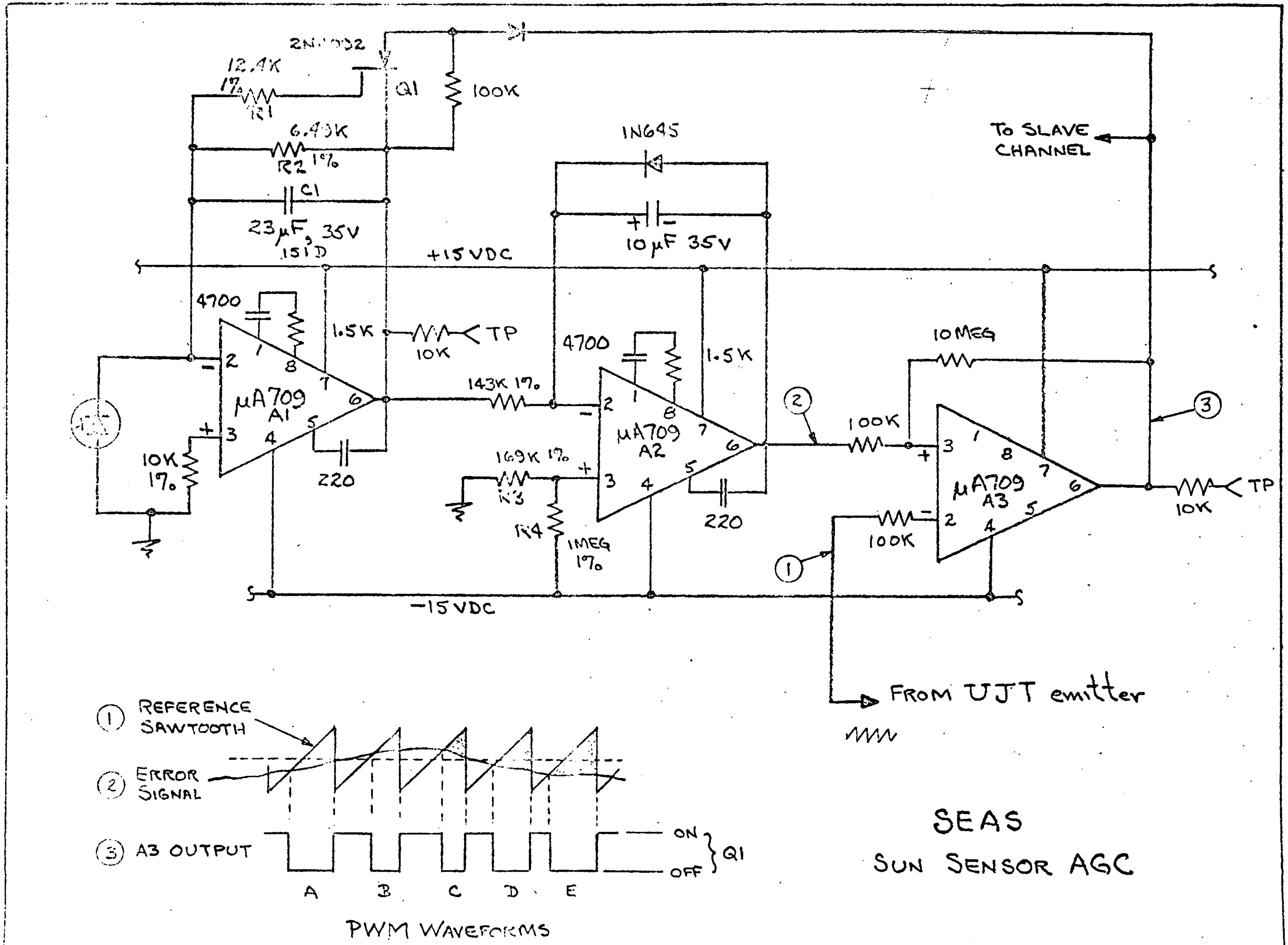

Figure 4-13 - Sun Sensor Automatic Gain Control

SUN SENSOR AMPLIFIER

A matched dual field effect transistor is used as the input stage of a μA709 to achieve excellent dc stability in the sun sensor channel.

Both input current and voltage offsets must be kept extremely low in the sun sensor preamplifier to achieve desired system accuracy. Significant characteristics of the 2N3954 dual FET selected as the input stage for the integrated μA709 are summarized below.

Differential Gate Reverse Current (+125°C)	10 nA max.
Gate-Source Voltage Differential (+25°C)	5 mV max.
Gate-Source Voltage Differential temperature coefficient (-55 to +125°C)	10μV/°C max.
Transconductance Ratio G_{m1}/G_{m2}	0.97 min.to 1.0 max.
Transconductance (V_{DS} = 20V, V_{GS}= 0, f = 1 kHz)	1000 min. 3000 max μmho

The FET is connected as a differential stage with a voltage gain of approximately three,which places sufficient gain ahead of the μA709 to avoid significant summing of drift characteristics of the two devices as would occur if a simple source-follower circuit were employed. The input stage is included in the feedback loop, and the entire circuit becomes a conventional operational amplifier whose input characteristics are those of the 2N3954. Input offset can be precisely balanced out by trimming R1 until no output change occurs as first high, then low source impedances are presented to the amplifier.

The feedback path consists of a fixed resistor (R2) and a second resistor (R3) which is switched in and out at a 3 kHz repetition rate with variable pulse width to control the gain. The FET switch, Q2, is slaved to the AGC drive signal generated in the sun sensor AGC channel. As a result, the relative gain of the sun sensor is identical to that of the AGC preamplifier. To achieve this, the ratio of resistance, R3/R2, must equal the ratio of their counterparts in the AGC circuit although the absolute values need not be the same. Preamplifier output is fed to the output error amplifier, A2, where signals from both the sun sensor and collimator sensor are summed out of phase to provide the system output signal. Potentiometer R4 provides offset capability to permit nulling the system against vehicle or experiment references. A complete system would of course include an additional identical collimator and sun sensor channel for the other axis.

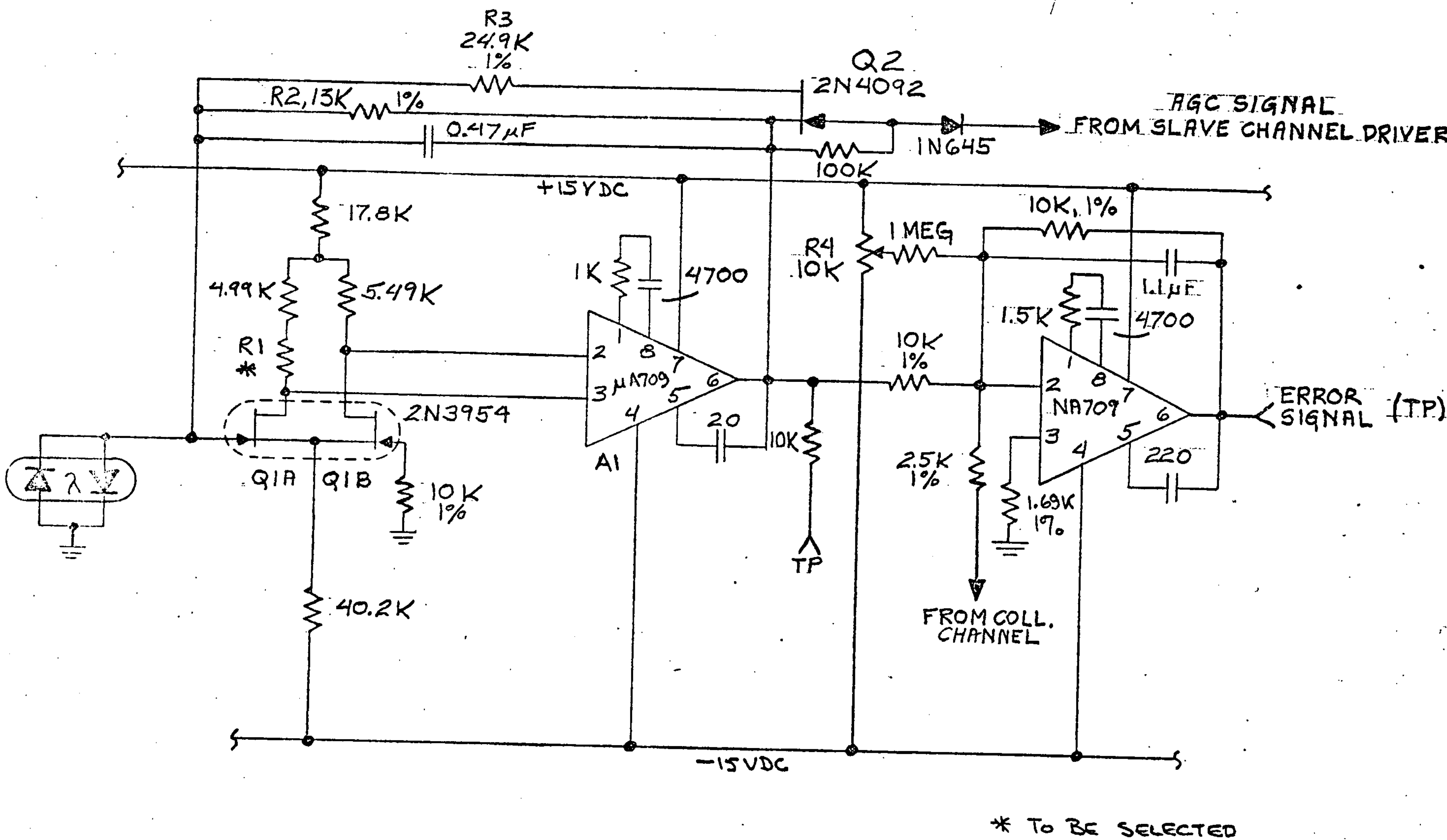

Figure 4-14 - Sun Sensor Amplifier

LIGHT SOURCE REGULATOR

Sensing and regulating the output of the light-emitting-diode (LED) provides stable collimator sensor gain over the required operating temperature.

The TIXL03 LED selected for the collimator light source exhibits a decrease in relative photon intensity of approximately 50% as the ambient temperature is raised from -20°C to + 70°C with constant drive current. In order to obtain a fixed gain, $dI/d\theta$, from the collimator sensor, a feedback regulator is required. A silicon cell, the LED intensity monitor, is positioned to see some of the emitted light. The signal from this sensor is amplified in preamplifier A1, demodulated by the half-wave synchronous switch Q1, and compared with a reference voltage (established by the resistive divider R1 and R2) at the input to regulating amplifier A2. This amplifier drives a cascaded complementary current gain stage (Q2, Q3, Q4) to obtain the necessary output power capability. The 1.5 kHz drive signal for the LED is obtained by applying a unidirectional pulse to the primary of transfer T1 by pulsing current-sinking switch Q5. The transformer achieves reasonable efficiency by matching the low impedance LED to the higher impedance regulator circuit.

Control of the drive current is accomplished as the essentially dc level of the regulator output (emitter of Q3) is varied, thus varying the peak voltage available to impress across the primary of T1. For example, as the light output from the LED diminishes with increasing temperature, the demodulated signal output across C1 becomes smaller (more negative) with respect to the positive reference for A2. Since A2 is inverting, the output of Q3 rises, providing more LED drive.

A demodulator is used at the output of the preamp (A1), rather than an asynchronous detector, to avoid offsets resulting from scattered sunlight falling on the LED intensity monitor sensor.

A small current sampling resistor, R4, is inserted in the LED return line to facilitate checkout and calibration. Also, a filter made up of R3 and C5 isolates the relatively high transformer-drive current pulses from the regulated ± 15 volt busses.

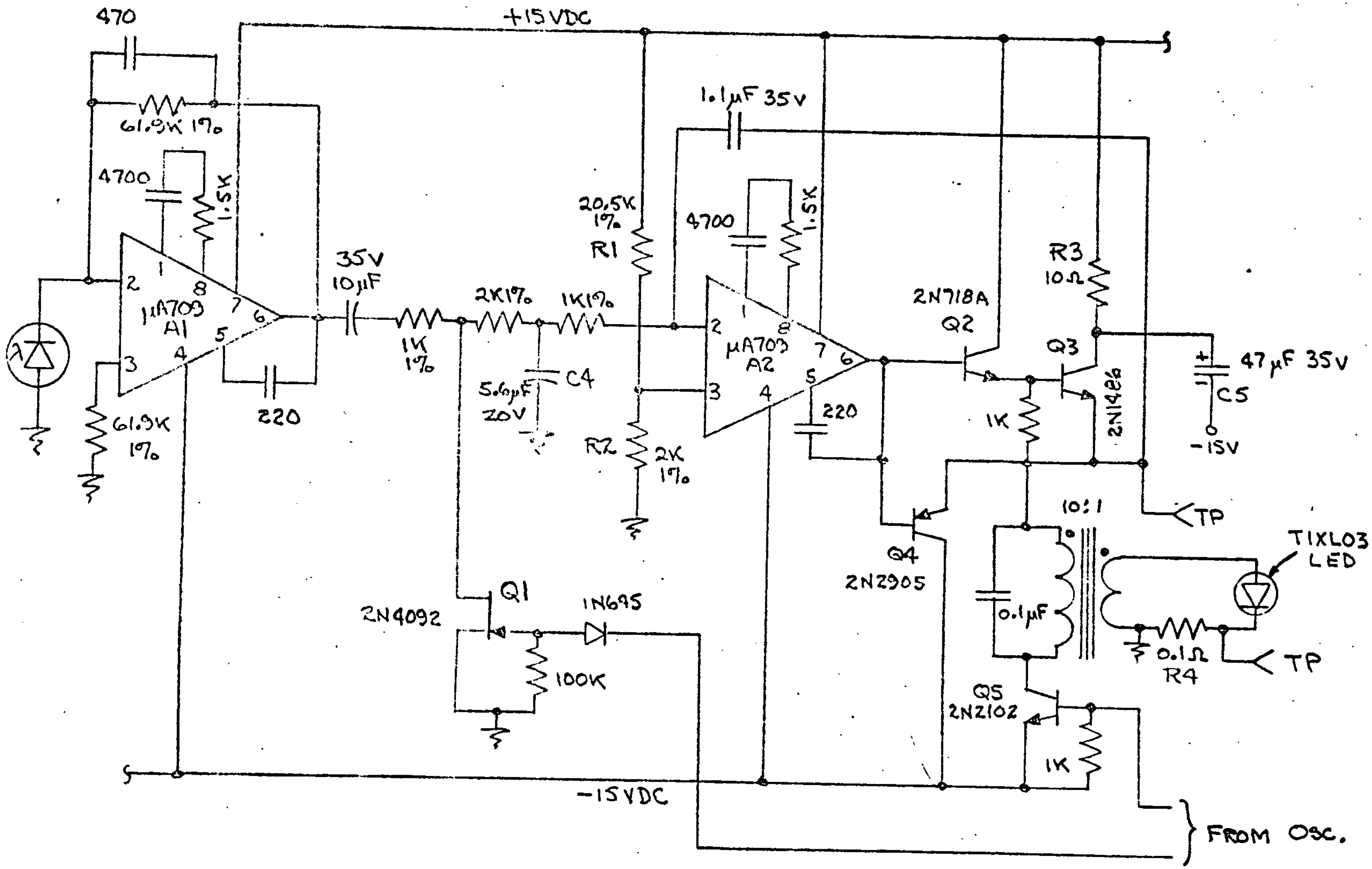

Figure 4-15 - Light Source Regulator

COLLIMATOR SENSOR CHANNEL

Integrated operational amplifiers perform the functions of preamplifier, ac amplifier, and synchronous full-wave demodulator in a high gain 1.5 kHz collimator sensor channel.

The collimator sensor channel processes the signal received from the light emitting diode prior to summing it with the error signal from the sun sensor amplifier. Since high dc stability is not required in the ac-coupled preamplifier, a μA709 is employed without an FET input stage such as is used in the sun sensor circuit. A differential input connection is used to achieve common mode noise rejection. The output is fed to a voltage-follower-type ac amplifier whose high input impedance permits the use of a relatively small coupling capacitor, C3. This amplifier has a gain equal to (R7+R8)/R7 and is non-inverting.

The ac amplifier drives a full-wave synchronous demodulator employing only one operational amplifier by applying alternately switched signals to both the inverting and non-inverting inputs. Field effect transistor choppers are used in the shunt connection to avoid inserting gate bias current into the signal path. The two 2N4092 N-channel switch FET's (Q1 and Q2) have a low ON resistance, <50 ohms, which is small compared to the 10 K ohm signal impedance at the switch point. This large ratio renders negligible the effect of small changes in R_{on} with temperature. Bandwidth of the demodulator is approximately 0.2 Hz which is ample for the collimator channel. Drive for the synchronous switches is provided by a conventional flip-flop driven from a unijunction transistor relaxation oscillator. This oscillator receives a sync signal from the 6 kHz dc to dc converter to prevent beating of the two oscillators. The unijunction divides that signal by two to obtain a 3 kHz output. Of course, the flip-flop further divides the frequency by two, thus supplying 1.5 kHz drive for the demodulators and through emitter-follower Q3, to the LED drive circuitry. Also, the 3 kHz sawtooth waveform appearing at the emitter of the unijunction is used as the reference signal for the sun sensor AGC comparator.

Overall gain of the autocollimator sensor channel is approximately 7.6×10^7 volts/amp.

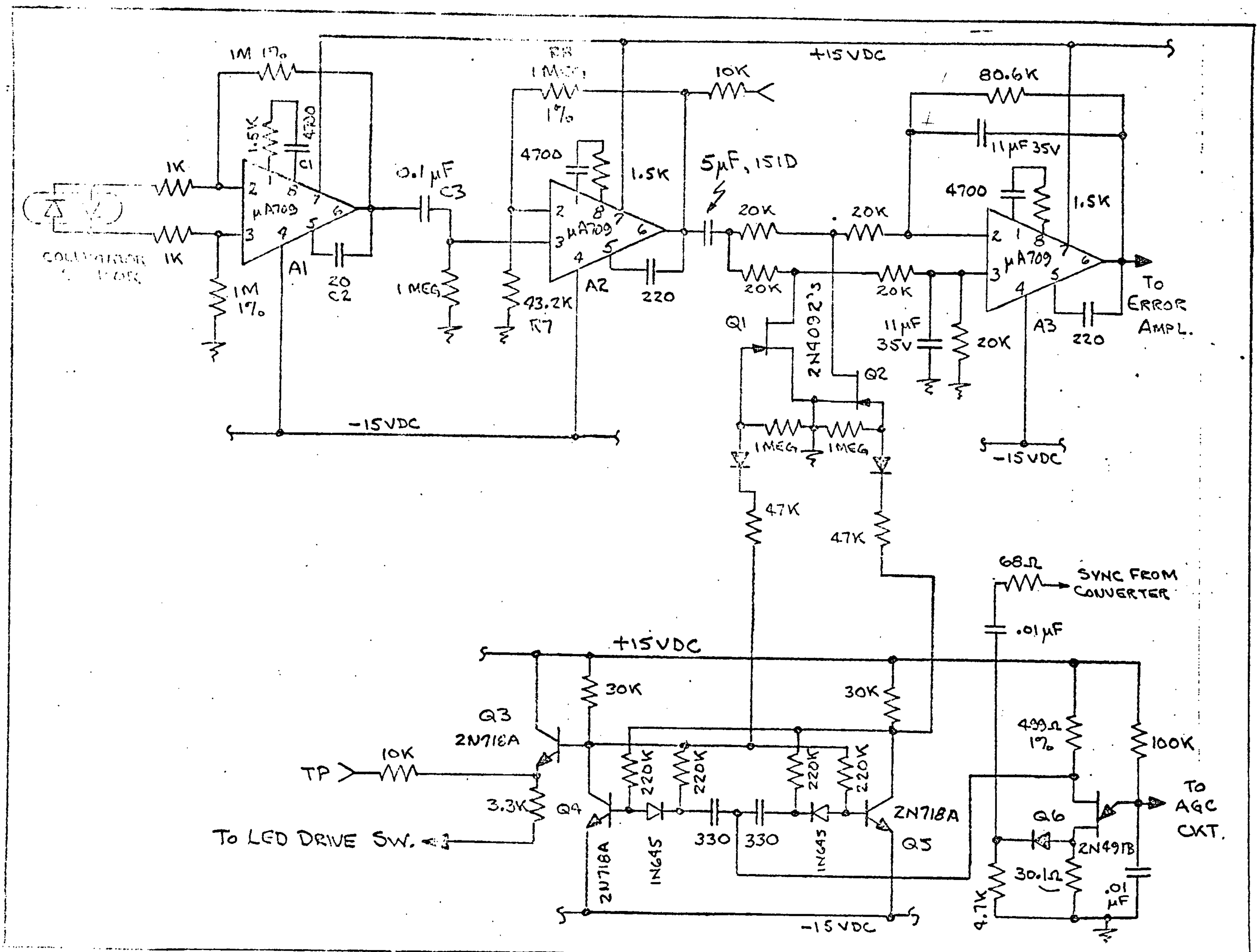

Figure 4-16 - Collimator Sensor Channel

SECTION 5 - Test Program

SUBSECTION - Test Description

SUMMARY OF TEST PROGRAM GOALS

The purpose of the SEAS test program was to establish performance characteristics of the SEAS system which could be evaluated in terms of the original performance goals.

In order to evaluate the SEAS in terms of its performance goals, a comprehensive series of tests were performed to isolate and characterize critical parameters. A complete list of performance parameters and the subsystems which influence them are given in Table 5-1.

Basic Solar Sensor Characteristics - By measuring the solar sensor and collimator-sensor transfer characteristics, it is possible to determine the following:

1. Dynamic Range
2. Linearity

Thermal tests at null can be used to determine null stability.

Automatic Gain Control Performance - The automatic gain control system is primarily responsible for establishing solar-sensor gain stability so that all aspects of the system must be checked including sensor and electronics performance.

LED Infrared Source Characteristics - Since the LED intensity controls collimator-sensor gain, the overall performance of this system must be checked. In addition, the properties of the fiber bundle and stray IR energy levels should be determined to gauge its influence on potential experiments.

Performance Parameter	Subsystems Which Influence Parameter
Null Stability	Solar Sensor null stability Collimator Sensor null stability Preamplifier stability
Dynamic Range	Solar Sensor (Transfer Characteristic) Collimator Sensor (Transfer Characteristic)
Linearity	Solar Sensor (Transfer Characteristic) Collimator Sensor (Transfer Characteristic)
Gain Accuracy	AGC Subsystem including AGC Detector and Electronics. IR source regulator
Radiation Source	Fiber bundle and Optical System

TABLE 5-1 Summary of Performance Parameters And Subsystems Which Affect Them

SECTION 5 - Test Program

SUBSECTION - Test Description

OUTLINE OF OPTICAL TEST SET UP AND FACILITIES

A complex optical test facility including an experiment telescope, a solar simulator, an autocollimator, a theodolite, precision turntables and miscellaneous optical components were required to align and test the SEAS system.

Figure 5-1 is a photograph of the SEAS test set-up showing the optical components assembled on a granite slab.

One of the primary requirements for testing the SEAS system was a simulated solar experiment. This requirement was fulfilled adequately by one of the early SPARCS performance-payload experiments which consisted of a specially designed Questar telescope having a focal length of approximately one meter. It was provided with a reticle inscribed on a quartz substrate in the focal plane which was used as a pointing reference.

The solar simulator employed for these tests was an Exotech Model 5T which uses a 2800°Kelvin, tungsten source whose image is projected on a precisely machined aperture at the focus of a collimating system. The aperture diameter is such that a disc subtending 32 arc minutes is observed when looking into the simulator. To facilitate testing, the simulator beam was reflected off a flat mirror attached to a precision lever mechanism so that angular motion of the solar image alone could be obtained.

For most tests, the SEAS was mounted on a turntable to permit angular motion of the sensor with respect to both the sun and the experiment. Actual angular changes were measured by autocollimating from a flat mirror mounted on the turntable.

A camera behind the experiment focal plane was used to photograph the telescope's solar image in some alignment tests.

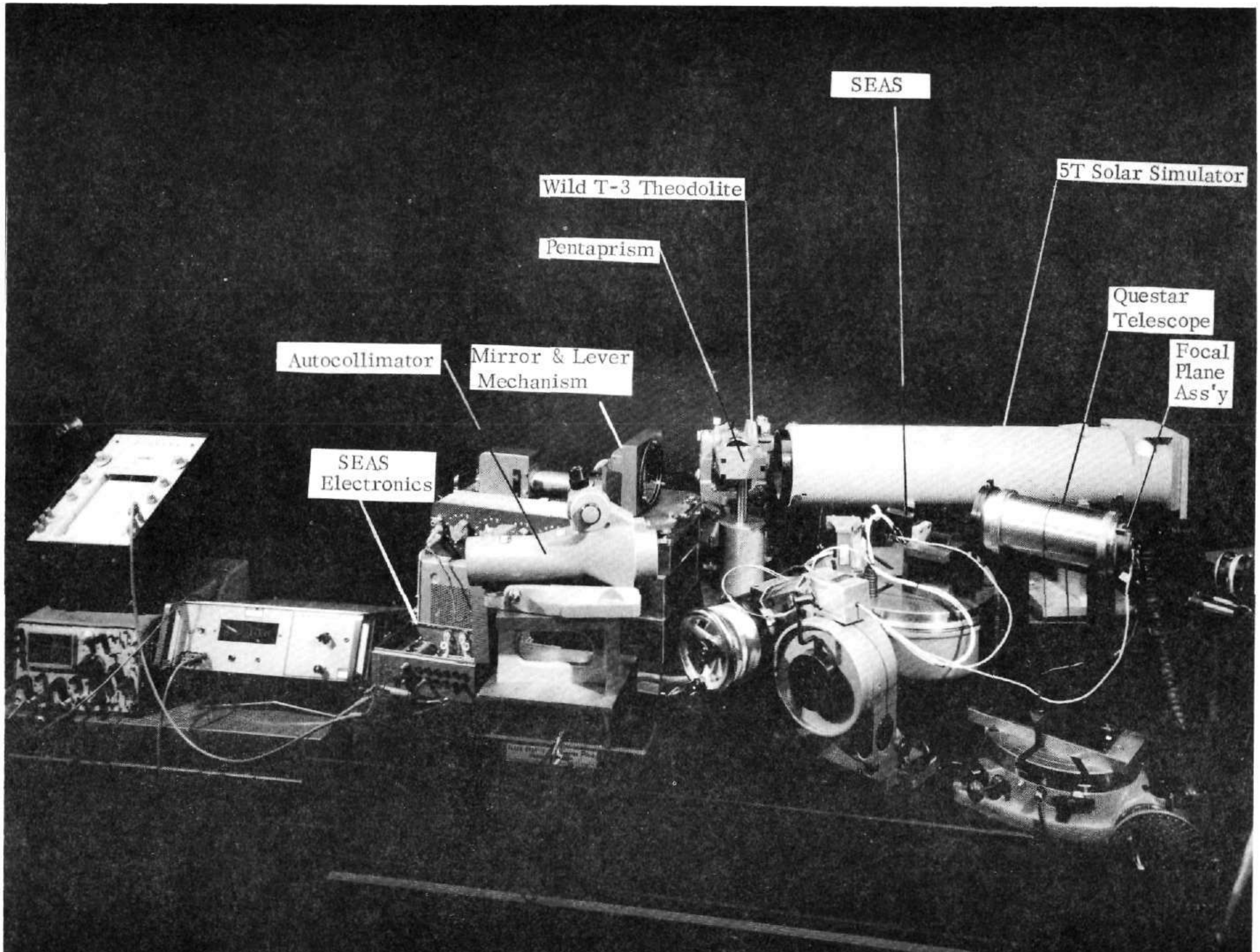

Figure 5-1 SEAS Test Set Up

SECTION 5 - Test Program

SUBSECTION - Test Description

OUTLINE OF THE SEAS TEST PROGRAM

The SEAS test program was begun with a series of electronic system tests to establish the influence of electronics on subsequent optical system tests.

Since a wide variety of system parameters had to be characterized, a test program was carefully devised to permit the determination of individual parameters isolated from other effects which would tend to obscure basic data. For example, it is essential to know that apparent sensor drift during a temperature test is due to the sensor alone, and not due to an electronic drift which could be caused by changing detector impedance if a large input offset voltage was present in the sensor preamplifier. A first step in this direction was an exhaustive series of electronics tests to define all important parameters of this system, particularly those which affect the sensor-electronics interface. A complete list of measured parameters is given below:

Electronics System

1. Preamplifier performance
   - (a) Input offset current and voltage
   - (b) Temperature coefficient of input offsets from -20°C to + 70°C
   - (c) Equivalent input noise characteristics

2. Solar Sensor AGC performance
   - (a) Tracking of AGC Solar Sensor amplifiers with changing inputs (± 20%)
   - (b) Thermal stability

3. LED Regulator performance
   - (a) Thermal stability

4. Power Supply Regulator performance
   - (a) Line regulation
   - (b) Load regulation
   - (c) Thermal stability
   - (d) Power consumption

Sensor

1. Sensor transfer characteristics
   (a) Solar sensor transfer curves
   (b) Collimator sensor transfer curves

2. Sensor operating performance
   (a) Tracking of sensor signals as the SEAS is rotated in front of the experiment
   (b) Dynamic thermal null stability
   (c) Thermal cycling stability
   (d) Correction of experiment misalignments due to thermal gradients

3. Infrared Source Performance
   (a) Stray radiation levels
   (b) Collimator sensor sensitivity

2

SECTION 5 - Test Program

SUBSECTION - Test Results

ELECTRONICS SYSTEM TEST RESULTS

A series of electronics system tests were carried out to establish electronics performance levels.

Preamplifier Performance

Sun Sensor Preamp:	Input offset current	10 nA	
	Input offset voltage	<0. 5 mV	
Temperature Coefficients: (Measured at output of summing amplifier)	-20 to 70°C	Sun Sensor Channel .0007 arc sec/°C	
		Collimator Sensor Channel .01 arc sec/°C	
Combined Noise Characteristics:	Equivalent noise angle .4 arc seconds peak to peak (see record)		

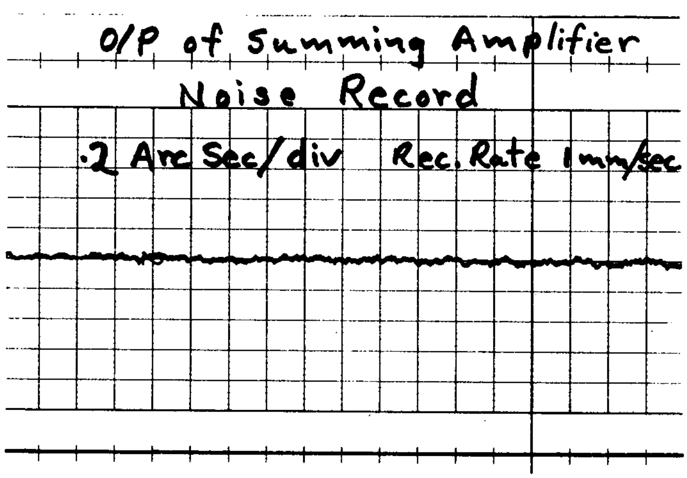

Note: Further improvements in noise performance are possible through the adoption of a low noise preamplifier and improved optical coupling of the LED to the focal plane IR aperture.

Solar Sensor AGC Performance

Gain Tracking: 0.1% over a gain range of ± 20%

Equivalent Temperature Drift -20 to 70°C: .01% total

LED Regulator Performance

The best results were obtained during preliminary tests with PASS cells when an overall temperature coefficient of .02%/°C was obtained. The SEAS cells were not as well matched at .92 microns but the preliminary tests demonstrated what could be achieved.

Power Supply Regulator Performance

Characteristic	Test Conditions	Output Variation
Line Regulation	30 ± 2V	± <1.0 mV
Load Regulation	Δ100 ma	Δ<0.5 mV
Temperature Drift	± 45°C	± 0.1%
Power Consumption	LED Full On	300 Ma @ 30V
Estimated Power Consumption for two axis electronics		400 Ma @ 30V

SECTION 5 - Test Program

SUBSECTION - Test Results

SOLAR SENSOR TRANSFER CHARACTERISTICS

A solar aspect sensor transfer characteristic was obtained which had a maximum deviation from linearity of ± 1.6% over ± 16 arc minute dynamic range.

Two types of solar-sensor transfer curves were obtained. The first was a wide range curve obtained by rotating the sensor turntable in front of the solar simulator over a range of ± 15 degress from null. The curve obtained (Figure 5-2a) is typical of imaging type sensors, having a high gain near null followed by a broad range of high constant output which falls off at angles of 6 to 8 degrees. The large dip occurring at approximately 1.8 degrees is due to a mask on the detector cell which can be easily eliminated in future SEAS. However, for this initial program the region of primary interest was within ± 20 minutes of null, so a second transfer curve of great precision was obtained over this range by reflecting the simulator beam off a flat mirror which could be accurately rotated over a small angular range to give an apparent solar vector shift. The device used for this purpose was an Opto Mechanisms "Micro Positioner" which employs a micrometer - type lead screw to deflect a precision lever mechanism attached to a five inch diameter flat mirror. A deflection accuracy of better than one arc second was obtained.

The actual transfer curve obtained over a ± 20 arc minute range was extremely linear so that the only meaningful method of presentation was to compute a best fit straight line from the data, and then plot a high resolution deviation curve as shown in Figure 5-2b.

Of primary interest is transfer curve linearity, which affects the ability of the collimator sensor and solar sensor to track one another. Deviations from linearity may be easily computed from the slope of the deviation curve, where the steepest slope over a ± 16 arc minute range is S_1 having a slope of approximately 1 sec/minute or 1.6 %. At larger deflections up to ± 20 arc minutes the slopes increase, indicating a deviation from linearity of about 5%.

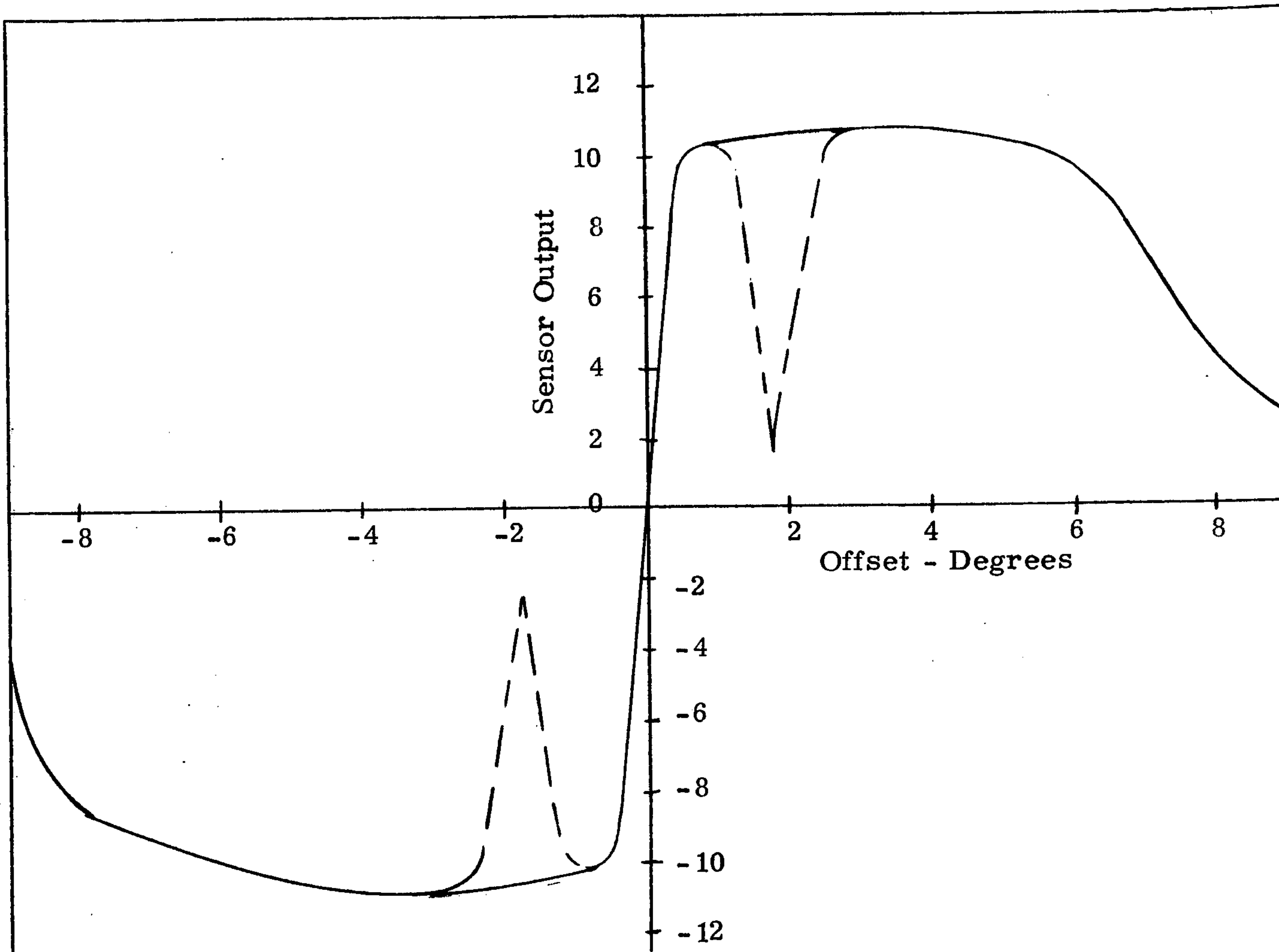

Figure 5-2a - Solar Aspect Sensor Transfer Characteristic

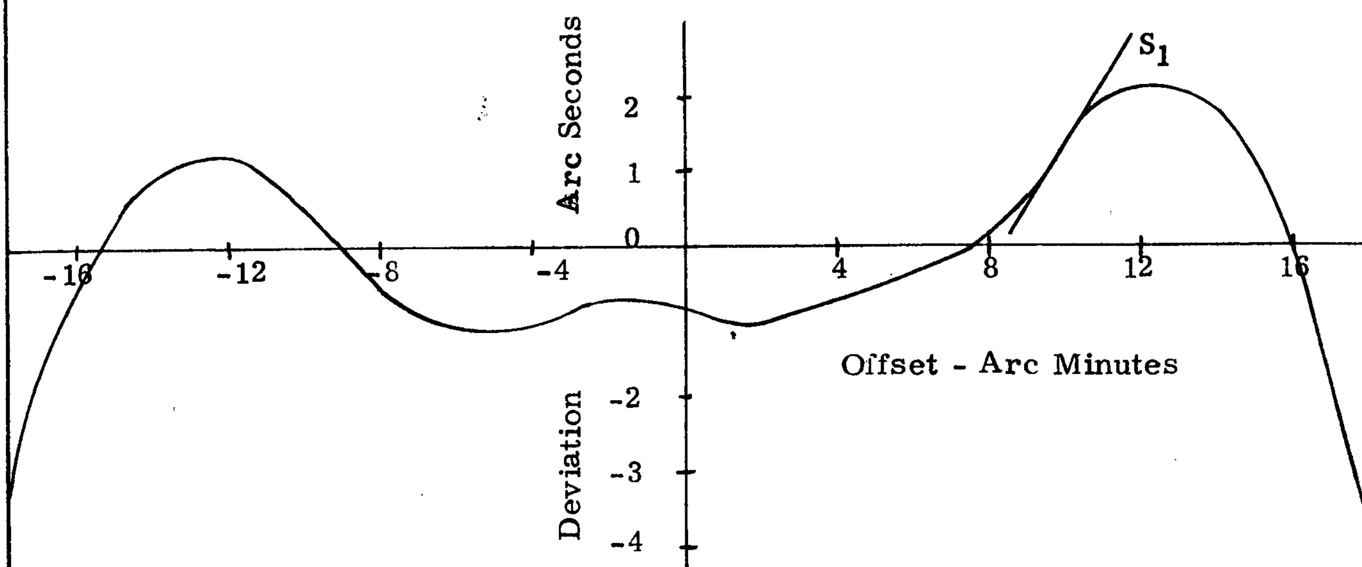

Figure 5-2b - Deviation of Transfer Curve From Best-Fit Straight Line

SECTION 5 - Test Program

SUBSECTION - Test Results

COLLIMATOR-SENSOR TRANSFER CHARACTERISTICS

A collimator-sensor transfer characteristic was obtained which had a linearity of ± 1% over a ± 1 arc minute range, and was capable of tracking the solar sensor transfer curve to better than one arc second over a ± 2 arc minute range.

A collimator sensor transfer characteristic covering ± 5 arc minutes was obtained by rotating the sensor in front of the experiment which remained rigidly fixed on the granite test surface. Angular measurements were made with a Davidson D638 autocollimator. As in the case of the solar sensor, a very linear curve was obtained, so a straight line was fitted to the data, and a deviation curve was drawn as shown in Figure 5-3a. Its basic shape is similar to that of the solar-sensor deviation curve. The extra dip on the left-hand hump is probably due to an intensity variation in the focal plane radiation aperture.

Maximum departure from linearity is about ± 1.3% in the ± 1 arc minute range, while 4% variations were noticed at larger offsets. However, sensor/experiment movements should be restricted to the ± 1 arc minute range.

In order to check overall solar-sensor/collimator-sensor tracking as the sensor moves in front of the experiment, a test was performed which involved rotating the sensor with the solar simulator and focal plane source operating. Ideally there should be no output change, and,as illustrated in Figure 5-3b, it was limited to less than one arc second over a ± 2 arc minute deviation range.

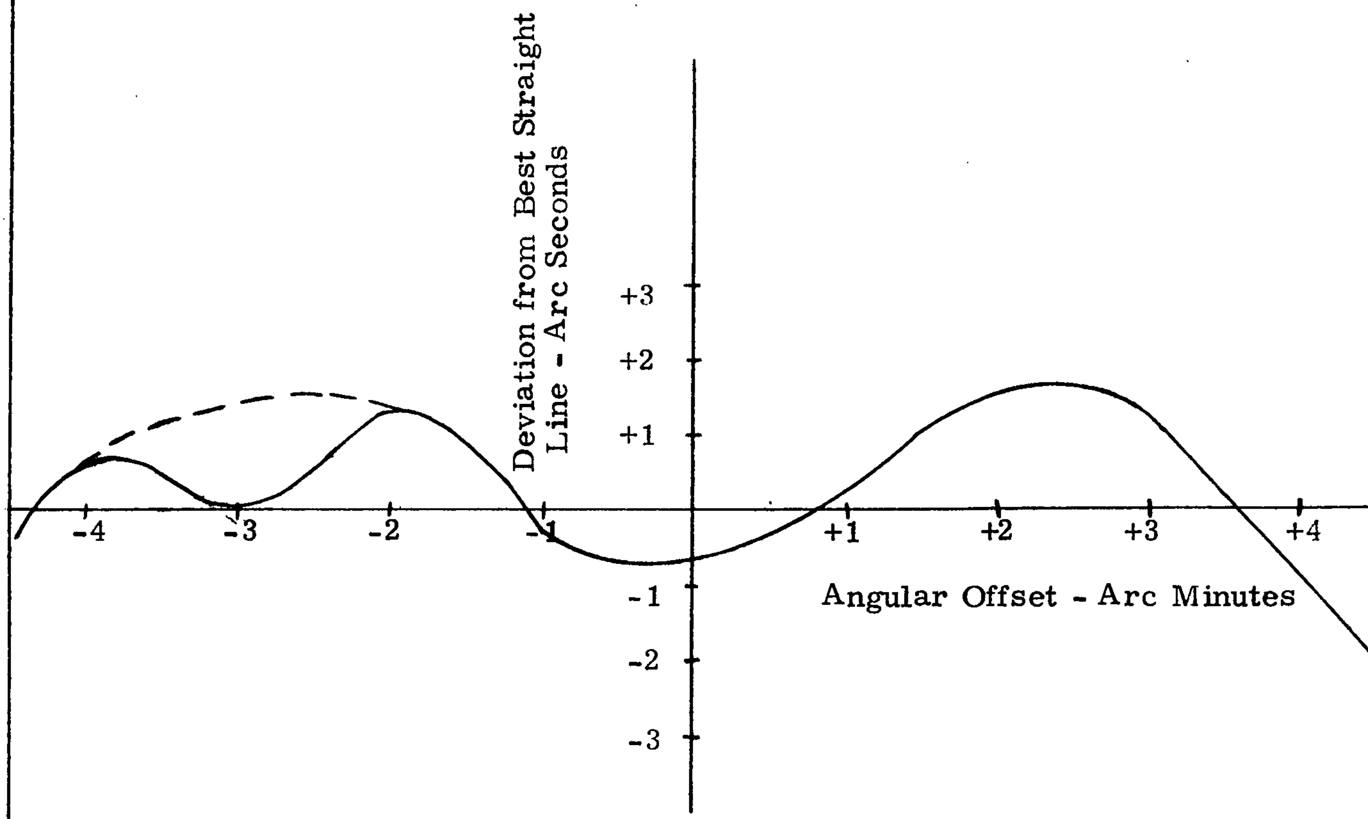

Figure 5-3a - Collimator-Sensor Deviation Curve

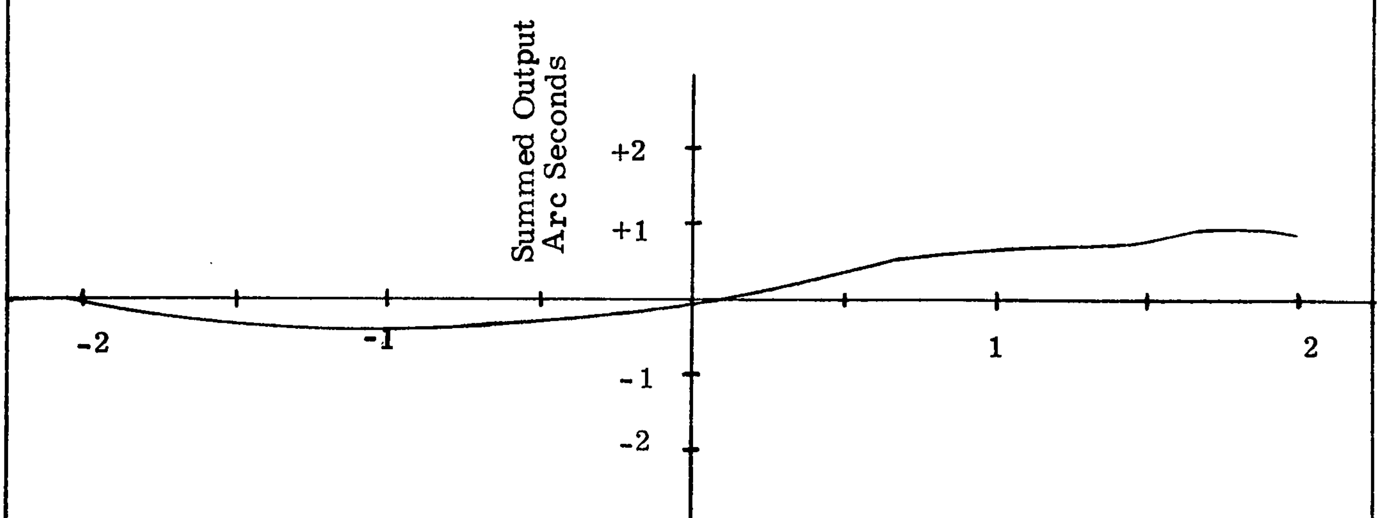

Figure 5-3b - Solar Sensor/Collimator Sensor Tracking

SECTION 5 - Test Program

SUBSECTION - Test Results

VARIATION OF RESPONSIVITY IN THE COLLIMATOR SENSOR SILICON CELLS

An unexpected change in collimator sensor output as the solar simulator was turned on or off was discovered to be caused by a change in silicon cell responsivity with ambient light. See Appendix D for the results of an investigation of this effect.

During the test program an unexpected phenomenon manifested itself in the form of a variation in the incremental responsivity of the collimator sensor cells. This was first noticed as a shift in the collimator sensor output when the solar simulator was turned on or off, and subsequent tests confirmed that reflected sunlight falling on the collimator cells caused a differential change in responsivity to the chopped infrared from the experiment aperture. Subsequently, a series of experiments was carried out in which a single silicon cell was illuminated by very low-level chopped (1.5 KHz) infrared from a LED source. The sensor output at 1.5 KHz was monitored on a harmonic analyzer tuned to the chopping frequency while the ambient light level was increased by changing the aperture in the solar simulator, which was also flooding the cell. As the ambient light level increased, the silicon cell output at 1.5 KHz was observed to increase even though the LED output was constant.

The results are summarized in Figure 5-4 which shows the change in incremental responsivity of the silicon cell with ambient light. Apparently this was not a frequency or spectral dependent phenomenon since an incremental change in illumination produced by turning a small pilot lamp on and off resulted in an increasing change in output as the ambient light was increased.

The most obvious effect of this phenomenon would be a shift in collimator sensor output between ground and space sun conditions. This shift would occur if unequal amounts of reflected or scattered sunlight fell on the collimator sensor cells causing a differential change in responsivity. Presumably this effect could be reduced by placing a narrow band spectral filter in front of the sensor which would reduce solar illumination but not the IR from the focal plane aperture.

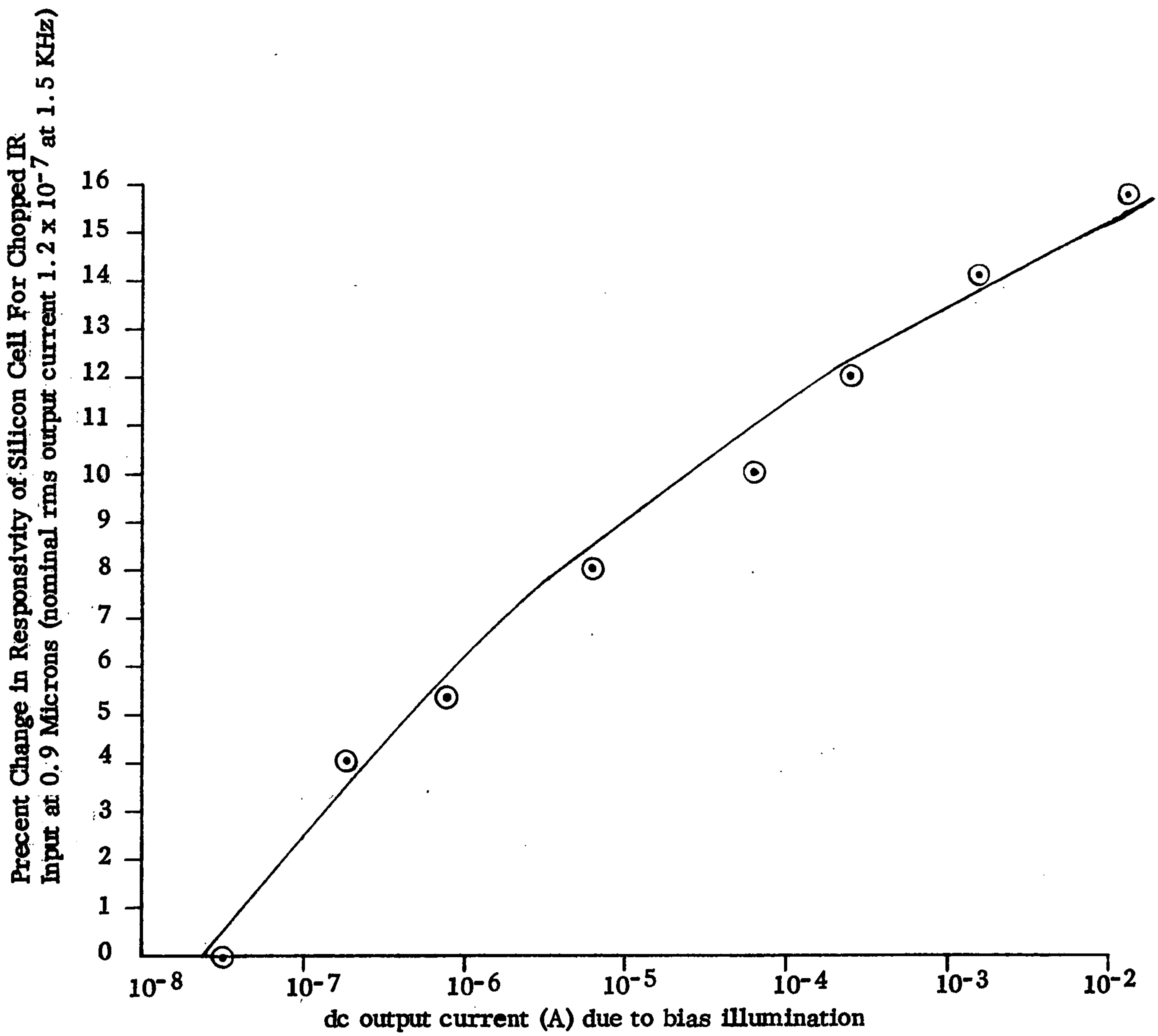

Figure 5-4 Variation In Responsivity of Silicon Photovoltaic Cell With Bias Illumination

SECTION 6 - Conclusions

SUBSECTION - Test Results

SUMMARY OF TEST RESULTS

A summary of test results indicates that performance levels of the SEAS closely approach or exceed the design goals.

A summary of performance levels for the SEAS system is given below. For most parameters worst case errors were calculated from observed thermal coefficients for an assumed temperature change of ± 20°C.

Note: All thermal stabilities are based on a ± 20°C change from a Nominal 25°C

	Observed or Estimated Performance	Performance Goals From Page 10
Null Stability		
Solar Sensor Optical/Mech. Null Stability	± 0.5 * sec	
Solar Sensor Elect. Equivalent Null Stability	± 0.014 sec	
Collimator Sensor Optical/Mech. Null Stability	± 0.5 * sec	
Collimator Sensor Elect. Equivalent Null Stability	± 0.20 sec	
Combined Null Stability	± 1.21 sec	< 2 sec
Dynamic Range		
Dynamic Range of Solar Sensor	> 20 min	
Dynamic Range of Collimator Sensor	> 5 min	>2 min
Linearity		
Solar Sensor Deviation from Linearity over ± 16 min Range	1.6%	1%
Collimator Sensor Deviation from Linearity	1.3%	1%
Worst Case Combined Deviation	2.9%	
Worst Case Error for 1 min Sensor Shift $\frac{2.9 \times 60}{100}$ =	1.74 sec	

* These values were estimated since thermal tests were not completed.

	Observed or Estimated Performance	Performance Goals From Page 10
Gain Accuracy		
Solar Sensor Calibration Error (Estimated)	± 0.5 sec	
Solar Sensor Combined AGC & Cell Stability	± 0.2%	.1%
Solar Sensor Offset error At Limb $\frac{.2}{100} \times 1000$	2 sec	
Collimator Sensor Calibration Error (Estimated)	± 0.5 sec	
Collimator Sensor Gain Stability	0.8%	
Collimator Sensor Error for 1 min shift $\frac{.8}{100} \times 60$	± 0.48 sec	
Worst Case Error ± .5 ± 2 ± .5 ± .48 =	± 3.48 sec	

Combined worst case error for limb pointing

Null Stability Error	-	1.21 sec
Linearity Stability Error	-	1.74 sec
Gain Stability Error	-	3.48 sec
		6.43 sec

It may be seen that performance appears adequate for solar limb pointing and for feature pointing provided accurate roll control is maintained.

SECTION 6 - CONCLUSIONS

SUBSECTION - Recommendations

RECOMMENDATIONS FOR FURTHER INVESTIGATION

The success of the SEAS investigation proves that the concept is feasible and should be employed in a flight mission.

Because the earth's orbit is slightly elliptical with an eccentricity of .01673 the solar radius vector varies periodically on an annual basis. This results in small changes in the solar constant, and apparent sun diameter. The intensity variations are not particularly important because the solar-sensor AGC system compensates for variations of this type, and its effect is to keep the peak sensor output constant regardless of solar intensity. However, in an imaging type sensor the transfer-characteristic gain is proportional to the ratio of peak output to dynamic range, the latter being a function of apparent source diameter which, in the case of the sun, varies as shown in Figure 6-1. This effect can be overcome by suitable gain compensation taking into account the time of year, but the required compensation can only be found by extensive testing with various size suns in a solar simulator or by computer analysis. The latter approach is complicated by the fact that the sensor image is slightly defocussed.

Another area of concern is the effect of solar limb darkening which is a wavelength dependent phenomenon. Its immediate effect is to alter the energy density distribution in the sensor focal plane which in turn affects sensor gain. The problem may not be severe because of the defocussed sensor but it is felt that some analysis and testing in this area are warranted to improve confidence in sensor performance.

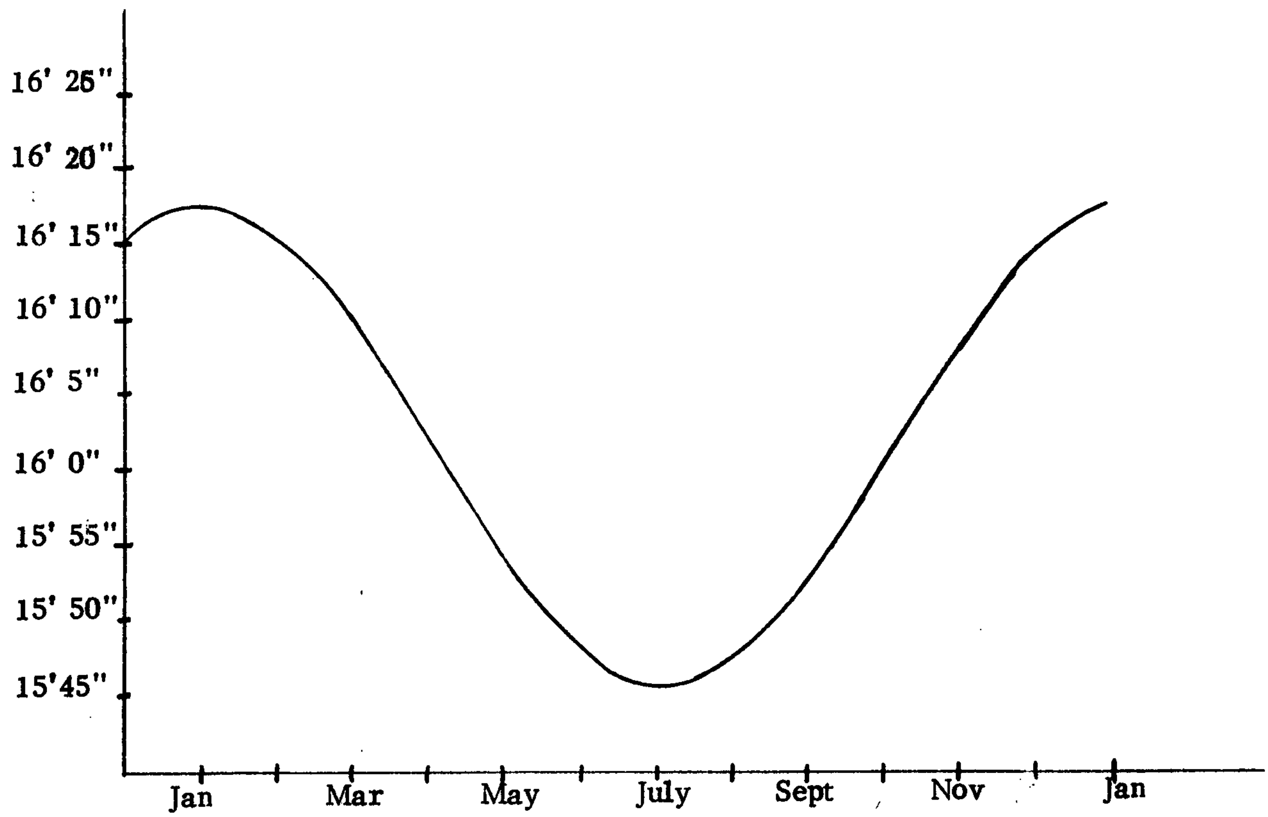

Figure 6-1 Variation In Apparent Solar Radius

Appendix A - Photographs

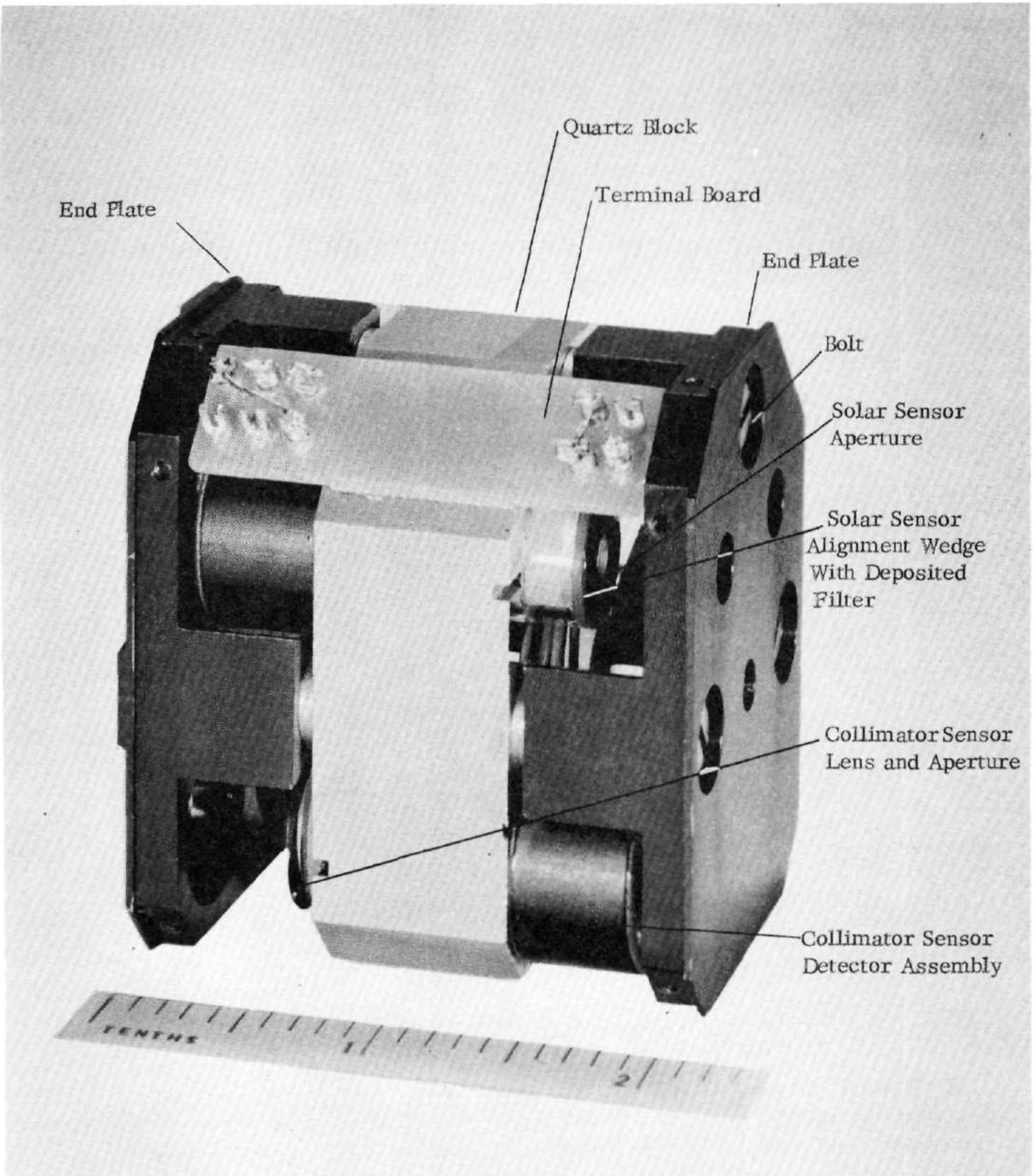

Figure A-1 SEAS With Cover Removed

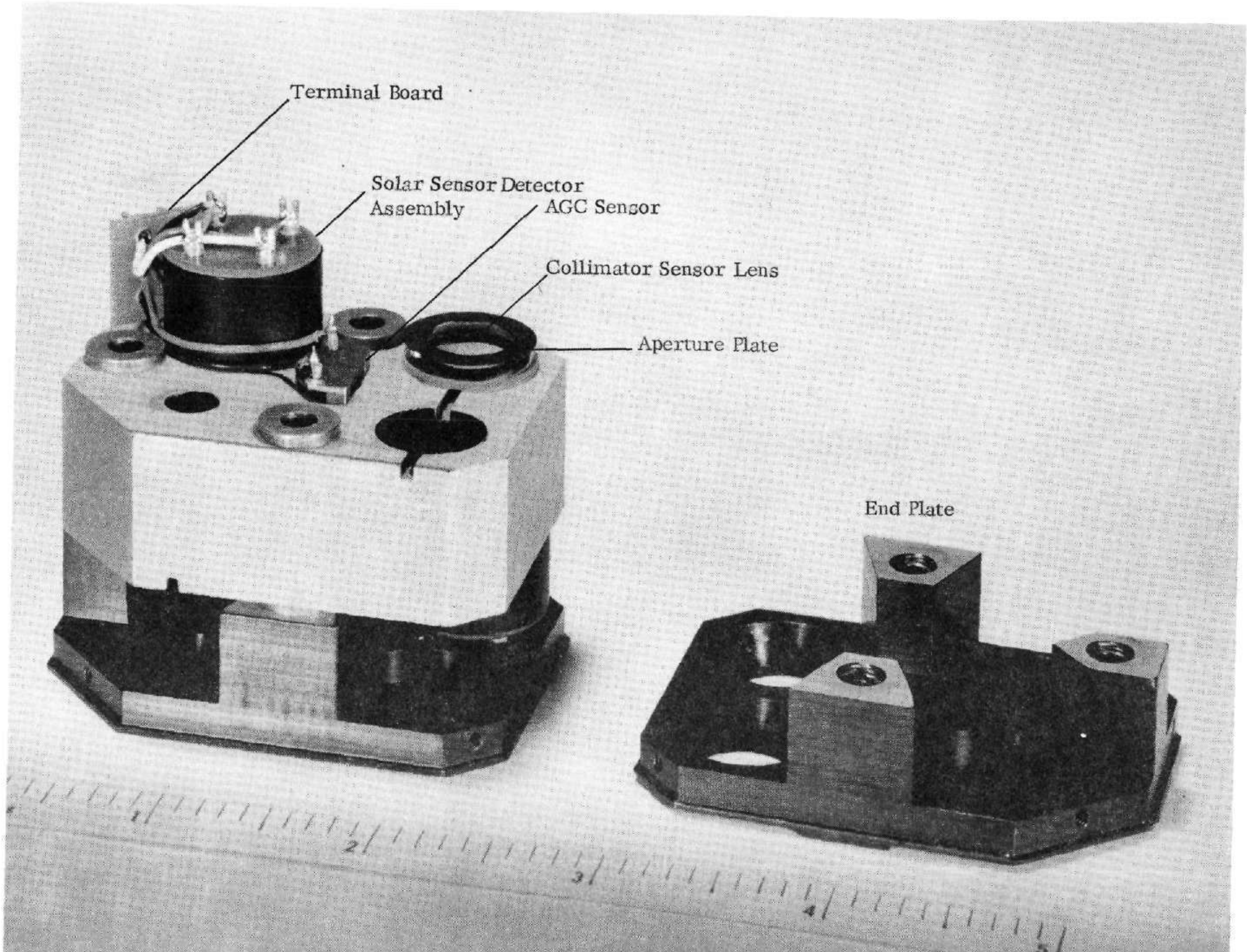

Figure A-2 SEAS With One End-Plate Removed

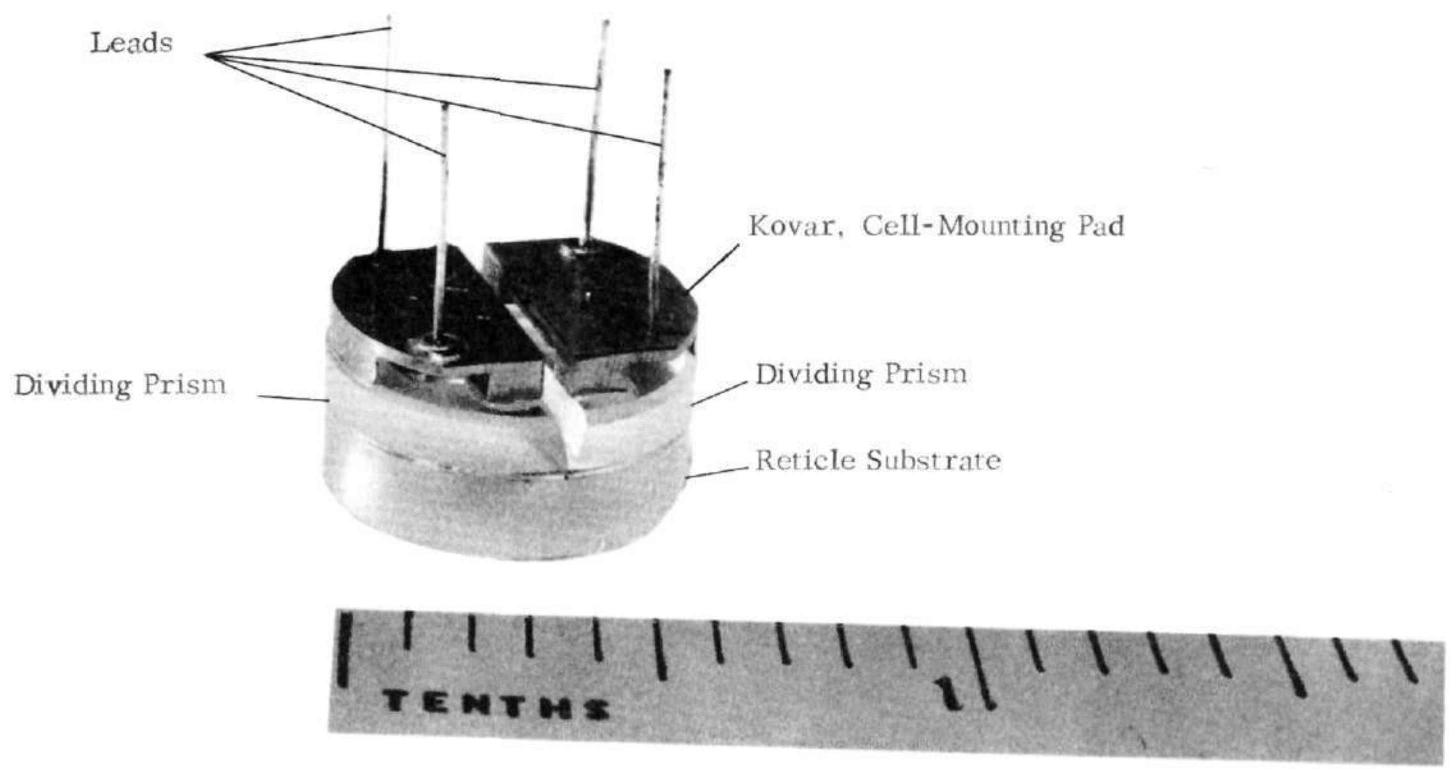

Figure A-3 Rear View of Reticle Assembly

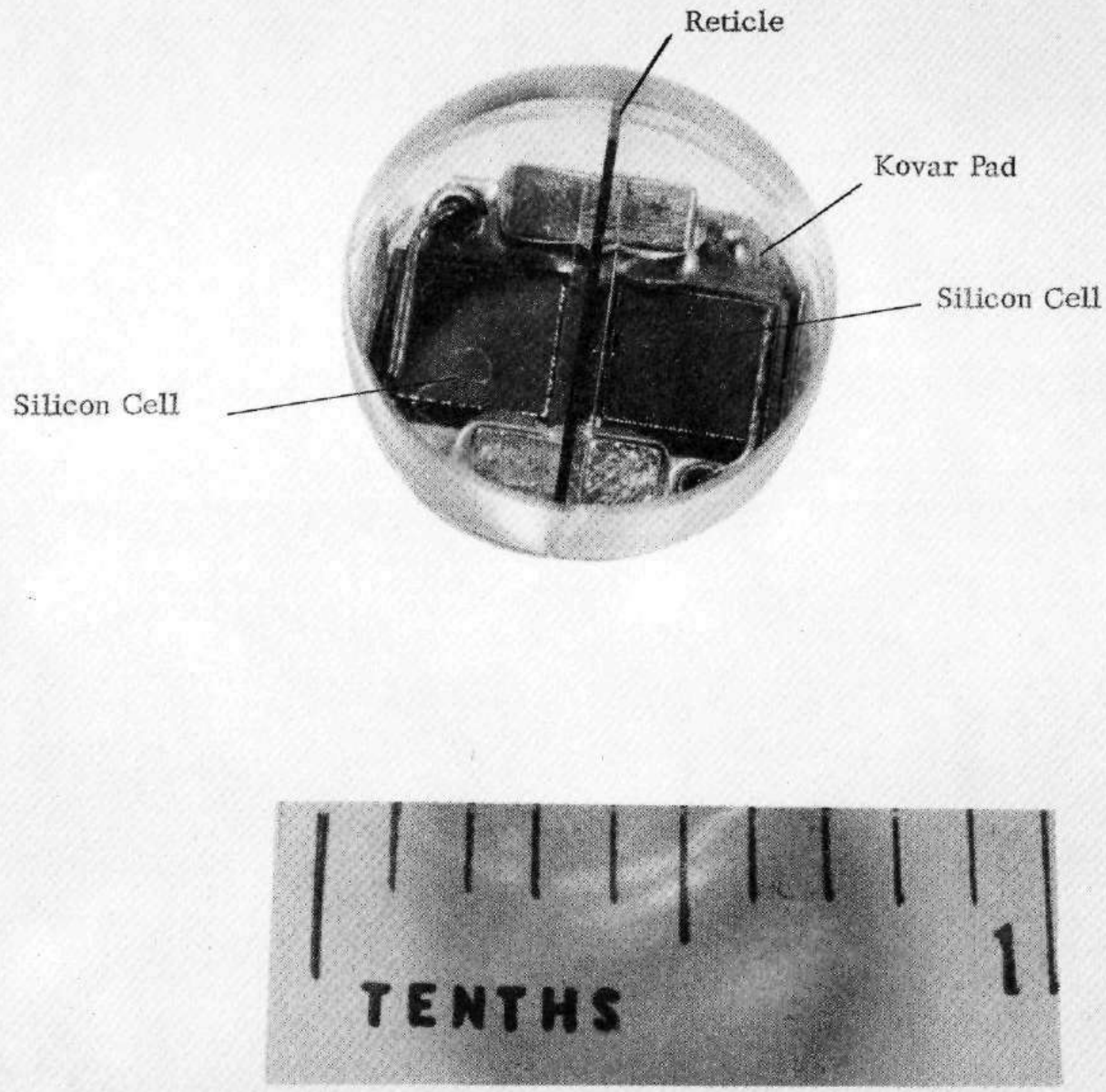

Figure A-4 Front View of Reticle Assembly

Appendix B - Data Sheets

TYPE TIXL03
P-N PLANAR GALLIUM ARSENIDE DIODE LIGHT SOURCE

TYPICAL CHARACTERISTICS

RELATIVE SPECTRAL CHARACTERISTICS

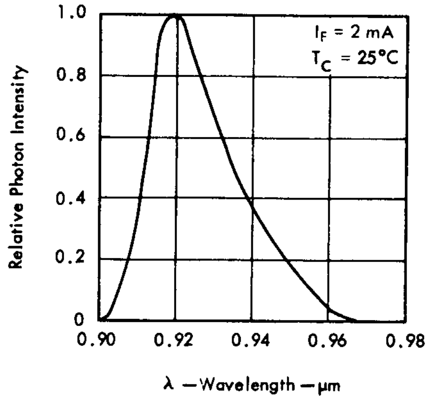

FIGURE 1

RELATIVE PHOTON INTENSITY
vs
ANGULAR DISPLACEMENT

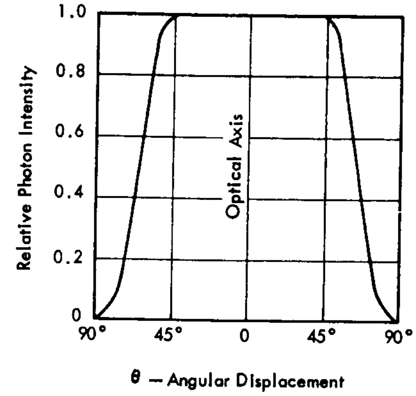

FIGURE 2

RELATIVE PHOTON INTENSITY
vs
CASE TEMPERATURE

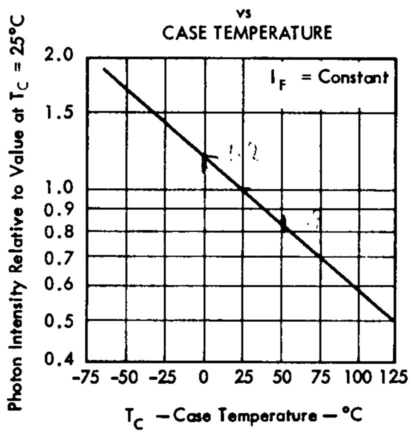

FIGURE 3

CHANGE IN WAVELENGTH OF PEAK INTENSITY
vs
CASE TEMPERATURE

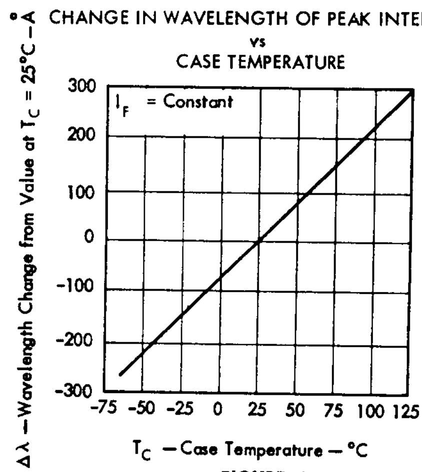

FIGURE 4

RELATIVE PHOTON INTENSITY
vs
FORWARD CURRENT

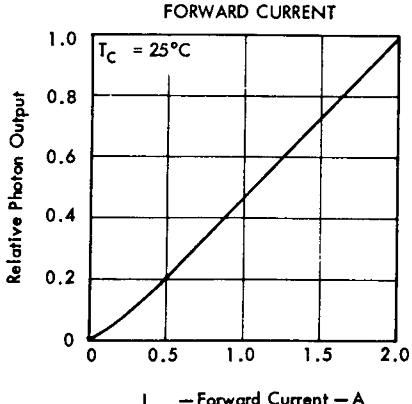

FIGURE 5

FORWARD CONDUCTION CHARACTERISTICS

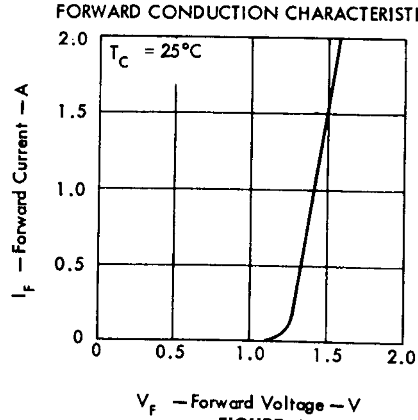

FIGURE 6

P-N PLANAR GALLIUM ARSENIDE DIODE LIGHT SOURCE

TYPE TIXL03
BULLETIN NO. DL-S 679788, FEBRUARY 1967

DESIGNED TO EMIT NEAR-INFRARED LIGHT WHEN FORWARD BIASED

(Improved Version of SNX110)

Light Source Spectrally Matched to Silicon Sensors

mechanical data

This device is in a hermetically sealed package with a flat glass window in the top of the case. The emitting surface of the GaAs material is hemispherical, 0.07 inch in diameter. The cathode is in electrical contact with the case and adjacent solder lug. The anode is in electrical contact with the stud, which is insulated from the case by a glass-to-metal seal.

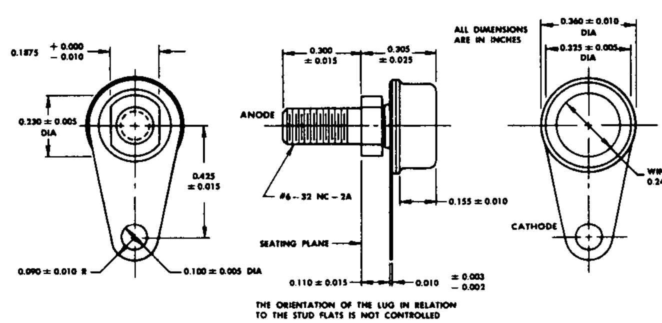

Torque between stud and can or lug must be avoided. Flats are provided on the stud for tightening to heat sink.

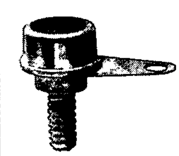

absolute maximum ratings

Reverse Voltage at 25°C Case Temperature . . . . 2 V
Continuous Forward Current at (or below) 25°C Case Temperature (See Note 1) . . . . 2 A
Storage Temperature Range . . . . −65°C to 150°C
Solder Lug Temperature for 10 Seconds (See Note 2) . . . . 240°C

operating characteristics at 25°C case temperature

PARAMETER		TEST CONDITIONS	MIN	TYP	MAX	UNIT
P_O	Radiant Power Output	$I_F = 2$ A	15			mW
λ_{peak}	Wavelength at Peak Emission			0.92		μm
BW_λ	Spectral Bandwidth Between Half-Power Points			225		Å
θ	Emission Beam Angle Between Half-Power Points			130		deg
V_F	Static Forward Voltage			1.6	2.2	V

NOTES: 1. Derate linearly to 125°C case temperature at the rate of 20 mA/deg.
2. Soldered connections should not be made directly to the stud because of the low-thermal-resistance path between the stud and emitting element.

PRELIMINARY DATA SHEET:
Supplementary data will be published at a later date.

TEXAS INSTRUMENTS
INCORPORATED
SEMICONDUCTOR-COMPONENTS DIVISION
POST OFFICE BOX 5012 • DALLAS, TEXAS 75222

Appendix C

CEMENT EVALUATION TESTS FOR THE SEAS PROGRAM

Appendix C

CEMENT EVALUATION TESTS FOR THE SEAS PROGRAM

INTRODUCTION

One of the basic operational principles of both the SEAS and the PASS optical heads is that the relative alignment between the sun sensor and the collimator sensor axes does not change. The absolute accuracy of the SEAS system depends upon accurately knowing what the sun sensor to collimator sensor alignment is and knowing that it does not change by more than a fraction of second of arc from the time of initial calibration,through the period of environmental testing,and to the end of its operation in space. In order to ensure the maximum of dimensional stability for the SEAS optical head a construction method was devised where the major structural element is a block of fused quartz,and the sensor lenses and reticle-detector assemblies, also made from fused quartz, are permanently cemented to the structural block. Of prime importance in this method of construction is that the components that are cemented to the quartz structural block do not move relative to the block after the calibration has been performed. A transitional motion of five millionths of an inch of a reticle relative to its lens would cause a system error of one second of arc. Therefore, it is obvious that the dimensional stability of cement joints is of great concern and it is because of this that the cement evaluation test was carried out.

TEST PREPARATION

Four cements were selected for the test program; two epoxy cements and two optical cements. They are each formulated and recommended by their manufacturers specifically for the purpose of bonding glass to glass to produce a joint of high optical quality. In addition, the two epoxy cements are formulated to have a low flexural modulus of elasticity and are therefore also recommended for bonding glass to metal. Although the most critical cement joints in SEAS are not in the optical path and could actually be opaque, it was felt that the elimination of pigments and fillers from the cements would be advantageous because the same cement could be used in those places where optical clarity is required. Also, the fillerless cements would generally have a lower viscosity which would allow for the formation of thin cement lines and would absorb less thermal radiation because of their transparency. Table 1 lists most of the important properties of the selected cements. (Much of the physical properties information for the optical cements was unobtainable from the manufacturer.)

Cement	Cement Type	Color	Shelf-life	Mix Viscosity	Coeff. of Expansion in/in/^{o}F	Tensile Shear Strength	Modulus of Elasticity	De-cementing	Recommend Cure
Armstrong #A-271	Epoxy 2 component	Light Amber	12 Mos.	14,000 cps	$4x10^{-5}$	2800 psi	$4.9x10^{4}$ psi	Difficult	30 min @ 200^{o}F
Hysol #0151	Epoxy 2 component	Light Amber	12 mos.	8,000 cps	$7x10^{-5}$	1950 psi	$1.1x10^{4}$ psi	Difficult	2 hrs @ 140^{o}F
Summers Lab Lens Bond C-59	Polyester resin with catalyst	Clear	18 mos non-refrig.	Very low	N/A	N/A	N/A	above 480^{o}F	2-3/4 hrs @ 160^{o}F
American Optical, Optical Cement #805	thermo-plastic single component	Clear	6 mos when refrig-erated	Very low	N/A	N/A	N/A	above 230^{o}F	3 hrs @ 160^{o}F

TABLE C-1 Physical Properties of Cements

Sixteen one inch cubes of a commercial optical grade of fused quartz were purchased for the cement tests. The quartz cubes each had two opposite faces polished to at least five fringes flatness; the other cube faces were fine ground flat, but were not polished. The one inch cube shape of test blocks was selected to provide a symmetrical and physically stable test piece with a sufficient surface area for both cementing and measuring. When two cubes are cemented together with their entire faces in contact the maximum tensile stress in the cement due to a 1 g acceleration is about the same as that similarly produced between the SEAS quartz structure block and the reticle-detector assemblies.

Each of the four test cements were prepared according to the manufacturers instructions. The cements were applied between the ground faces of the cubes and the cubes were manually pressed together to spread the cement and remove bubbles in the standard optical manner. The cemented test assemblies were than placed in an oven with no clamps and were positioned so that the cement planes were horizontal with one cube above another and temperature cured according to the manufacturers recommended time and temperature. Two pairs of the quartz cubes were cemented together with each of the cements to form eight test blocks.

In order to enable precision measurements of the test blocks to be made, it was necessary to establish a very accurate reference surface on each cube in a test block. In order to do this one of the 1 x 2 inch faces of each of the eight test blocks was optically polished to a flatness of close to 1/10 fringe, except near the edges and the cement line. It should be pointed out that the achievement of this degree of flatness across the cement line took considerable effort on the part of the optical polisher because of the relative flexibility of the cement joint and it required that the test blocks be imbedded in a rigid plaster polishing block instead of the normally used pitch block.

After the polishing operation was completed and the test blocks were removed from the plaster polishing block, the surface contours of the polished faces were checked by the use of an optical flat. Two things were immediately evident: First, all of the eight test blocks exhibited a depression with maximum depth of about 15 millionths of an inch and extending about 1/16 inch on either side of the cement line. This depression is attributed to the cement line loading up with polishing compound and causing the area immediately next to the cement line to receive a greater amount of polishing action. This phenomena is of particular importance for the PASS type of autocollimator reticle assembly which required polishing across a cement line to produce a reticle. Secondly, some of the test blocks exhibited an immediate twisting of the two halves relative to each other. This immediate twisting can be attributed to the relatively high stresses induced into the cement during the polishing operation and is the type of movement that is commonly seen in cemented optical prisms after they are polished. An inspection of the test block cement lines from the side of the polished faces with a

100X microscope was made in order to determine the cement thickness and the extent of edge chips around the cement line. Table 2 indicates the results of the cement line microscope inspection.

The only practical and easy to interpret measuring method that would indicate the relative motion between the cube faces on a test block with an accuracy of less than one second of arc is by autocollimation. The polished faces of the test blocks were silvered by a silvering solution of silver nitrate to increase their reflectivity and make them suitable for use as autocollimation mirrors. Measurements were made by placing a test block in front of a Davidson Model D-638 autocollimator with one of the polished cube faces covered and determining the angular orientation of the other polished cube face in two perpendicular axes. The cube face cover was then shifted to the other cube face and the angular orientation of the second cube face was then determined; the angular differences between the two cube faces in each of the two axes is the tilt between the two polished cube faces on a test block. The direction of the axes was chosen so that motion about one of them indicated a twist between the cubes and motion about the other indicated a tilt. The accuracy of this method of measurement was checked by using the same procedure with a precision optical flat masked to the shape and size of a test block polished face instead of a test block. Repeated measurements with this calibration set-up indicated a measurement error of less than 0.2 arc second.

TESTS

It was felt that both thermal cycling and a high temperature soak would accelerate any motion of the halves of the test blocks relative to each other. The eight test blocks were divided into two groups of four blocks with one of each of the cements in each group. One group was considered the control group and was not subjected to any environment other than that of the laboratory; the other was subjected to three different tests at a temperature of +65°C. Autocollimation measurements of all of the test blocks were made prior and subsequent to the thermal tests in addition to measurements made during the thermal tests. For the thermal tests the test blocks were put in a temperature controlled oven at +65°C. The oven door was equipped with a window consisting of a six inch diameter by one inch thick optical flat through which the autocollimation measurements of the test blocks could be made, however, careful examination of the data obtained at +65°C revealed that the one inch thick Pyrex optical flat, used for the oven window, was warping due to the temperature gradient across it with the result that the autocollimator readings were in error by two-three seconds.

Approximately 175 autocollimation measurements were made on the eight test blocks over a period of four months time. The results of the measurements are plotted graphically in Figure 4-4.

Cement	Cement Line Thickness	Comments
Hysol #0151	#1 0.0004 inches #2 0.00126 inches	free of polish chips approx. .0005
Armstrong A-271	#3 0.0014 inches #4 0.0008 inches	Similar to Hysol
Summers Lab C-59	#5 0.0005 inches #6 0.0006 inches	free of polish chips approx. 0.0006 and more regular than those on epoxy blocks
American Optical 805	#7 0.00035 inches #8 0.0005 inches	loaded with polish most extensive chips approx. 0.0007

TABLE C-2 **Cement Line Properties**

CONCLUSIONS

The observed motions of the test blocks are believed to be caused by the normal aging processes of the cements and the gradual recovery from possibly high stresses induced in the cements by the optical polishing operation. It is apparent that a period of at least two weeks from the time of cementing and/or mechanically induced stress should pass before critically cemented components are considered stable. Exposure to a temperature of 65°C does not seem to appreciably either accelerate or stabilize block motion.

As for selecting the best of the four cements, the data indicates not too much difference between them. The block cemented with the American Optical #805 cement had the largest initial motion of approximately nine seconds immediately after release from the polishing block as compared to 0.1 seconds for one of the blocks cemented with the Summers Lab C-59. The Summers Lab C-59 cement was selected for SEAS because of its high stability, low viscosity and relative ease of decementing. This cement also makes satisfactory bonds between quartz and metal and was also used in SEAS for the quartz to metal bonding.

APPENDIX D - Detector Investigation

1.0 INTRODUCTION

During the final SEAS (Contract NAS 2-4835) prototype testing at Exotech an apparent increase in detector responsivity with increased level of illumination was observed. This phenomena, if proven to be real, would make ground calibration of the SEAS sensors extremely difficult and could decrease the absolute accuracy of the present SEAS system in other than center pointing modes of operation. At that time a cursory survey of literature and detector users did not yield sufficient information to enable a solution to the problem to be found.

This study was begun in order to sufficiently define the phenomena and to determine what, if any, SEAS design changes would be necessary.

2.0 DETECTOR INVESTIGATION

The detector investigation was divided into three parts. The first part was to examine the literature and to contact detector manufacturers in order to get a theoretical understanding of the detector responsivity non-linearity phenomena and to ascertain if it would be possible to obtain detectors that exhibited a minimum of non-linearity. The second part was to construct an experimental test set-up that could accurately measure the detector non-linearity and to then check a variety of detectors from different manufacturers. The last part of the detector investigation was to determine what course of action should be taken in future SEAS programs to ensure that detector non-linearity will not affect the sensor absolute accuracy.

2.1 Phenomena Investigation

The initial literature search and detector vendor contacts established that there was little understanding of the non-linearity phenomena and much conflicting information. None of the detector vendors contacted (Heliotek, Philco-Ford, EG&G, Electro-Nuclear, United Detector) could establish a theoretical basis for predicting the observed non-linearity of their detectors or could they be sure that they could consistently produce detectors with the same amount of non-linearity. Therefore, it was decided that further investigation into the theoretical aspects of the non-linearity phenomena at this time would not be fruitful. Particularly, until enough empirical data is obtained to adequately characterize the non-linearity phenomena.

2.2 Experimental Test Set-Up

An experimental set-up was designed and constructed which would allow for a reproducible change of several orders of magnitude of the incident energy on the test detector while simultaneously allowing for an accurate determination of the detector responsivity. The number of experimental variables that could be measured for this study were far too many for the current scope. Therefore, the study was limited to the following:

1. Incident illumination in the range of 10^{-8} to 10^{-2} watts/cm^2.
2. Illumination wavelength of tungsten filiments at approximately 2800°K.
3. Effects of two bandpass filters to alter the incident energy spectrum.
4. Thermal effect at +50°C.
5. Data for seven different detectors.

Figure #1 and Table #1 shows the experimental set-up. An experimental run was made in the following manner.

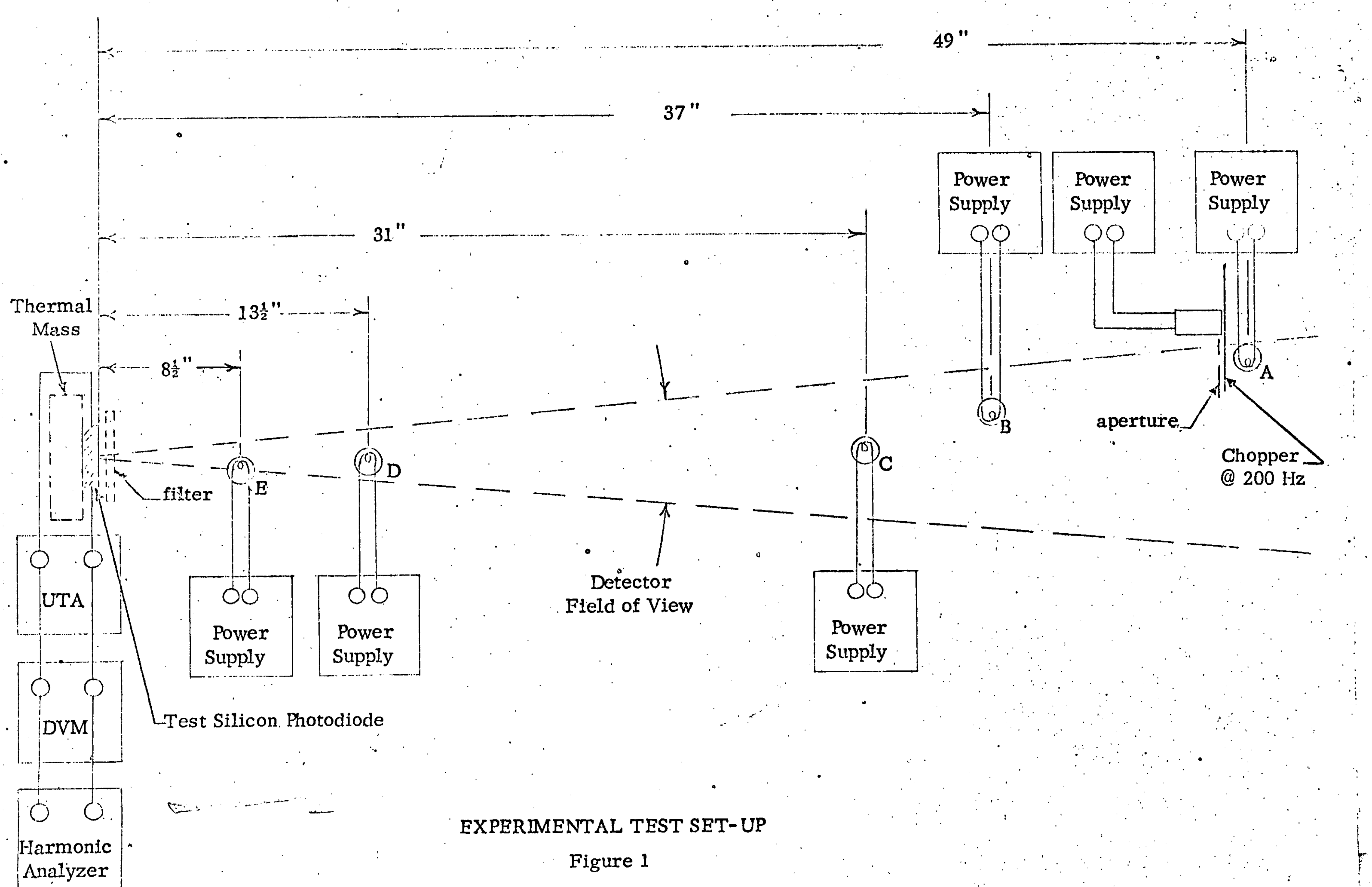

EXPERIMENTAL TEST SET-UP

Figure 1

LAMPS USED DURING DETECTOR LINEARITY TEST PROGRAM

MANUFACTURER		MFG. NO.	VOLTAGE	WATTAGE
A =	Chicago Miniature	327	28 V	1.12 W
B =	General Electric	18A-T10-1P	6 V	108 W
C =	General Electric	1024	12 V	15.6 W
D =	Kay Electric	3030	2.7 V	84 mW
E =	General Electric	345	6 V	240 mW

TABLE I

1. The test detector was mounted in the test set-up.

2. Lamp A, the reference light, was turned on behind a rotating blade chopper. The chopper frequency was set at approximately 200 Hz.

3. The detector under test was mounted on a large thermal mass to ensure temperature stability and was connected to a high sensitivity Universal Test Amplifier, UTA.

4. The UTA output was connected to a harmonic analyzer which was carefully tuned to the chopper frequency.

5. Measurements of the detector output were first made with only the reference lamp on. Then lamps, B, C, D, and E were turned on one at a time and the detector output re-measured - each succeeding lamp supplying greater amounts of illumination on the test detector.

6. The above measurement sequence was repeated with the thermal mass at 50°C for some detectors.

7. The measurements were also repeated with spectral filters in front of the test detector. See Figure 9 for the filter characteristics.

2.3 Data Analysis

The experimental data for the seven test detectors is plotted in Figures 2 through 8. The horizontal axis is an approximate value for the total useable incident energy falling on the detector in watts/cm^2. The vertical axis is the per cent deviation in the detector responsivity from its initial value with only the reference lamp on. In other words, the graphs are a plot of the increased detector responsivity with increasing illumination.

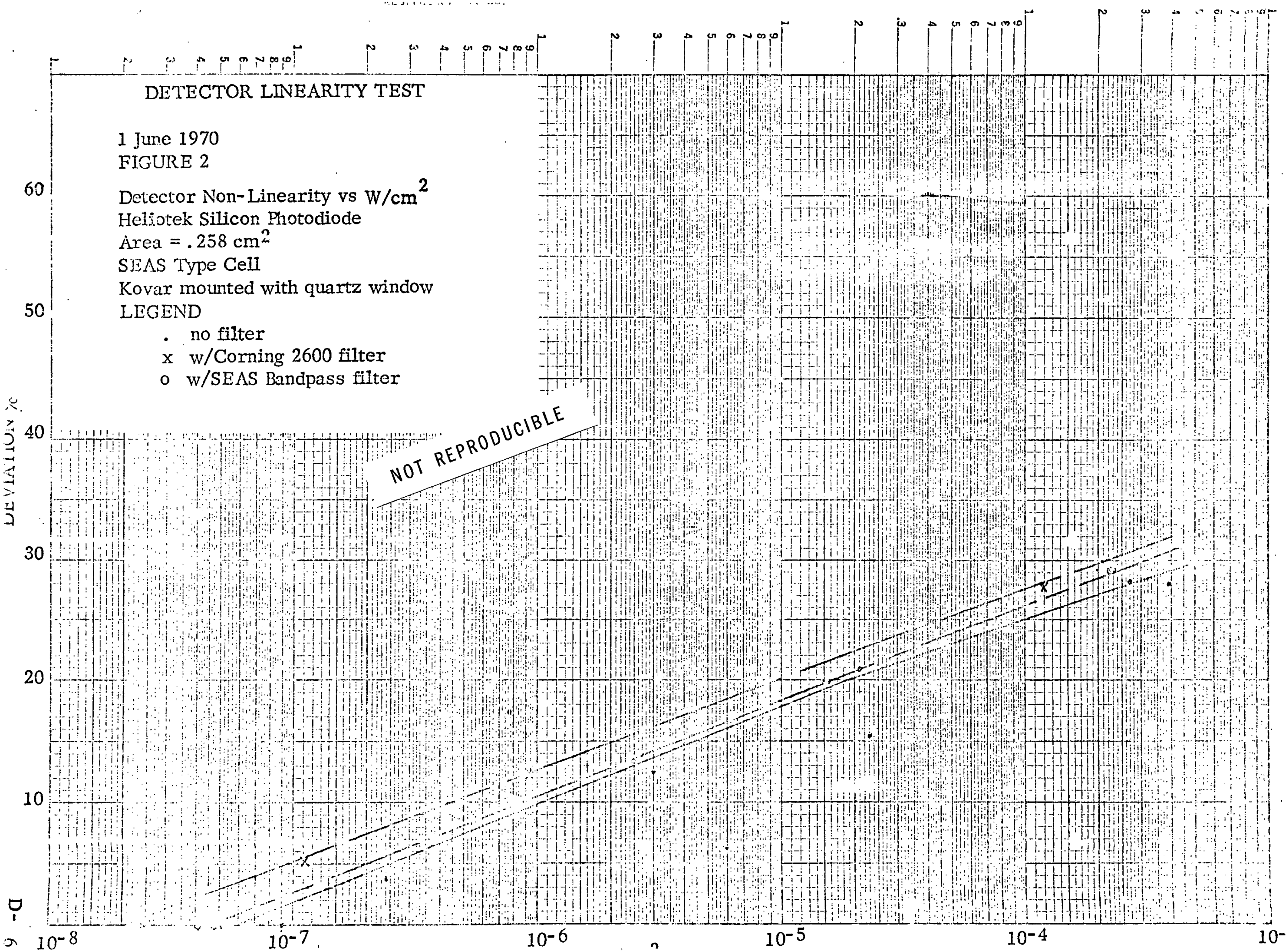

DETECTOR LINEARITY TEST
1 June 1970
FIGURE 2
Detector Non-Linearity vs W/cm^2
Heliotek Silicon Photodiode
Area = .258 cm^2
SEAS Type Cell
Kovar mounted with quartz window
LEGEND
. no filter
x w/Corning 2600 filter
o w/SEAS Bandpass filter
NOT REPRODUCIBLE
DEVIATION %
60
50
40
30
20
10
10^{-8}
10^{-7}
10^{-6}
10^{-5}
10^{-4}

D-9

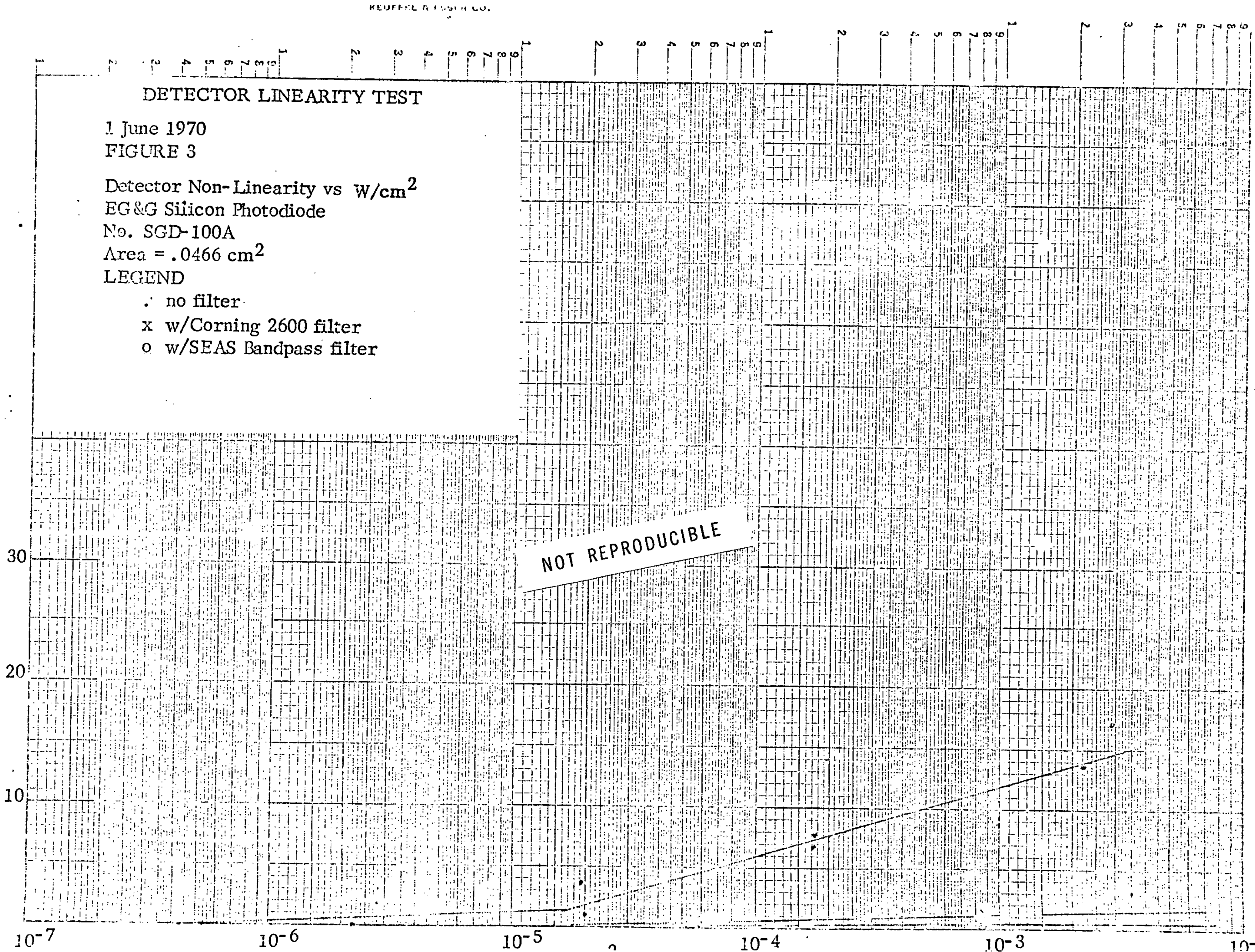

KEUFFEL & ESSER CO.
DETECTOR LINEARITY TEST
1 June 1970
FIGURE 3
Detector Non-Linearity vs W/cm²
EG&G Silicon Photodiode
No. SGD-100A
Area = .0466 cm²
LEGEND
· no filter
x w/Corning 2600 filter
o w/SEAS Bandpass filter
DEVIATION %
30
20
10
10⁻⁷
10⁻⁶
10⁻⁵
10⁻⁴
10⁻³
NOT REPRODUCIBLE

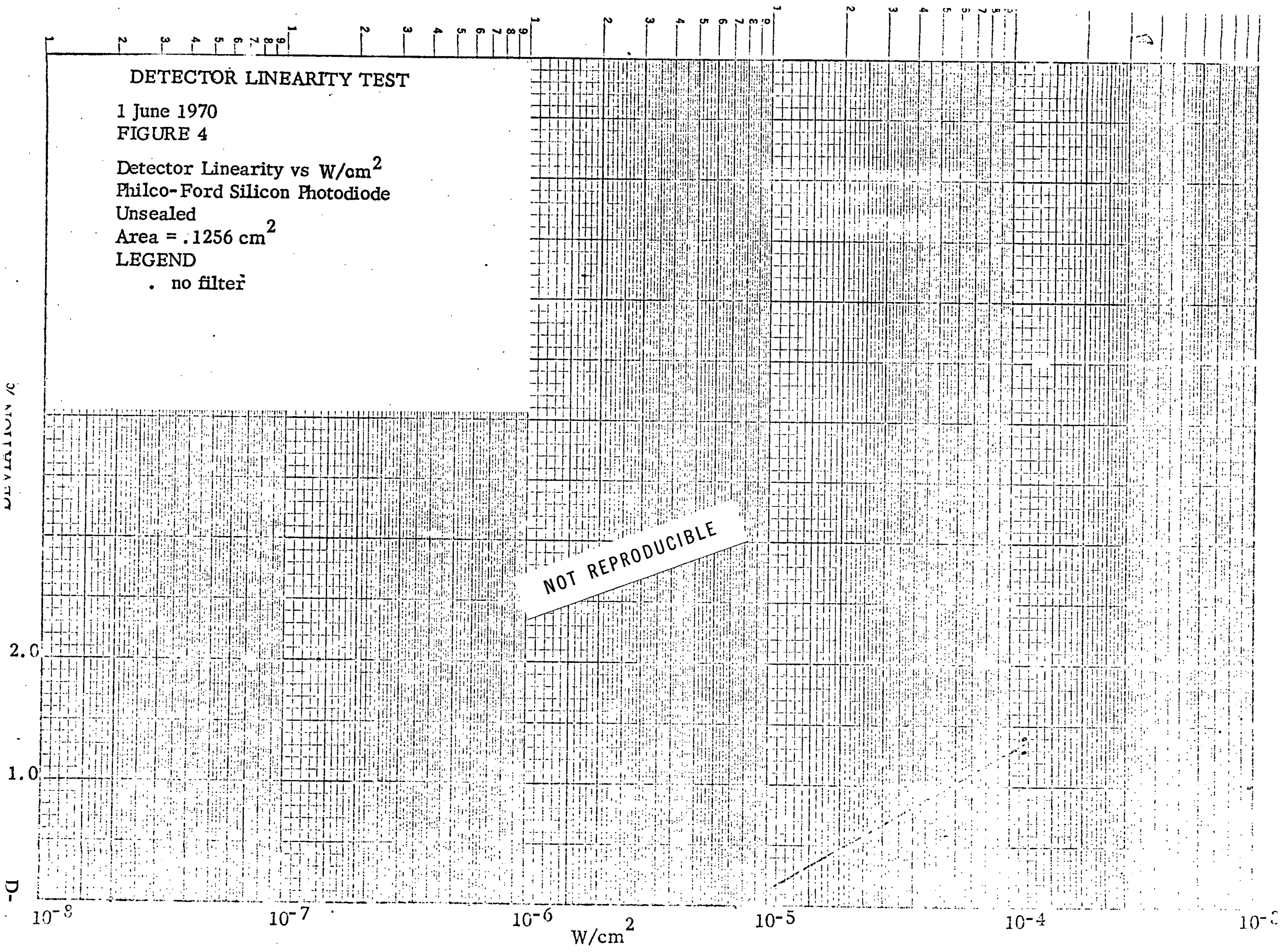
DETECTOR LINEARITY TEST
1 June 1970
FIGURE 4
Detector Linearity vs W/cm2
Philco-Ford Silicon Photodiode
Unsealed
Area = .1256 cm2
LEGEND
. no filter
NOT REPRODUCIBLE
2.0
1.0
10-8
10-7
10-6
10-5
10-4
W/cm2

D-

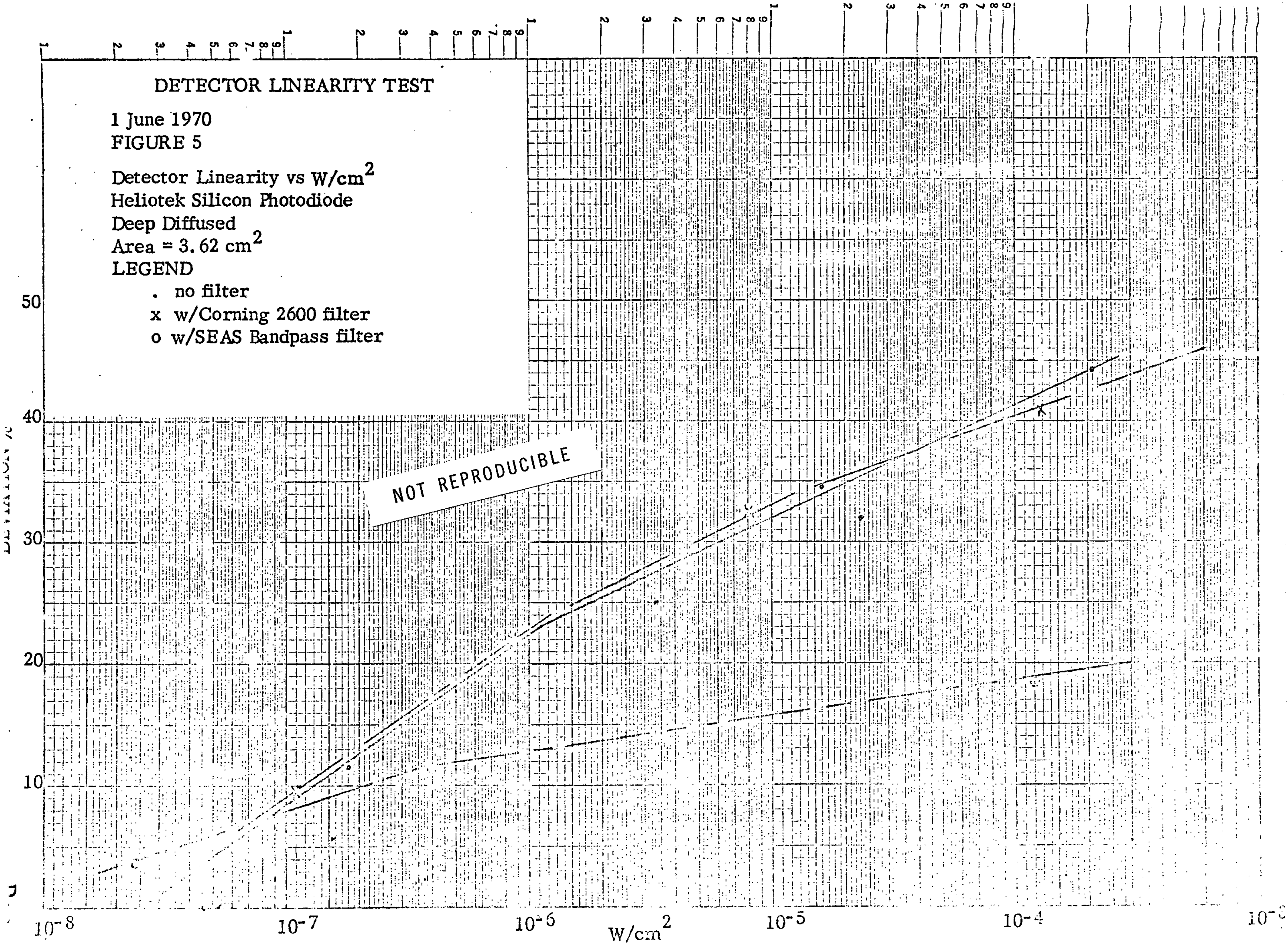

DETECTOR LINEARITY TEST
1 June 1970
FIGURE 5
Detector Linearity vs W/cm²
Heliotek Silicon Photodiode
Deep Diffused
Area = 3.62 cm²
LEGEND
. no filter
x w/Corning 2600 filter
o w/SEAS Bandpass filter
NOT REPRODUCIBLE
50
40
30
20
10
10⁻⁸
10⁻⁷
10⁻⁶
10⁻⁵
10⁻⁴
W/cm²

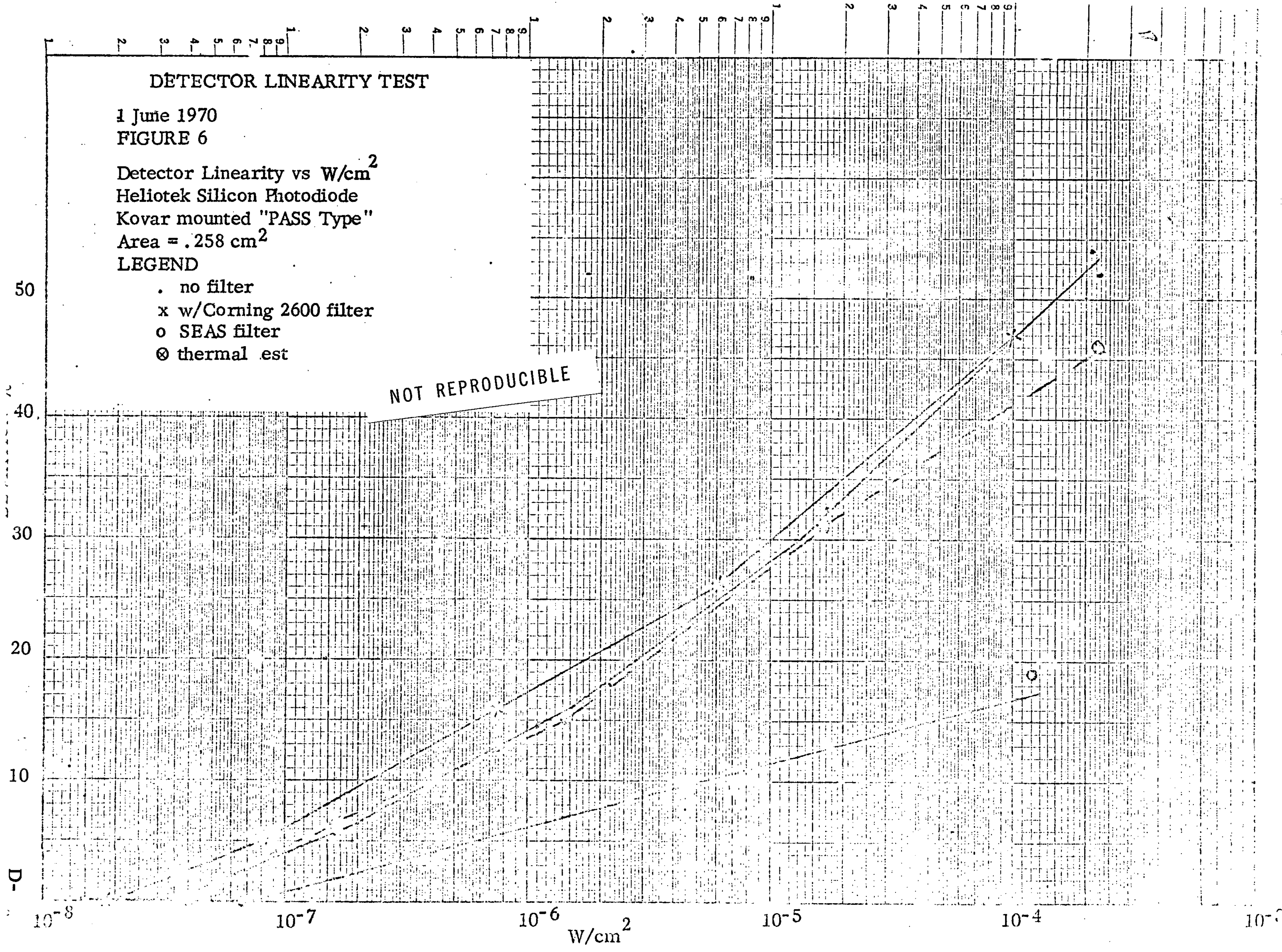
DETECTOR LINEARITY TEST
1 June 1970
FIGURE 6
Detector Linearity vs W/cm^2
Heliotek Silicon Photodiode
Kovar mounted "PASS Type"
Area = .258 cm^2
LEGEND
. no filter
x w/Corning 2600 filter
o SEAS filter
⊗ thermal est
NOT REPRODUCIBLE
50
40
30
20
10
D-
10^{-8}
10^{-7}
10^{-6}
10^{-5}
10^{-4}
W/cm^2

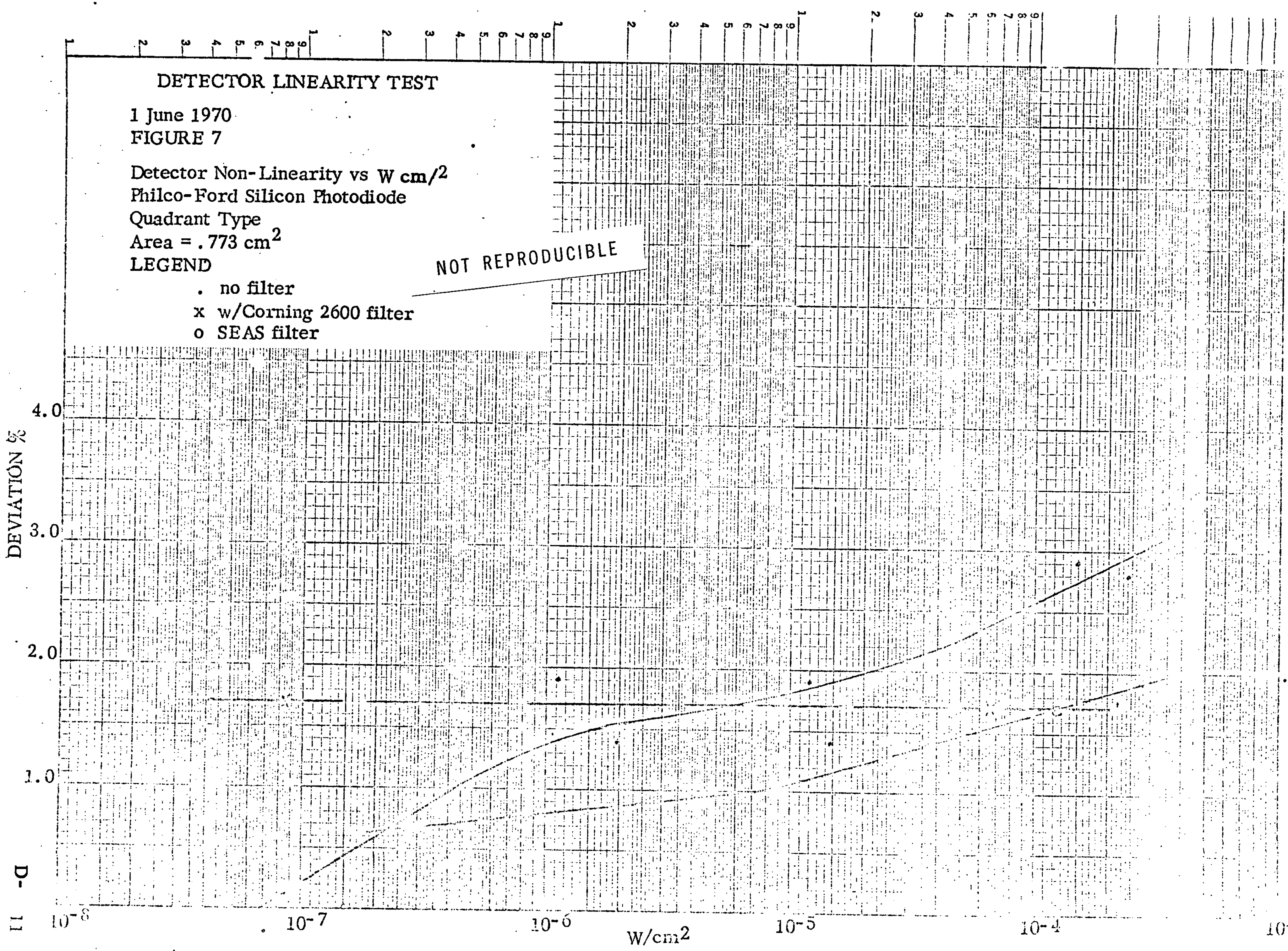
DETECTOR LINEARITY TEST
1 June 1970
FIGURE 7
Detector Non-Linearity vs W cm/2
Philco-Ford Silicon Photodiode
Quadrant Type
Area = .773 cm2
LEGEND
. no filter
x w/Corning 2600 filter
o SEAS filter
NOT REPRODUCIBLE
DEVIATION %
4.0
3.0
2.0
1.0
10-8
10-7
10-6
10-5
10-4
W/cm2

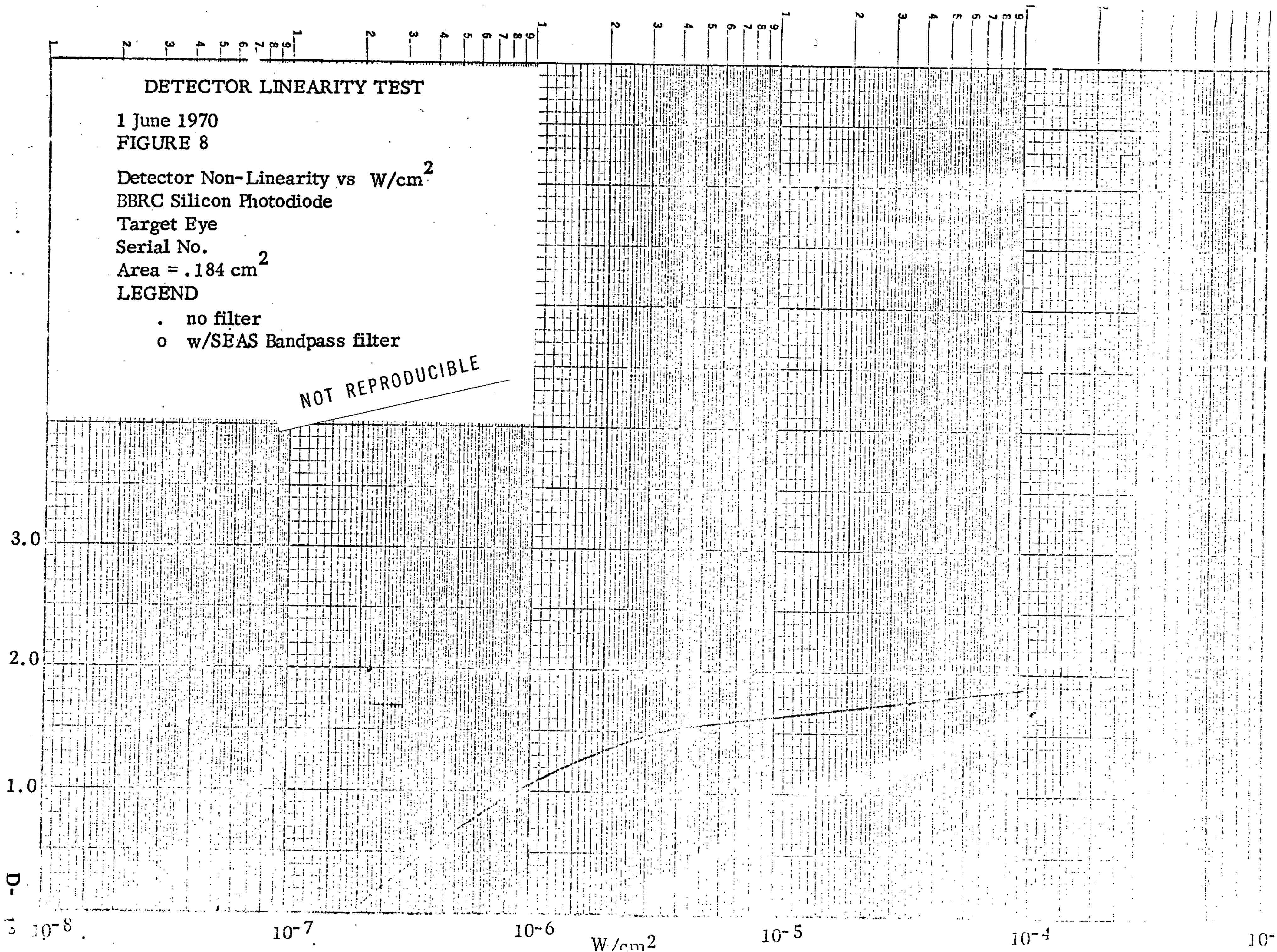
DETECTOR LINEARITY TEST
1 June 1970
FIGURE 8
Detector Non-Linearity vs W/cm^2
BBRC Silicon Photodiode
Target Eye
Serial No.
Area = .184 cm^2
LEGEND
. no filter
o w/SEAS Bandpass filter
NOT REPRODUCIBLE
3.0
2.0
1.0
10^{-8}
10^{-7}
10^{-6}
10^{-5}
10^{-4}
10^{-3}
W/cm^2

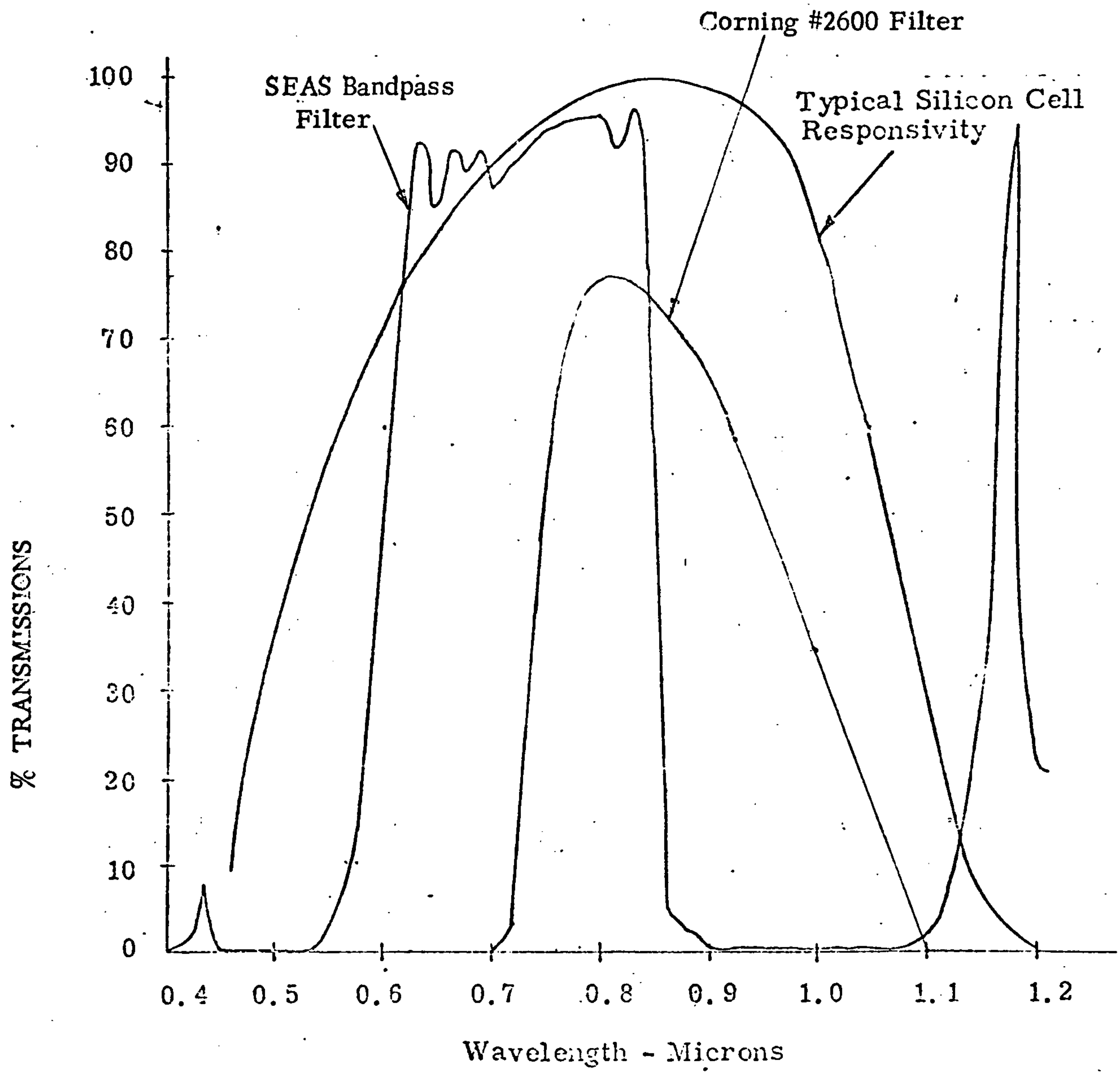

Figure 9 - FILTER CHARACTERISTICS

2.4 Conclusions

The data obtained is not sufficient to draw too many valid conclusions. However, certain generalities are quite apparent.

1. Of those detectors tested the PASS type and SEAS types exhibited the worst non-linearities.

2. The Ball Brothers Target Eye purchased for the SES Program, which used a Heliotek detector with the same nominal specifications as the PASS and SEAS detectors, had a relatively low non-linearity. (The BBRC target eye uses a Corning #2600 filter internally).

3. The Philco-Ford planar diffused P on N photodiodes exhibited a significantly reduced non-linearity effect.

4. Some detectors indicated a significant change in their non-linearity when the incident illumination was spectrally filtered. Blockage of wavelengths below 0.7 microns seemed to produce significant reductions in detector non-linearities on certain detectors.

5. Increasing the detector temperature to 50°C (only the PASS type cell was so tested) produced no significant change in detector non-linearity.

The results of the experiments suggest that the Philco-Ford planar diffused diodes should be used in those applications where detector non-linearities will be important. Also, because there seems to be a considerable variation in detector non-linearity in detectors of the same type and from the same manufacturer, it will be important to measure each detector's non-linearity and select them for matched characteristics.

In the SEAS solar axis variations in detector responsivity with illumination changes from simulator testing to space use will not cause any changes in the absolute accuracy of the sensor if all of the solar detectors, including the AGC detector, have identical amounts of non-linearity. The same holds true for the SEAS experimental axis, except that changes in the detector illumination will be caused by stray light and reflections in the experiment. As a result of this the location of the SEAS experiment AGC detector has been changed from the focal plane source to the sensor head to reduce the probability of the AGC detector being illuminated by a different amount of stray light than the alignment detectors.

REFERENCES

1. NASA CR-73620 , Final Report on The Design, Development, and Fabrication of a Precision Autocollimating Solar Sensor, NAS 2-4050, Exotech, Inc., Rockville, Maryland - 1968

2. Hansen, Q. M., Gabris, E. A., Pearson, M. D., Leonard, B. S., A Gyroless Solar Pointing Attitude Control System for the Aerobee Rocket - Journal of Spacecraft and Rockets, Vol. 4, Number 11, November 1967

3. Melugin, R. K., Bancroft, J. R., Fain, M. Z., "A Solar Experiment Alignment Sensor" - Electro-Optical Systems Design Conference, September 1970